On the Polarization of Gravitational Waves

Dissertation

zur

Erlangung der naturwissenschaftlichen Doktorwürde

(Dr. sc. nat.)

vorgelegt der

Mathematisch-naturwissenschaftlichen Fakultät

der

Universität Zürich

von

Lionel Antoine Philippoz

von

Leytron VS

Promotionskommission

Prof. Dr. Philippe Jetzer (Vorsitz und Leitung)
Prof. Dr. Laura Baudis
Dr. Edward Porter
Dr. Carlos Sopuerta

Zürich, 2018

Summary

More than one hundred years after its formulation, Einstein's General Relativity (GR) has so far proven to be the most accurate theory describing gravity, successfully passing all the tests submitted to it. And even more recently with the first direct detection of gravitational waves (GW) from a binary black hole merger, back in 2015. While GR is well suited to describe the interactions of massive bodies or the evolution of the Universe on cosmological scales, it however faces difficulties to account for the effects described by quantum physics, and this has led to the development of numerous alternative theories of gravity over the years. Since those theories, including GR, sometimes provide different explanations to some phenomenons, for instance dark matter, one needs to rely on their predictions and compare them to the actual observations.

One powerful tool to discriminate between alternative theories, and at the same time serve as an additional test of GR, is given by gravitational waves. In particular, these waves deform space-time in some specific directions - the so-called polarizations of GW - relatively to their direction of propagation. While GR, as every other theory, predicts the existence of two tensor polarizations, some alternative frameworks also expect the existence of additional vector or scalar modes. These discrepencies can therefore be used as a suitable criterion to test gravity, depending on the (non)-observation of those additional modes.

In this thesis, we first tackle the issue of the GW polarizations in alternative theories of gravity, in particular for the so-called $f(R)$ theories, which aim at generalizing GR. The basic idea of this framework consists in replacing the Ricci scalar R found in the Einstein-Hilbert action - that one needs to minimize in order to establish the field equations - by a general function $f(R)$. The new field equations then depend on this function f, on which specific conditions can be applied. We show that in the general case, GW possess two tensor modes as well as two scalar modes. If the connection is assumed to be non-metric, we then only have the existence of the two tensor polarizations. Thanks to theses results, the (non-)detection of additional modes within a GW signal can therefore provide a useful way to test GR and put constraints on $f(R)$ theories.

In a further phase of this thesis, we focus our attention on future GW detectors, and in particular on their sensitivity to the polarization content of a stochastic GW background (GWB). So far, only binary black holes and binary neutron stars have been detected through their emission of GW, but it is possible that GW could have been emitted during the very first moments of the Universe, at a time when space-time was subject to huge accelerations. These early emissions could provide a GWB analog to the CMB for electromagnetic waves, which would still be obervable today and thus allow a direct access to the early Universe. We investigate the characteristic sensitivity achievable with a network of Earth-based detectors of current and next generation, such as the Einstein Telescope (ET), as well as with the future space-borne detector LISA and find that those combinations would be sufficient to detect a GWB. We also show that a correlation of ET with the space-detector DECIGO provides a interesting time-variation of the sensitivity for some polarization modes, depending on their configuration within the network. This result could also provide a way to determine the existence of additional modes, or at least put contraints on their strength.

Zusammenfassung

Mehr als hundert Jahre, nachdem Einstein sie entwickelt hat, scheint seine Allgemeine Relativitätstheorie (ART) die genaueste Theorie der Gravitation zu sein, und bis jetzt konnte sie alle Tests bestehen, die ihr vorgelegt wurden. Dies wurde sogar noch vor kurzem bestätigt mit dem ersten direkten Nachweis von Gravitationswellen (GW) in 2015, die durch zwei umkreisende Schwarze Löcher erzeugt wurden. Obwohl die ART geeignet ist, die Wechselwirkungen zwischen massiven Körper oder die Entwicklung des Universums auf kosmologischen Skalen zu beschreiben, hat sie jedoch Schwierigkeiten, die von der Quantenphysik beschriebenen Effekte zu erklären, was mit der Zeit zur Entwicklung von zahlreichen alternativen Gravitationstheorien geführt hat. Da diese Theorien - einschliesslich ART - für einige Phänomene, z.B. dunkle Materie, verschieden Erklärungen liefern, muss man auf ihre Vorhersagen verlassen und sie mit tatsächlichen Beobachtungen vergleichen.

Ein mächtiges Werkzeug, um zwischen alternativen Theorien zu unterscheiden und gleichzeitig als zusätzlicher Test von ART zu dienen, wird durch GW gegeben. Insbesondere verformen diese Wellen die Raumzeit in bestimmten Richtungen relativ zu ihrer Ausbreitungsrichtung - die sogenannten Polarisationszustände der GW. Während die ART, wie jede andere Theorie, die Existenz von zwei Tensor-Polarisationszustände vorhersagt, werden in einigen alternativen Rahmen die Existenz zusätzlicher Vektor- oder Skalarzustände erwarten. Diese Abweichungen können daher als ein geeignetes Kriterium zum Testen der Gravitation in Abhängigkeit von der (Nicht-) Beobachtung dieser zusätzlichen Polarisationszustände verwendet werden.

In dieser Dissertation beschäftigen wir uns zunächst mit der Frage der GW-Polarisation in alternativen Theorien der Gravitation, insbesondere für die sogenannten $f(R)$-Theorien, die auf eine Verallgemeinerung von der ART abzielen. Die Grundidee besteht darin, den in der Einstein-Hilbert-Wirkung gefundenen Ricci-Skalar R durch eine allgemeine Funktion $f(R)$ zu ersetzen, und diese neue Wirkung dann zu minimieren, um die Feldgleichungen zu bestimmen. Die neuen Feldgleichungen hängen von dieser Funktion f ab, auf die bestimmte Bedingungen angewandt werden können. Wir zeigen, dass die ART im Allgemeinen zwei Tensor-Polarisationszustände sowie zwei Skalarzustände besitzt. Wenn angenommen wird, dass der Zusammenhang nicht metrisch ist, haben wir nur die Existenz der zwei Tensor-Polarisationszustände. Dank dieser Ergebnisse kann die (Nicht-) Detektion zusätzlicher Moden innerhalb eines GW-Signals daher eine nützliche Möglichkeit bieten, um die ART zu testen und Einschränkungen für $f(R)$-Theorien zu setzen.

In einer weiteren Phase dieser Arbeit fokussieren wir uns auf zukünftige GW-Detektoren und insbesondere auf ihre Empfindlichkeit gegenüber der Polarisationszuständen eines stochastischen GW-Hintergrunds (GWB). Bisher wurden nur binäre Schwarze Löcher und binäre Neutronensterne durch ihre Emission von GW entdeckt, aber es ist möglich, dass GW in den allerersten Momenten des Universums zu einer Zeit emittiert wurden, als die Raumzeit sehr stark beschleunigt wurde. Diese frühen Emissionen könnten ein GWB analog zum CMB für elektromagnetische Wellen verfügen, der heute noch beobachtbar wäre und somit einen direkten Zugang zum frühen Universum ermöglichen würde. Wir untersuchen die charakteristische Empfindlichkeit, die mit einem Netzwerk von auf der Erde basierten Detektoren aktueller und zukünftiger Generationen, wie das Einstein Telescope (ET), sowie mit dem zukünftigen weltraumbasierten Detektor LISA erreicht werden kann, und stellen fest, dass diese Kombinationen zur Detektion eines GWB ausreichen würden. Wir zeigen auch, dass eine Korrelation von ET mit dem weltraumgestützen DECIGO eine interessante Zeitvariation der Empfindlichkeit für einige Polarisationsmoden liefert, abhängig von ihrer Konfiguration innerhalb des Netzwerks. Dieses Ergebnis könnte auch eine Möglichkeit bieten, die Existenz zusätzlicher GW-Polarisationszusände zu bestimmen oder zumindest ihre Stärke einzuschränken.

Acknowledgements

Now has come the time to step back and think about the many adventures I had the chance to experience during my doctoral studies in Zürich. Surely those times were not spent alone, and I would like to express some special thanks to some of the many people who accompanied me on that road; since they are quite numerous, I will probably forget some names, but be reassured: only on this page, not in real life.

First of all, I would like to express my deepest gratitude to my supervisor, Philippe Jetzer, for having given me the privilege to embark on this journey. Thanks to him, I had the opportunity to enter the exciting world of gravitational waves, take part in many conferences and schools, and meet fascinating researchers. Not only did he constantly provide good advice on the research aspects of my studies, but he also helped me navigate through the turbulent waters of the academic world, and I am grateful to have been able to count on his support to find solutions when challenges arised. More than a supervisor, he was also a mentor, and I will always remember our numerous discussions often going beyond physics.

I would also like to deeply thank Diethard Klatte, who offered me the possibility to work at the Departement of Business Administration as a teaching assistant in mathematics, and later take over the coordination of the course. Thanks to his trust, I was able to finance my doctorate, but also enjoy a great time in Zentrum.

Over the years, I always experienced a positive and stimulating atmosphere at work, mostly due to all my incredible colleagues. I am thankful to all of them, and in particular Mario, Cédric, Lorenzo, Simone, Andreas, Rafael and Yannick, with whom we shared many memories beyond the academic life; in that sense, they have all become friends more than work colleagues. I could also count on many great colleagues during my stays in Zentrum, and I would like to thank in particular Elef, Daniela, Markus and Luca for the great times we shared together.

Beyond research and teaching lies an unsettling jungle, that of the administration, regardless of the Departement considered. In that regard, I can only thank Regina, Carmelina, Monika, Renate and Rahel, who at one time or another, definitely eased my time by taking care of all the necessary administrative tasks I was confronted to, and with whom I shared many joyful moments.

Last, but not least, I would like express my profound gratitude to my parents, Dominique and Antoine. I probably would not be where I am standing today without their unstinting support and encouragement over all those years.

Thank you again to everyone.

Lionel Philippoz Zürich, 16 May 2018

Sombre couple céleste avide d'unité
Deux étoiles déchues ont débuté leur danse;
Les voilà dans la ronde, tournant en silence,
Intriguante ballade dans l'obscurité.

Le rythme s'accélère, tout semble agité,
L'approche a commencé pour les corps noirs et denses;
Se réduit la distance, augmente la cadence,
Bientôt la réunion pour une éternité.

Tout n'est pas sans repos dans l'espace et le temps:
Intenses vibrations durant quelques instants,
L'on pourrait presque ouïr des deux trous noirs la voix.

Du cosmique concert, un souvenir latent.
Quelques notes diffuses, un écho de ce chant.
Plus un bruit alentour. Univers calme et froid.

Publications

Chapter 4 is based on works published in Phys. Rev. D **93**, 124071 (2016). [1, 2]

Chapter 5 is based on works published in Phys. Rev. D **98**, 044025 (2018). [3]

Chapter 6 is based on works published in J. Phys.: Conf. Ser. **840**, 012057 (2017) and in *Proceedings of the 52nd Rencontres de Moriond*, ASRIF (2017) pp. 69-72. [4, 5]

Table of Contents

Chapter 1

Introduction

"When I ask myself what are the great things we got from the Renaissance, it's the great art, the great music, the science insights of Leonardo da Vinci. Two hundred years from now, when you ask what are the great things that came from this era, I think it's going to be an understanding of the universe around us. This is culture and I think it's culture that the human mind and spirit embrace."

Kip Thorne

After the formulation of his theory of General Relativity (GR) in 1915, Albert Einstein showed just one year later that in the weak-field limit, his linearized field equations can admit wave-like solution, the so-called gravitational waves (GW). These waves, generated by time-varying quadrupole moments of a mass distribution, propagate at the speed of light and locally deform space-time. The expected effect was however so tiny that Einstein himself had his doubts about the possibility to ever be able to detect them, and it led him to think that the energy radiated by a source would be negligible. The debate even grew within the scientific community to know whether those waves were actually real or an artifact of the gauge freedom.

In the 60s, Joseph Weber built one of the first GW detector, based on the principe of a resonant mass. The idea consists in using massive cylinders — historically known as Weber bars — as an antenna with a resonance frequency of 1660 Hz, connected to very sensitive piezo-electric sensors, to supposedly detect a GW signal. He even claimed to have detected a signal, but his results were finally discredited. The expected effect is actually much weaker than his claim, and one should expect relative length change typically of the order 10^{-20} on Earth for a signal emitted by a distant source in the Universe.

One had to wait until 1974 for the first evidence of the existence of GW, with the discovery of a binary pulsar by Robert Hulse and Russel Taylor. This particular system consists of a pulsar — a rapidly rotating neutron star, with a period of 59 ms — and another neutron star rotating around their center of mass, with a period of 7.75 h. By analyzing the decay of the orbital period, they showed that the binary system was losing energy by emitting GW, and thus slowing down. Long-term observations have shown that the ratio of observed to predicted decay rate was 0.997 ± 0.002, and demonstrate a spectacular agreement with the prediction of GR. The discovery of the Hulse-Taylor pulsar led to the 1993 Nobel Prize in Physics and the first indirect detection of GW.

The search for a direct detection started with the pioneering works of Mikhail Gertsenshtein, Vladislav Pustovoit, and Rainer Weiss sketching the concept of what would become the modern laser interferometric detectors. In 1983, Rainer Weiss, Ronald Drever and Kip Thorne founded LIGO, the Laser Interferometer Gravitational-Wave Observatory, which currently consists of two Michelson interferometer in the USA, one located in Hanford/Washington and the second one in Livingston/Louisiana. On the 14th September 2015, LIGO made the very first direct detection of a GW signal emitted by the merging of two black holes of respective masses $36M_\odot$ and $29M_\odot$. Most of the energy carried away, the equivalent of $3M_\odot$, was emitted in less than 200 ms as GW. Up to now (2018), several additional black hole mergers have been detected, as well as a binary neutron star merger, opening a new era in the GW astrophysics.

So far, several second generation detectors are operational, like LIGO or VIRGO in Italy, or about to be built (LIGO India, KAGRA in Japan), and projects for third-generation ground-based detectors are already under way, like the Einstein Telescope (ET). The access to lower frequency in the GW band requires larger detectors, and space-borne detectors are also planned, like LISA or DECIGO. In the case of the former, the LISA Pathfinder mission, thought as a technology test for LISA, was already a success, exceeding the sensitivity expectations. Both space and ground detectors will allow to cover frequencies ranging from 0.1 mHz to 10 kHz without any gap, and thus enable the observation of small to supermassive black holes, neutron star binaries or extreme-mass-ratio inspirals, to name only a few systems.

Thanks to GW, not only will we be able to observe the mentioned systems or even the very first moments of the Universe, but also to test GR at unprecedented precisions. Currently, every attempt to unify quantum field theories with GR have failed, and consequently led to the developement of alternative theories to account for all fundamental forces within a unified framework. Many of these theories diverge from GR in their predictions, and GW could be of help to not only test GR in the strong field regime, but also clear the zoo of gravitation theories, or at least put constraints on them.

In this thesis, we will focus on one characteristic of GW, namely the concept of polarization. GW indeed deform space-time in some specific directions relatively to their direction of propagation. If GR expects the existence of two tensor polarizations transverse to the direction of propagation, modification of the field equations can lead to the existence of additional vector or scalar modes.

In Chapter 2, we introduce the basic ideas and the formalism of GW theory and have a look at some examples of alternative theories of gravitation. In Chapter 3, we review the formalism used for data analysis that we will apply in subsequent chapters for multiple types of detectors.

In Chapter 4, we investigate the question of gravitation wave polarization within the frame of alternative theories to general relativity, and more specifically within the framework of $f(R)$ theories.

In Chapter 5, we study the correlations between the Einstein Telescope (ET) and ground-based detectors, as well as ET and DECIGO, a space-borne detector, in order to determine the sensitivity of the considered network to a GW background.

In Chapter 6 we study the possibilities offered by the LISA project to detect the polarization content of a GW signal, especially in the case of a GW background.

In Chapter 7 we summarize the main results from the previous chapters and give a short outlook.

Chapter 2

The Theory of General Relativity

"The whole fabric of the space-time continuum is not merely curved, it is in fact totally bent."

Douglas Adams, *The Restaurant at the End of the Universe*

2.1 An Introduction to General Relativity

The theory of General Relativity (GR) can be described by the so-called *Einstein's field equations* at any point x on a four-dimensional manifold - the *spacetime* - with $x = (x^0 = ct, x^1, x^2, x^3)$:

$$R_{\mu\nu} - \frac{1}{2} g_{\mu\nu} R = \frac{8\pi G}{c^4} T_{\mu\nu}, \tag{2.1}$$

or equally (taking the trace and replacing R with T),

$$R_{\mu\nu} = \frac{8\pi G}{c^4} \left(T_{\mu\nu} - \frac{1}{2} g_{\mu\nu} T \right). \tag{2.2}$$

Here, c is the speed of light, G is Newton's gravitational constant and t denotes the time coordinate. To our present understanding, all physical processes in the macroscopic universe are governed by these equations. The left-hand side renders information about the local curvature of spacetime while the right-hand side incorporates the local energy-momentum density. It is thus that non-zero energy creates non-zero spacetime curvature which governs the motion of test-masses. To quote John A. Wheeler: *"Matter tells spacetime how to curve, and curved spacetime tells matter how to move."*

The energy-momentum density on the right-hand side is represented by the *energy-momentum tensor* $T_{\mu\nu}$ which contains all curvature-generating energy fields. The curvature on the left-hand side is expressed via the *Riemann tensor* $R^{\rho}{}_{\sigma\mu\nu}$ that can be seen as a measure of how parallel-transported vectors change when transported along two different paths. The *Ricci tensor* $R_{\mu\nu} = R^{\alpha}{}_{\mu\alpha\nu}$ and the *scalar curvature* $R = R^{\mu}{}_{\mu}$ are contractions of the Riemann tensor (repeated indices are always summed over). Because Einstein's field equations are formulated only in terms of tensors, they are form-covariant, i.e. they are invariant under the choice of coordinates. The tensor $g_{\mu\nu}$ represents the metric on the curved manifold and allows to express a length element as $\mathrm{d}s^2 = g_{\mu\nu} dx^{\mu} dx^{\nu}$, where the dx^{μ} are coordinate differentials. The metric tensor is used in tensor algebra to raise and lower indices.

In order to establish a connection between the Riemann and the metric tensor, one needs to impose an *affine connection* that defines the parallel transport of vectors. Conveniently, this is done through the definition of a covariant derivative $\nabla_{\partial_\mu} \partial_\nu = \Gamma^{\rho}_{\mu\nu} \partial_\rho$ which defines how one tangent space basis vector $\partial_\mu \equiv \frac{\partial}{\partial x^{\mu}}$ is derivated along another

basis vector ∂_ν at a certain point on the manifold. The symbols $\Gamma^\rho_{\mu\nu}$ are called *Christoffel symbols*, a convenient choice (to enforce $\nabla g = 0$) in terms of the metric is

$$\Gamma^\rho_{\mu\nu} = \frac{1}{2} g^{\rho\sigma} \left(g_{\mu\sigma,\nu} + g_{\nu\sigma,\mu} - g_{\mu\nu,\sigma} \right), \tag{2.3}$$

where the comma ',' denotes partial derivation. Similarly, the Riemann tensor can be expressed through Christoffel symbols and their derivatives:

$$R^\rho{}_{\sigma\mu\nu} = \partial_\mu \Gamma^\rho_{\sigma\nu} - \partial_\nu \Gamma^\rho_{\sigma\mu} + \Gamma^\rho_{\alpha\mu} \Gamma^\alpha_{\sigma\nu} - \Gamma^\rho_{\alpha\nu} \Gamma^\alpha_{\sigma\mu}. \tag{2.4}$$

Test particles on a curved spacetime move on *geodesics*. A geodesic represents the worldline minimising the distance between two points and is described through the *geodesic equation*

$$\frac{\mathrm{d}^2 x^\rho}{\mathrm{d}\tau^2} + \Gamma^\rho_{\mu\nu} \frac{\mathrm{d}x^\mu}{\mathrm{d}\tau} \frac{\mathrm{d}x^\nu}{\mathrm{d}\tau} = 0, \tag{2.5}$$

which can be found by variation of the action $\int \mathrm{d}s^2 = \int \mathrm{d}\tau \sqrt{g_{\mu\nu} \frac{\mathrm{d}x^\mu}{\mathrm{d}\tau} \frac{\mathrm{d}x^\nu}{\mathrm{d}\tau}}$. In flat space, the metric tensor reduces to the Minkowski tensor

$$\eta_{\mu\nu} = \begin{pmatrix} -1 & 0 & 0 & 0 \\ 0 & 1 & 0 & 0 \\ 0 & 0 & 1 & 0 \\ 0 & 0 & 0 & 1 \end{pmatrix}. \tag{2.6}$$

It is straightforward that the Christoffel symbols as well as the Riemann tensor vanish in flat space.

This is indeed a very brief review of the concepts behind GR and serves mainly to establish the notions used throughout this work. More sophisticated reviews can be found e.g. in [6–8].

Conventions

In the following, repeated indices always imply summation, Greek indices stand for four-dimensional vector indices such as x^μ with $\mu = 0, 1, 2, 3$ and Latin indices refer to three-dimensional spatial vector components such as x^i with $i = 1, 2, 3$. Time derivatives are usually abbreviated with a dot, as for example $\dot{\Phi} = \frac{\mathrm{d}\Phi}{\mathrm{d}t}$. Throughout this work, we use the metric signature $(-, +, +, +)$ of (2.6), such that (by general covariance) $\mathrm{d}s^2 = g_{\mu\nu} \mathrm{d}x^\mu \mathrm{d}x^\nu = -c^2 \mathrm{d}\tau$. Boldface symbols stand for three-dimensional vectors such as $\boldsymbol{r}$ with an absolute value of r. Unit vectors are denoted by a hat, such as $\hat{\boldsymbol{n}}$.

2.2 Principles of gravitational-wave theory

Gravitational waves are ripples propagating and acting on the spacetime manifold itself. In order to gain an understanding of how fast they travel and what they exactly do to spacetime, one can introduce a perturbation to the underlying metric. In the following, we build up basic structures that serve to explore how gravitational waves are generated and how they propagate.

Linearisation of Einstein's field equations

Suppose that we find ourselves in a vacuum far away from gravitational sources, where the flat space Minkowski metric applies. Adding a perturbation $h_{\mu\nu}$ with $|h_{\mu\nu}| \ll 1$ to it results in the perturbed metric tensor

$$g_{\mu\nu} = \eta_{\mu\nu} + h_{\mu\nu}. \tag{2.7}$$

To compute the *linearized* Einstein equations, we follow the ladder from the Christoffel symbols $\Gamma^{\rho}_{\mu\nu}$ up to the Ricci tensor $R_{\mu\nu}$. The linear approximation consists of neglecting terms of the order $\mathcal{O}(h^2)$. To this end, we raise and lower indices with the ordinary flat space metric η. The Christoffel symbols are then

$$\Gamma^{\rho}_{\mu\nu} = \frac{1}{2}\eta^{\rho\sigma}(\partial_\nu h_{\mu\sigma} + \partial_\mu h_{\nu\sigma} - \partial_\sigma h_{\mu\nu}) + \mathcal{O}(h^2)\ . \tag{2.8}$$

We can thus write the Riemann tensor as

$$R^{\mu}{}_{\nu\rho\sigma} = \frac{1}{2}\left(\partial_\nu\partial_\rho h^{\mu}_{\ \sigma} + \partial^\mu\partial_\sigma h_{\nu\rho} - \partial^\mu\partial_\rho h_{\nu\sigma} - \partial_\nu\partial_\sigma h^{\mu}_{\ \rho}\right) + \mathcal{O}(h^2), \tag{2.9}$$

and the Ricci tensor becomes

$$R_{\mu\nu} = R^{\alpha}{}_{\mu\alpha\nu} = \frac{1}{2}\left(\partial^\alpha\partial_\mu h_{\alpha\nu} + \partial^\alpha\partial_\nu h_{\alpha\mu} - \Box h_{\mu\nu} - \partial_\mu\partial_\nu h\right) + \mathcal{O}(h^2), \tag{2.10}$$

where $\Box = \partial_\mu\partial^\mu$ is the d'Alembert operator and $h \equiv \eta^{\mu\nu}h_{\mu\nu}$ is the trace of $h_{\mu\nu}$. The corresponding scalar curvature is

$$R = R^{\mu}_{\ \mu} = \partial^\alpha\partial^\mu h_{\alpha\mu} - \Box h + \mathcal{O}(h^2). \tag{2.11}$$

This takes us at linear order in h to

$$\frac{1}{2}\partial^\alpha\partial_\mu h_{\alpha\nu} + \frac{1}{2}\partial^\alpha\partial_\nu h_{\alpha\mu} - \frac{1}{2}\Box h_{\mu\nu} - \frac{1}{2}\partial_\mu\partial_\nu h - \frac{1}{2}\eta_{\mu\nu}\partial^\alpha\partial^\rho h_{\alpha\rho} + \frac{1}{2}\eta_{\mu\nu}\Box h = \frac{8\pi G}{c^4}T_{\mu\nu}. \tag{2.12}$$

The above equations can be simplified by expressing them in terms of the trace-reversed metric $\bar{h}_{\mu\nu} = h_{\mu\nu} - \frac{1}{2}\eta_{\mu\nu}$. Then (2.12) reduces to

$$\Box\bar{h}_{\mu\nu} + \eta_{\mu\nu}\partial^\rho\partial^\sigma\bar{h}_{\rho\sigma} - \partial^\rho\partial_\nu\bar{h}_{\mu\rho} - \partial^\rho\partial_\mu\bar{h}_{\nu\rho} = -\frac{16\pi G}{c^4}T_{\mu\nu}. \tag{2.13}$$

We can simplify the resulting field equations further by taking advantage of gauge freedom, in analogy to electrodynamics. An infinitesimal coordinate transformation

$$x^\mu \to x'^\mu = x^\mu + \xi^\mu(x), \qquad |\partial_\mu\xi_\nu| = \mathcal{O}(h) \tag{2.14}$$

transforms the metric perturbation (at linear order in h) to

$$h_{\mu\nu}(x) \to h'_{\mu\nu}(x') = h_{\mu\nu}(x) - \left(\partial_\mu\xi_\nu + \partial_\nu\xi_\mu\right), \tag{2.15}$$

because $g'_{\mu\nu} = g_{\alpha\beta}\frac{\partial x^\alpha}{\partial x'^\mu}\frac{\partial x^\beta}{\partial x'^\nu}$ under coordinate transformations. In terms of the trace-reversed metric, one finds

$$\bar{h}_{\mu\nu}(x) \to \bar{h}'_{\mu\nu}(x') = \bar{h}_{\mu\nu}(x) - \left(\partial_\mu\xi_\nu + \partial_\nu\xi_\mu - \eta_{\mu\nu}\partial_\rho\xi^\rho\right)\ . \tag{2.16}$$

The gauge transformation (2.14) can be interpreted in a very natural way: we are free to choose our frame of reference and thus our coordinate system. Although an event is described differently in different reference frames, it still describes the same physical process. In the context of GR, fixing the gauge means going to a fixed frame; this is what we are going to do now.

One way to fix the gauge freedom (2.14) is the so-called *De Donder gauge* (in analogy to the Lorenz gauge in electrodynamics)

$$\partial^\nu\bar{h}_{\mu\nu} = 0. \tag{2.17}$$

The transformation behaviour of $\partial^\nu\bar{h}_{\mu\nu}$ is $\partial^\nu\bar{h}_{\mu\nu} \to \left(\partial^\nu\bar{h}_{\mu\nu}\right)' = \partial^\nu\bar{h}_{\mu\nu} - \Box\xi_\mu$, what enables us to achieve $(\partial^\nu\bar{h}_{\mu\nu})' = 0$ by fixing $\Box\xi_\mu = \partial^\nu\bar{h}_{\mu\nu}$. Thus we find the linearized field equations

$$\Box\bar{h}_{\mu\nu} = -\frac{16\pi G}{c^4} T_{\mu\nu}. \tag{2.18}$$

By differentiating (2.18) and applying the De Donder gauge, one immediately arrives at the flat space energy-momentum conservation law

$$\partial^{\nu} T_{\mu\nu} = 0. \tag{2.19}$$

Thus, at linear order in h, gravitational waves do not enter the energy-momentum tensor and higher order will have to be taken into account in order to compute the energy of a GW [9].

To study the propagation of GWs and their interaction with test masses, it is interesting to look at vacuum solutions of (2.18) where $T_{\mu\nu} = 0$. There the linearized field equations reduce to

$$\Box\bar{h}_{\mu\nu} = 0. \tag{2.20}$$

As $\Box = \boldsymbol{\nabla}^2 - \frac{1}{c^2}\partial_t^2$, this implies that gravitational waves travel at the speed of light. Since the De Donder gauge allows a further coordinate transformation of the form of (2.14) as long as it satisfies $\Box\xi_\mu = 0$, we have four additional degrees of freedom ξ_μ left to simplify our equations. ξ_0 can be chosen such that the trace $\bar{h}$ vanishes (then $h_{\mu\nu} = \bar{h}_{\mu\nu}$). The three spatial components ξ_i can then be fixed in such a way that $h_{0i} = 0$. Then, by applying (2.17), we also find that $\partial^0 h_{00} = 0$, i.e. h_{00} is constant in time and thus we can fix $h_{00} = 0$ for all time. The so-called *transverse-traceless (TT) gauge* is thus defined by

$$h_{0\mu} = 0, \qquad h^{i}{}_{i} = 0, \qquad \partial^{j} h_{ij} = 0. \tag{2.21}$$

A metric perturbation in the TT gauge will from now on be denoted as h_{ij}^{TT}. One can easily verify that the plane wave $h_{ij}^{TT}(x) = e_{ij}(\boldsymbol{k})\, e^{ikx}$ with $k^\mu = (\omega/c, \boldsymbol{k})$ and $\omega/c = |\boldsymbol{k}|$ solves (2.20) and that $\partial^j h_{ij} = 0$ can be interpreted in this case as $k^j h_{ij} = 0$. Here, e_{ij} represents the 4×4 polarisation tensor. Without loss of generality, we pick $\boldsymbol{k} = (0, 0, 1)$ for a plane wave propagating in the z-direction. Then, one finds as a solution in the TT gauge

$$h_{ab}^{TT}(t, z) = \begin{pmatrix} h_+ & h_\times \\ h_\times & -h_+ \end{pmatrix} \cos\left[\omega\left(t - \frac{z}{c}\right)\right], \tag{2.22}$$

for a plane wave moving along the z-axis and acting on the (x, y) plane with $a, b = 1, 2$ (all other components of e_{ij} are zero). Considering an infinitesimal rigid rod lying in the (x, y) plane, its length element oscillates as

$$\mathrm{d}s^2 = (h_+ \mathrm{d}x^2 - h_+ \mathrm{d}y^2 + 2h_\times \mathrm{d}x\mathrm{d}y) \cos\left[\omega\left(t - \frac{z}{c}\right)\right]. \tag{2.23}$$

Note the mixing of $\mathrm{d}x$ and $\mathrm{d}y$ in the last term. If one looks at multiple freely-floating point-masses distributed on a circle, one finds two transverse polarisation modes, a '+' (plus) and a '×' (cross) polarisation, as depicted in Fig. 2.1. The indices in the decomposition of $h_{ab}^{TT}(t, z)$ into h_+ and $h_\times$ in (2.22) were chosen accordingly.

It is possible to define a projector which is able to project every metric perturbation onto its transverse-traceless part. Consider the projection

$$P_{ij}(\hat{\boldsymbol{n}}) = \delta_{ij} - n_i n_j, \tag{2.24}$$

which is transverse along the direction $\hat{\boldsymbol{n}}$ ($n^i P_{ij} = 0$) and has the trace $P_{ii} = 2$. This allows us to construct the Lambda tensor which renders every rank 2 tensor transverse and traceless along $\hat{\boldsymbol{n}}$:

$$\Lambda_{ij,kl}(\hat{\boldsymbol{n}}) = P_{ik} P_{jl} - \frac{1}{2} P_{ij} P_{kl}. \tag{2.25}$$

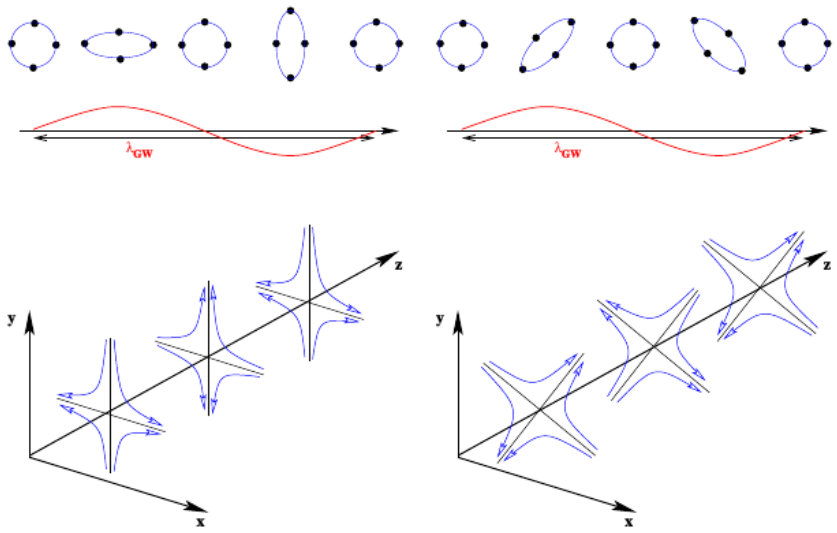

Figure 2.1: *Gravitational waves allow for two different transverse polarisation modes: plus (left) and cross (right) polarisation. Here, a GW that travels along the z-axis and acts on the (x, y) plane is depicted. Picture reproduced from [10].*

If we deal with a plane wave $h_{\mu\nu}$ in the De Donder gauge, we are able to project it to the TT gauge through

$$h_{ij}^{TT} = \Lambda_{ij,kl} h_{kl}, \tag{2.26}$$

where summation is implied for repeated indices. We have destroyed the general covariance of GR by linearising it, jumping to a preferred reference frame. It can be shown from geodesic deviation (see e.g. [9]) that the TT frame is the one where the coordinate difference of two test masses is constant when a gravitational wave passes by.

So far we have investigated the propagation of perturbations on the spacetime manifold. To gain a deeper understanding of gravitational waves, we will need to look at the sources that generate them; this will be covered in the next subsection.

2.3 Alternative theories of gravitation - Particular examples

So far, many alternative theories of gravity have been developed in order to describe physical effects that GR cannot: Scalar-tensor, Brans-Dicke, Einstein-Aether, $f(R)$, tensor-vector-scalar, bi-gravity, quintessence, non-commutative geometry, braneworld, ... to name only a few. Many of them have not been ruled out yet, and this naturally calls for ways of discriminating between them. In that sense, gravitational waves can certainly provide some help.

In the following we introduce selected examples of alternative theories that have been proposed. Let us emphasise once more that a detailed review of alternative theories can be found in [11–13]; in this work we are not interested in a particular theory to be true or false, but rather in GR being consistent with the measured data or not. After possible evidence that GR is not the best theory to describe the data that has been gathered by our detectors, selected alternative theories could then be investigated more closely.

Einstein's equations can be derived by variation of the Einstein-Hilbert action

$$S = \int R \sqrt{-g}\, \mathrm{d}^4x + S_M(\psi_M, g_{\mu\nu}), \tag{2.27}$$

where R represents the scalar curvature, g denotes the determinant of the metric and S_M is the matter action that universally couples a matter field ψ_M to the metric tensor. Any cosmological constant shall be ignored for the time being. Since S has to be scalar, R is the most-general scalar that can be formed from the metric in GR and $\sqrt{-g}\, d^4x$

is the invariant integration mass of GR, there are no alternative actions that could lead to Einstein's field equations. In the following, let us introduce some examples for alternative theories that modify this action.

Scalar-tensor theories

Scalar-tensor theories [14–16] are very popular in unification schemes such as string theory or quantum gravity. Moreover, scalar fields are used to provide a model for cosmological inflation. In addition to the metric tensor, such theories contain a scalar function $\varphi(x)$ that can be incorporated into the Einstein-Hilbert action using minimal coupling, where a potential $V(\varphi)$ and a coupling function $A(\varphi)$ are used:

$$S = \int \left[R - 2g^{\mu\nu}\partial_\mu\varphi\,\partial_\nu\varphi - V(\varphi)\right]\sqrt{-g}\,\mathrm{d}^4x + S_M(\psi_M, A^2(\varphi)g_{\mu\nu}). \tag{2.28}$$

This representation (in the so-called *Einstein frame*) is non-metric as here matter couples also to $A(\varphi)$. A metric representation can be found by defining the physical metric $\tilde{g}_{\mu\nu} \equiv A^2(\varphi)g_{\mu\nu}$ (*Jordan frame*), then,

$$S = \int \left[\phi\tilde{R} - \phi^{-1}\omega(\phi)\tilde{g}^{\mu\nu}\partial_\mu\phi\,\partial_\nu\phi - \phi^2 V\right]\sqrt{-\tilde{g}}\,\mathrm{d}^4x + S_M(\psi_M, \tilde{g}_{\mu\nu}), \tag{2.29}$$

with

$$\phi = A(\varphi)^{-2}, \qquad \omega(\phi) = \frac{1}{2}\left[\left(\frac{d(\log A(\varphi))}{d\varphi}\right)^{-2} - 3\right]. \tag{2.30}$$

The modified field equations in the Jordan frame are then found by a variation of the action to be

$$\tilde{\Box}\phi = \frac{1}{3+2\omega(\phi)}\left(8\pi T^M - \frac{d\omega}{d\phi}\tilde{g}^{\mu\nu}\partial_\mu\phi\,\partial_\nu\phi\right), \tag{2.31}$$

$$\tilde{G}_{\mu\nu} = \frac{8\pi G}{\phi}T^M_{\mu\nu} + \frac{\omega(\phi)}{\phi^2}\left(\partial_\mu\phi\,\partial_\nu\phi - \frac{1}{2}\tilde{g}_{\mu\nu}\tilde{g}^{\rho\sigma}\partial_\rho\phi\,\partial_\sigma\phi\right) + \frac{1}{\phi}\left(\partial_\mu\partial_\nu\phi - \tilde{g}_{\mu\nu}\tilde{\Box}\phi\right), \tag{2.32}$$

where $T^M_{\mu\nu}$ is the energy-momentum tensor constructed from $\tilde{g}_{\mu\nu}$. A special case is *Brans-Dicke* theory (or also referred to as *massless Jordan-Fierz-Brans-Dicke* theory) that assumes $\omega(\phi) \equiv \omega_{\mathrm{BD}}$ to be a constant. Brans-Dicke theory reduces to GR for $\omega_{\mathrm{BD}} \to \infty$. The Brans-Dicke parameter could be constrained using the Cassini spacecraft to $\omega_{\mathrm{BD}} > 4\times10^4$ through measurements of the Shapiro time delay [17].

In the context of compact binaries and gravitational radiation, the dominant effects of scalar-tensor theories on GW generation are the introduction of an additional scalar breathing polarisation mode and the production of dipole radiation through the non-trivial variation of the scalar field in the finite-sized bodies (see e.g. [13]). Thus the orbital energy of the binary is (to leading order) modified by a dipole term that enters one post-Newtonian order before the first contribution from GR. In terms of the gravitational waveform in the stationary phase approximation, this can be written as [18]

$$\tilde{h}(f) = \tilde{h}_{\mathrm{GR}}(f)\,e^{-i\beta_{\mathrm{BD}}u^{-7/3}}, \tag{2.33}$$

where

$$\beta_{\mathrm{BD}} = \frac{5}{3584}\frac{S^2}{\omega_{\mathrm{BD}}}\eta^{2/5}, \tag{2.34}$$

and we recall that $u = G\mathcal{M}\pi f/c^3 = \eta^{3/5}x^{3/2}$. Here, S compares the self-gravitational binding energy per unit mass for the two bodies and essentially depends on their equations of state: this is the point where the SEP is violated. For binary black hole systems, $S = 0$, and hence there is no dipolar radiation in the inspiral waveform [19]; we will therefore not go further into this theory, as it is irrelevant for the context of this work. Furthermore, scalar-tensor theories can be better constrained using weak-field experiments [13]. Nevertheless, they pose a nice pedagogical example of an alternative theory that has undergone a considerable amount of studies.

Vector-tensor theories

Similar to the previous approach, one can introduce an additional gravitational field with vectorial character to the Einstein-Hilbert action that will introduce Lorentz-violating preferred-frame effects to the theory. The most general such action up to quadratic derivatives in the vector is given by [11]

$$S = \int \left[(1 + \omega u_\mu u^\mu) R - K^{\mu\nu}_{\alpha\beta} \nabla_\mu u^\alpha \nabla_\nu u^\beta + \lambda (u_\mu u^\mu + 1) \right] \sqrt{-g}\, \mathrm{d}^4 x + S_M(\psi_M, g_{\mu\nu}), \tag{2.35}$$

where

$$K^{\mu\nu}_{\alpha\beta} = c_1 g^{\mu\nu} g_{\alpha\beta} + c_2 \delta^\mu{}_\alpha \delta^\nu{}_\beta + c_3 \delta^\mu{}_\beta \delta^\nu{}_\alpha - c_4 u^\mu u^\nu g_{\alpha\beta}. \tag{2.36}$$

The coefficients c_i can be chosen arbitrarily, while λ is a Lagrange multiplier that serves to incorporate constraints that are imposed by different subtheories, such as Will-Nordvedt theory, Hellings-Nordvedt theory and Khronometric theory. Einstein-Aether theory was introduced to account for the aether, a preferred frame for the propagation of light. However, vector-tensor theories suffer several serious defects [11]; consequently, to date nobody has computed their effect on gravitational waves.

It is possible to create a relativistic theory that reduces to MOND in the weak field by including a scalar gravitational field (tensor-vector-scalar theory, TeVeS). MOND [20] tries to account for a correct description of galaxy rotation curves (without resorting to dark matter) by introducing short-range corrections to gravitational fields. TeVeS is not considered here since MOND-like modifications to strong-field binary dynamics seem to be negligibly small [21].

Modified quadratic gravity / Chern-Simons theory

Instead of incorporating additional fields, one can also account for higher powers of the Riemann curvature. This will introduce effects that manifest in the untested strong-field regime of GR. The most general action for modified quadratic gravity reads [13, 22]

$$\begin{aligned} S = \int \Big[& \kappa R + \alpha_1 f_1(\vartheta) R^2 + \alpha_2 f_2(\vartheta) R_{\mu\nu} R^{\mu\nu} + \alpha_3 f_3(\vartheta) R_{\mu\nu\rho\sigma} R^{\mu\nu\rho\sigma} \\ & + \alpha_4 f_4(\vartheta) R_{\mu\nu\rho\sigma}\, {}^*R^{\mu\nu\rho\sigma} - \frac{\beta}{2} \left[\nabla_\mu \vartheta \nabla^\mu \vartheta + 2V(\vartheta) \right] \Big] \sqrt{-g}\, \mathrm{d}^4 x + S_M(\psi_M, g_{\mu\nu}), \end{aligned} \tag{2.37}$$

where α_i, β and $\kappa = 1/(16\pi G)$ are coupling constants, f_i are functionals on the same field ϑ (which is a restriction; in general the f_i could act on different fields) and ${}^*R^{\mu\nu\rho\sigma} = (1/2)\epsilon_{\rho\sigma}{}^{\alpha\beta} R^\mu{}_{\nu\alpha\beta}$ is the dual Riemann tensor. The term proportional to β represents a potential and a kinetic energy term in order to achieve minimal coupling. By choosing different values for the coupling constants, one can construct different theory subspaces, such as *Einstein-Dilaton-Gauss-Bonnet gravity* with $(\alpha_1, \alpha_2, \alpha_3, \alpha_4) = (1, -4, 1, 0)\, \alpha_{\mathrm{EDGB}}$ [23] or *dynamical Chern-Simons gravity* with $(\alpha_1, \alpha_2, \alpha_3, \alpha_4) = (0, 0, 0, -1/4)\, \alpha_{\mathrm{dCS}}$ [13, 24]. Both of these theories arise when considering the low-energy expansion of string theory; dynamical Chern-Simons gravity appears also when one considers loop quantum gravity [25, 26].

The effect of dynamical Chern-Simons gravity on gravitational-wave generation has recently been under deeper investigation [22]; to leading order, the GR waveform in the stationary phase approximation is modified to

$$\tilde{h}(f) = \tilde{h}_{\mathrm{GR}}(f)\, e^{-i\beta_{\mathrm{dCS}} u^{-1/3}}, \tag{2.38}$$

where

$$\beta_{\mathrm{dCS}} = \frac{1549225}{11812864} \frac{\zeta_4}{\eta^{14/5}}, \tag{2.39}$$

with the dynamical Chern-Simons coupling parameter $\zeta_4 = \alpha_4^2/(\beta\kappa M^4)$ and the total mass M. Through the R^*R term, dynamical Chern-Simons gravity leads to parity violation that can let the plus and the cross polarisation travel

at different speeds. It is important to emphasise that, in contrast to the two types of theories introduced before, modified quadratic gravity has no physical motivation, but rather aims to describe higher-order corrections that enter by an even more complicated underlying theory. Modified quadratic gravity should therefore be interpreted as an effective theory of a more fundamental theory that is truncated at quadratic order.

$f(R)$ theories

In $f(R)$ theories [27] the scalar curvature R in the Einstein-Hilbert action is replaced with a function of it:

$$S = \int f(R)\sqrt{-g}\,\mathrm{d}^4x + S_M(\psi_M, g_{\mu\nu}). \tag{2.40}$$

$f(R)$ theories are very popular in cosmology as they can be used to create models that explain inflation and late-time acceleration (dark energy) of the universe. It has to be emphasised here that $f(R)$ theories are rather mathematical toys instead of being physically motivated. Similar to modified quadratic gravity, they could be seen as effective theories. We will not delve further into classes of $f(R)$ theories as they are formally equivalent to a subclass of scalar-tensor theories, what can be shown by choosing the scalar field $\phi = \mathrm{d}f/\mathrm{d}R$ and the potential $V(\phi) = R\,\mathrm{d}f/\mathrm{d}R - f(R)$; it is then possible to map metric $f(R)$ theories to a Brans-Dicke theory with $\omega_{\mathrm{BD}} = 0$ and Palatini $f(R)$ theories to a Brans-Dicke theory with $\omega_{\mathrm{BD}} = -3/2$ [27]. We will investigate the question of GW polarization in those theories in Chapter 4.

Chapter 3

Detectors and Data Analysis

"Ladies and gentlemen, we have detected gravitational waves. We did it!"

David Reitze, *LIGO Press Conference, 11.02.2016*

In this chapter we review the tools that serve to analyze the data collected by gravitational-wave detectors and that can provide estimates of how accurately we will be able to measure the astrophysical parameters of compact binary inspirals. As GWs can be buried deep in noise, which is often considerably larger than the actual signal itself, the most suitable instrument to recover GWs from compact binaries is *matched filtering*. Matched filtering is the process of cross correlating the detector data with a set of signal templates. A template that matches (to some extent) a GW signal present in the data will lead to a signal-to-noise ratio that is above a certain detection threshold. Using matched filtering has the consequence that one has to know a priori what potential signals could be in the data and needs to have a bank of templates ready or generate them on the fly, what requires an immense amount of computation for compact binary model templates with 9-17 free parameters. It is therefore crucial that data analysis algorithms remain highly accurate, but are made the fastest possible. In the following we review the frequentist and the Bayesian approach to gravitational-wave astronomy that allow us both, albeit with different methods, to assess the parameter estimation capabilities of a LISA-like detector. As our interest lies mainly in how a LISA-like detector will perform in doing astronomy with GWs, we will use the notion 'gravitational-wave astronomy' here instead of the commonly used term 'data analysis'.

3.1 Detector response and antenna patterns

A single detector channel of a LISA-like detector will give us a one-dimensional output: an electric signal $h_{\rm out}(t)$, the so-called *response function*. The GWs that reach the detector, however, come as a metric perturbation tensor $h_{ij}^{\rm TT}(t)$. In the following, let us summarise how one can relate these two quantities.

The induced relative length change $h(t)$ of a detector arm can be computed by a projection of $h_{ij}^{\rm TT}(t)$ onto the detector arm which is essentially a function of source and detector orientation. In the so-called *low-frequency approximation* (LFA) [28, 29], this can be achieved with a linear combination of the waveform polarisations $h_{+,\times}$, weighted with the *antenna pattern functions* $F_k^{+,\times}$ (for detector channel k) that depend on the orientation of the source in the sky:

$$h_k(t;\mathbf{\Theta}) = h_+[\xi(t);\mathbf{\Theta}]\, F_k^+(t;\psi,\theta,\phi) + h_\times[\xi(t);\mathbf{\Theta}]\, F_k^\times(t;\psi,\theta,\phi), \tag{3.1}$$

with [28, 30]

$$F_k^+(t;\psi,\theta,\phi) = \frac{1}{2}\left[\cos(2\psi)\,D^+(t;\psi,\theta,\phi,\lambda_k) - \sin(2\psi)\,D^\times(t;\psi,\theta,\phi,\lambda_k)\right], \tag{3.2}$$

$$F_k^\times(t;\psi,\theta,\phi) = \frac{1}{2}\left[\sin(2\psi)\,D^+(t;\psi,\theta,\phi,\lambda_k) + \cos(2\psi)\,D^\times(t;\psi,\theta,\phi,\lambda_k)\right], \tag{3.3}$$

where $\lambda_1 = 0$ and $\lambda_2 = \pi/4$, and the detector motion is taken into account by

$$\begin{aligned} D^+(t;\psi,\theta,\phi,\lambda) = \frac{\sqrt{3}}{64}\big[&-36\sin^2(\theta)\sin(2\alpha(t)-2\lambda) + (3+\cos(2\theta)) \\ &\times(\cos(2\phi)\{9\sin(2\lambda) - \sin(4\alpha(t)-2\lambda)\} + \sin(2\phi)\{\cos(4\alpha(t)-2\lambda) - 9\cos(2\lambda)\}) \\ &-4\sqrt{3}\sin(2\theta)(\sin(3\alpha(t)-2\lambda-\phi) - 3\sin(\alpha(t)-2\lambda+\phi))\big], \\ D^\times(t;\psi,\theta,\phi,\lambda) = \frac{1}{16}\big[&\sqrt{3}\cos(\theta)(9\cos(2\lambda-2\phi) - \cos(4\alpha(t)-2\lambda-2\phi)) \\ &-6\sin\theta\,(\cos(3\alpha(t)-2\lambda-\phi) + 3\cos(\alpha(t)-2\lambda+\phi))\big]. \end{aligned} \tag{3.4}$$

For a detector with arm length L, the LFA is valid for GW frequencies below the so-called *transfer frequency* $f_* = c/(2\pi L)$. When generating waveforms, one has therefore to make sure that the GW frequency stays below f_*: depending on L, the LFA breaks down for binaries with total masses below $\sim 10^5 M_\odot$. In the static limit, i.e. when the motion the detector with respect to the source is neglected, the above equations reduce to

$$\begin{aligned} F_1^+(\theta,\phi,\psi) &= \frac{\sqrt{3}}{2}\left[\frac{1}{2}\left(1+\cos^2(\theta)\right)\cos(2\phi)\cos(2\psi) - \cos(\theta)\sin(2\phi)\sin(2\psi)\right], \\ F_1^\times(\theta,\phi,\psi) &= F_1^+\left(\theta,\phi,\psi-\frac{\pi}{4}\right), \\ F_2^+(\theta,\phi,\psi) &= F_1^+\left(\theta,\phi-\frac{\pi}{4},\psi\right), \\ F_2^\times(\theta,\phi,\psi) &= F_1^+\left(\theta,\phi-\frac{\pi}{4},\psi-\frac{\pi}{4}\right). \end{aligned} \tag{3.5}$$

The detector translates $h(t)$ to the response function $h_{\rm out}(t)$. Most definitely, the detector will not be equally sensitive to all frequencies and will obey a *transfer function* $T(f)$ with

$$\tilde{h}_{\rm out}(f) = T(f)\,\tilde{h}(f). \tag{3.6}$$

In GW astronomy, we assume that the effects of $T(f)$ have already been removed from the data by multiplying $\tilde{h}_{\rm out}(f)$ with $T^{-1}(f)$ [9].

3.2 Modelling detector noise

In an actual experimental detector setup, there will not only be the gravitational-wave signal present, but also a multitude of noise sources. If one does not treat noise thoroughly , it will be impossible to recover the desired signals. Therefore it is of crucial importance to characterise how detector noise affects GW astronomy. The actual signal in the detector will be the gravitational-wave strain $h(t)$ superposed with noise,

$$s(t) = h(t) + n(t), \tag{3.7}$$

where $n(t)$ is the noise stream. In GW astronomy, the noise is usually assumed to be *stationary* and *Gaussian*. We will follow this assumption but emphasise that in real detections, we should be ready to face the challenge of understanding non-stationary non-Gaussian noise. Since noise is a stochastic process, let us introduce the *ensemble*

average (or expectation value) $\langle..\rangle$ that averages its argument for multiple samples taken subsequently from the data stream. In the following, let us also assume that $\langle n(t)\rangle = 0$.

The behaviour of noise can be investigated through the autocorrelation function

$$R(\tau) = \langle n(t+\tau)\, n(t)\rangle, \tag{3.8}$$

which can be expressed through its Fourier transform $\tilde{R}(f)$ as $R(\tau) = \int_{-\infty}^{\infty} \mathrm{d}f\, \tilde{R}(f)\, e^{-2\pi i f\tau}$. Since

$$R(0) = \langle n^2(t)\rangle = \int_{-\infty}^{\infty} \mathrm{d}f\, \tilde{R}(f) = \int \mathrm{d}f \int \mathrm{d}f'\, \langle \tilde{n}^*(f)\, \tilde{n}(f')\rangle\, e^{2\pi i(f-f')t}, \tag{3.9}$$

$\tilde{R}(f)$ can be identified with the power spectral density of the noise. In the following we use the *one-sided power spectral density* $S_n(f) = \frac{1}{2}\tilde{R}(f)$, such that $\langle n^2(t)\rangle = \int_0^{\infty} \mathrm{d}f\, S_n(f)$. Moreover, we are able to identify

$$\langle \tilde{n}^*(f)\, \tilde{n}(f')\rangle = \delta(f-f')\, \frac{1}{2} S_n(f). \tag{3.10}$$

It is crucial to know the exact form of the power spectral density $S_n(f)$ of the noise appearing in a LISA-like detector. For such a detector, there are two main types of noise:

- *Instrumental noise* is an umbrella term for all the noise sources in the detector, such as laser shot noise and uncertainties in the position and acceleration of the spacecraft.
- Since a LISA-like detector will only detect a certain number of sources that are significantly stronger than the general background, sources that are below the detection threshold blend in with the background and form a noise floor of unresolvable sources, so called *confusion noise*.

The resulting power spectral density will be the sum of the spectral densities of these two individual noise sources,

$$S_n(f) = S_n^{\mathrm{instr}}(f) + S_n^{\mathrm{conf}}(f). \tag{3.11}$$

3.3 Matched filtering

As introduced before, matched filtering is the cross correlation of a signal $s(t) = h(t) + n(t)$ in the detector with a filter $f(t)$:

$$o(\tau) = \int_{-\infty}^{\infty} s(t) f(t-\tau)\, \mathrm{d}t, \tag{3.12}$$

where $n(t)$ is the noise stream, $o(\tau)$ denotes the overlap for a filter that is shifted by τ and $h(t)$ is the GW signal. For conciseness, let us assume that the integral boundaries are always between $-\infty$ and ∞ in the following. The best match for the filter $f(t)$ is where $o(\tau)$ has its maximum. Let us assume that this maximum has been found at $\tau = \tau_0$ and let then $F(t) \equiv f(t-\tau_0)$ such that

$$o = \int s(t) F(t)\, \mathrm{d}t. \tag{3.13}$$

Given a signal $s(t)$ and a template $h(t)$, how can we know if the filter has found something? To this end, let us define the *signal-to-noise ratio* (SNR) under the action of the filter $F(t)$. For the nominator (signal) which we denote as S, let us take the average over many realisations of o when a signal is present:

$$\begin{aligned} S = \langle o\rangle &= \int \mathrm{d}t\, \langle s(t)\rangle F(t) \overset{\langle n(t)\rangle = 0}{=} \int \mathrm{d}t\, h(t) F(t) = \int \mathrm{d}t \int \mathrm{d}f \int \mathrm{d}f'\, e^{2\pi i(f-f')t}\, \tilde{h}(f)\, \tilde{F}^*(f') \\ &= \int \mathrm{d}f \int \mathrm{d}f'\, \delta(f-f')\, \tilde{h}(f)\, \tilde{F}^*(f') = \int \mathrm{d}f\, \tilde{h}(f)\, \tilde{F}^*(f), \end{aligned} \tag{3.14}$$

where we chose to work in frequency space and have used $F(t) = F^*(t)$. Note that since $h(t)$ is deterministic and has only one realisation, $\langle h(t)\rangle = h(t)$. Since $\langle n(t)\rangle = 0$, let us compute the denominator N through the variance of o in the absence of a gravitational-wave signal:

$$\begin{aligned} N^2 = \left[\langle o^2\rangle - \langle o\rangle^2\right]_{h=0} &= \int \mathrm{d}t \int \mathrm{d}t' \, \langle n(t)\, n(t')\rangle \, F(t)\, F(t') \\ &= \int \mathrm{d}t \int \mathrm{d}t' \int \mathrm{d}f \int \mathrm{d}f' \, e^{2\pi f t} \, e^{-2\pi f' t'} \, \langle \tilde{n}^*(f)\, \tilde{n}(f')\rangle \, F(t)\, F(t') \\ &= \int \mathrm{d}f \, S_n(f)\, |\tilde{F}(t)|^2, \end{aligned} \tag{3.15}$$

where (3.10) has been used. In order to write the SNR in a well-arranged way, let us introduce the inner product of two functions $g(t)$ and $h(t)$ as

$$(g|h) \equiv 2 \int_0^\infty \frac{\tilde{g}^*(f)\tilde{h}(f) + \tilde{g}(f)\tilde{h}^*(f)}{S_n(f)} \, \mathrm{d}f = 4 \, \mathrm{Re} \int_0^\infty \frac{\tilde{g}^*(f)\tilde{h}(f)}{S_n(f)} \, \mathrm{d}f, \tag{3.16}$$

where $S_n(f)$ in the denominator makes sure that contributions from frequencies where the detector noise level is higher are counted less. Using the definition $\tilde{k}(f) = S_n(f)\,\tilde{F}(f)$ allows us to write the SNR as

$$\rho = \frac{S}{N} = \frac{(h|k)}{\sqrt{(k|k)}}. \tag{3.17}$$

The quantity ρ is maximised if $k \propto h$, what leads us to the *optimal filter* $\tilde{F}(f) = \frac{\tilde{h}(f)}{S_n(f)}$. Plugging this into Eq. (3.17), one gets the optimal SNR of a single detector channel,

$$\rho_{\mathrm{opt}} = \sqrt{(h|h)}, \tag{3.18}$$

that can be achieved given that the parameter set $\boldsymbol{\Theta}$ of the template h is perfectly known. To compute the SNR of arbitrary data $d(t)$, one can evaluate

$$\rho = \frac{(d|h)}{\sqrt{(h|h)}} = \rho_{\mathrm{opt}} + \frac{(n|h)}{\sqrt{(h|h)}}. \tag{3.19}$$

Because of the presence of noise, $\rho(\boldsymbol{\Theta})$ will be maximised for a different parameter set $\boldsymbol{\Theta}$ than $\rho_{\mathrm{opt}}(\boldsymbol{\Theta})$, depending on the strength of the noise. More in-depth discussions on matched filtering can be found in [9] and [31]. Matched filtering is the basic tool used by the parameter estimation methods introduced in the following sections.

3.4 Frequentist statistics and likelihood maximisation

The frequentist approach to statistics regards probability as a long-run occurrence frequency. Through the conduction of a set of experiments, multiple random samples can be taken from the underlying probability distribution. If the underlying probability distribution depends on a set of parameters, then these parameters are considered to be fixed quantities that remain constant during the experiments. It is simply because we can only sample noisy instances of the truth that the true parameters remain hidden from our eyes. However, a large number of experiments will remove this noise and allow us to estimate the underlying parameters.

As in a gravitational-wave experiment we do not possess the power to set the binary black holes back to their initial position after they have merged, it is impossible to conduct the same experiment with similar initial conditions even twice. This renders the frequentist approach questionable and in general one should prefer a Bayesian approach as introduced in the next section. However, one can draw estimates for the true underlying parameter set $\boldsymbol{\Theta}_t$ through maximisationof a so-called *likelihood function*.

Assuming Gaussian detector noise, the probability for a particular noise realisation n_0 to appear in the detector is given by $p(n_0)$, where $p(n)$ is defined through the Gaussian distribution

$$p(n) = C \exp\left[-\frac{1}{2}(n|n)\right], \tag{3.20}$$

where C is a normalisation constant. Since $n = d - h$, it is possible to express the probability distribution for the data $d(t)$ to appear in the detector given the GW signal $h(t;\boldsymbol{\Theta})$ as

$$p(d|\boldsymbol{\Theta}) = C \exp\left[-\frac{1}{2}(d-h(\boldsymbol{\Theta})|d-h(\boldsymbol{\Theta}))\right]. \tag{3.21}$$

The parameter estimation methods that are introduced in this work (e.g. maximum likelihood) do not require the knowledge of the normalisation constant; this is a very useful property, as it is in general very difficult to compute.

One can define the *reduced log-likelihood* (reduced because the normalisation constant in (3.21) is dropped)

$$L(\boldsymbol{\Theta}) = -\frac{1}{2}(d-h(\boldsymbol{\Theta})|d-h(\boldsymbol{\Theta})). \tag{3.22}$$

The *maximum likelihood* method [9, 31, 32] provides us with an estimator $\hat{\boldsymbol{\Theta}}_{\mathrm{ML}}$ for the true underlying parameter set $\boldsymbol{\Theta}_t$ that can be found through

$$\left.\frac{\partial L(\boldsymbol{\Theta})}{\partial \Theta^i}\right|_{\boldsymbol{\Theta}=\hat{\boldsymbol{\Theta}}_{\mathrm{ML}}} = 0. \tag{3.23}$$

As $(d|d)$ is independent of $\boldsymbol{\Theta}$, an alternative definition of the log-likelihood that simplifies the computation of $\hat{\boldsymbol{\Theta}}_{\mathrm{ML}}$ is $\tilde{L}(\boldsymbol{\Theta}) = (d|h) - \frac{1}{2}(h|h)$. The (time-averaged) expectation value of $\tilde{L}$ can then also be expressed in terms of the signal-to-noise ratio (3.18) as $\langle\tilde{L}(\boldsymbol{\Theta})\rangle = \frac{1}{2}\rho^2$. Given a certain value of the log-likelihood, the SNR can thus easily be recovered with $\rho = \sqrt{2\langle\tilde{L}(\boldsymbol{\Theta})\rangle}$.

Due to the presence of noise in the data, $\hat{\boldsymbol{\Theta}}_{\mathrm{ML}}$ will in general be different from $\boldsymbol{\Theta}_t$ and show errors of $\Delta\Theta^i = \Theta^i_{\mathrm{ML}} - \Theta^i_t$. In the limit of high SNR, however, we expect that $\Delta\Theta^i \ll 1$. This allows us to expand the waveform template to quadratic order as

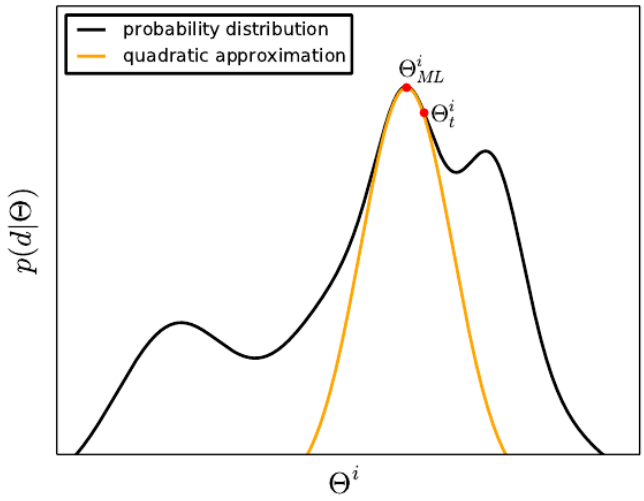

Figure 3.1: *The Fisher information matrix is a quadratic approximation of the likelihood function $p(d|\boldsymbol{\Theta})$ in the limit of a small difference between the maximum likelihood estimate $\boldsymbol{\Theta}_{ML}$ and the true underlying binary parameters $\boldsymbol{\Theta}_t$. Picture reproduced from [33].*

$$h(\hat{\boldsymbol{\Theta}}_{\rm ML}) \approx h(\boldsymbol{\Theta}_t) + \left.\frac{\partial h}{\partial \Theta^k}\right|_{\boldsymbol{\Theta}=\boldsymbol{\Theta}_t} \Delta\Theta^k + \frac{1}{2}\left.\frac{\partial^2 h}{\partial\Theta^k\partial\Theta^l}\right|_{\boldsymbol{\Theta}=\boldsymbol{\Theta}_t} \Delta\Theta^k\Delta\Theta^l, \tag{3.24}$$

and hence the reduced log-likelihood can be expressed as

$$L(\hat{\boldsymbol{\Theta}}_{\rm ML}) \approx -\frac{1}{2}\left[(n|n) - 2\Delta\Theta^k(n|h_k) - \Delta\Theta^k\Delta\Theta^l(n|h_{kl}) + \Delta\Theta^k\Delta\Theta^l(h_k|h_l)\right], \tag{3.25}$$

where $n = d - h(\boldsymbol{\Theta}_t)$ and the definitions $h_k = \left.\frac{\partial h}{\partial\Theta^k}\right|_{\boldsymbol{\Theta}=\boldsymbol{\Theta}_t}$ and $h_{kl} = \left.\frac{\partial^2 h}{\partial\Theta^k\partial\Theta^l}\right|_{\boldsymbol{\Theta}=\boldsymbol{\Theta}_t}$ have been used. In order to get a clearer understanding of how the SNR enters the calculations, let us define $h(\boldsymbol{\Theta}) = \rho\,\bar{h}(\boldsymbol{\Theta})$ with the optimal SNR $\rho = \sqrt{(h(\boldsymbol{\Theta}_t)|h(\boldsymbol{\Theta}_t))}$. Eq. (3.23) can then be expressed to first order in $\Delta\boldsymbol{\Theta}$ as [32]

$$\Delta\Theta^k(\bar{h}_k|\bar{h}_l) - \frac{1}{\rho}\left[(n|\bar{h}_l) + 2\Delta\Theta^k(n|\bar{h}_{kl})\right] = 0. \tag{3.26}$$

In the limit of large SNR, we expect the first term in the square brackets in Eq. (3.26) to dominate over the second one, leaving us with the error on the maximum likelihood estimator in the *linearized signal approximation*,

$$\Delta\Theta^k = \frac{1}{\rho}(\bar{h}_k|\bar{h}_l)^{-1}(n|\bar{h}_l). \tag{3.27}$$

The corresponding covariance matrix is then

$$\Sigma_{ij} = \langle\Delta\Theta^i\Delta\Theta^j\rangle = \frac{1}{\rho^2}(\bar{h}_i|\bar{h}_k)^{-1}\langle(n|\bar{h}_k)(n|\bar{h}_l)\rangle(\bar{h}_j|\bar{h}_l)^{-1} = \frac{1}{\rho^2}(\bar{h}_i|\bar{h}_j)^{-1} = \Gamma_{ij}^{-1}, \tag{3.28}$$

where it has been used that $\langle(g|n)(n|h)\rangle = (g|h)$ and

$$\Gamma_{ij} = \left(\frac{\partial h}{\partial\Theta^i}\middle|\frac{\partial h}{\partial\Theta^j}\right) \tag{3.29}$$

is the so called *Fisher information matrix* (FIM). In the limit of large SNR, the 1σ errors and the correlations among the parameters can therefore be estimated as

$$\Delta\Theta_i = \sqrt{\Gamma_{ii}^{-1}}, \quad C_{ij} = \frac{\Gamma_{ij}^{-1}}{\sqrt{\Gamma_{ii}^{-1}\Gamma_{jj}^{-1}}}, \tag{3.30}$$

respectively, with $C_{ij} \in [-1,1]$. This goes together with a Gaussian approximation of the likelihood surface, as $L(\hat{\boldsymbol{\Theta}}_{\rm ML})$ is in the approximation considered above

$$\begin{aligned} L(\hat{\boldsymbol{\Theta}}_{\rm ML}) &\approx L(\boldsymbol{\Theta}_t) + \left.\frac{\partial L}{\partial\Theta^i}\right|_{\boldsymbol{\Theta}=\boldsymbol{\Theta}_t}\Delta\Theta^i + \frac{1}{2}\left.\frac{\partial^2 L}{\partial\Theta^i\partial\Theta^j}\right|_{\boldsymbol{\Theta}=\boldsymbol{\Theta}_t}\Delta\Theta^i\Delta\Theta^j \\ &\approx L(\boldsymbol{\Theta}_t) + \rho\,(n|\bar{h}_i)\,\Delta\Theta^i - \frac{1}{2}\rho^2(\bar{h}_i|\bar{h}_j)\,\Delta\Theta^i\Delta\Theta^j, \end{aligned} \tag{3.31}$$

what corresponds to

$$p(\Delta\boldsymbol{\Theta}) \propto \exp\left[-\frac{1}{2}\Gamma_{ij}\,\Delta\Theta^i\Delta\Theta^j\right]. \tag{3.32}$$

In the case of multiple detector channels, the resulting Fisher matrix is the sum of the ones for the individual detectors, $\Gamma_{ij} = \sum_k \Gamma_{ij}^{(k)}$.

The FIM is widely used in parameter estimation studies to assess the measurement accuracy of GW detectors. As it requires only the derivatives of the considered waveform model and no realistic simulation of noise, it can be

computed very cheaply. However, the FIM suffers a couple of issues that should be handled with caution: For many considered sources, the limit of large SNR is not fulfilled. It is also quite unclear how large the SNR will have to be such that the assumption $\Delta\Theta^i \ll 1$ is justified. If the limit of large SNR is not reached, then the FIM might be a bad approximation of the covariance matrix. Consequently, errors found in parameter estimation studies may be under- or overestimated. Moreover, by apparent degeneracies in the parameter space of gravitational waves generated by black hole binaries, the FIM can often be ill-conditioned, making it very difficult to invert it numerically and harbouring potential errors [32]. Rodriguez et al. [34] found in the context of ground-based detectors that the FIM can greatly overestimate the errors (up to three orders of magnitude), even for considerably high SNR, leading to an underestimation of the science capabilities of GW detectors. Cornish and Porter [35] found that, for a classic LISA detector, the FIM overestimates the errors even for sources with an SNR as high as 450 by about a factor of two. They put this effect down to the fact that the FIM is unable to cope with the high correlations among the parameters.

It has to be emphasised again that the FIM is a frequentist tool, i.e. it considers the true underlying parameter set $\boldsymbol{\Theta}_t$ as fixed and treats the data as a random process. The FIM is not able to take prior information on the parameter set into account and provides no notion of how likely it is that a certain parameter set $\boldsymbol{\Theta}$ describes the measured data best; for such statements one has to resort to Bayesian techniques.

3.5 The Bayesian approach to parameter estimation

As mentioned before, frequentist statistics may not be the optimal tool for GW astronomy, as here we deal with single experiments that are non-repeatable and we may have prior information on the probability distribution at hand from previous astrophysical observations. In real life, we will ask ourselves how likely it is that a particular parameter set is the true one in the light of the detector data d. Frequentist statistics is by design not able to answer such questions.

The heart of Bayesian statistics is *Bayes' theorem*:

$$p(A|B) = \frac{p(B|A)\,p(A)}{p(B)}, \tag{3.33}$$

where A, B are two events and $p(A|B)$ is the conditional probability for A to take place given that B has already occurred. Taking for A the hypothesis that the set $\boldsymbol{\Theta}$ describes the parameters of the source best and for B the event that the particular data set d appears in the detector, we can write in terms of Bayes' theorem:

$$p(\boldsymbol{\Theta}|d) = \frac{p(d|\boldsymbol{\Theta})\,p(\boldsymbol{\Theta})}{p(d)}. \tag{3.34}$$

Here, $p(\boldsymbol{\Theta})$ is the *prior probability* for $\boldsymbol{\Theta}$ to be the true parameter set, i.e. what is known about $\boldsymbol{\Theta}$ before the experiment. In GW astronomy, these could e.g. be priors on the mass or distance distribution of black holes through astronomical observations. $p(d|\boldsymbol{\Theta})$ is the *likelihood* introduced in Eq. (3.21) and the quantity $p(d) = \int \mathrm{d}\boldsymbol{\Theta}\, p(d|\boldsymbol{\Theta})$ is the so-called *evidence*, marginalised over all possible values of $\boldsymbol{\Theta}$. As before, $p(d)$ is just a normalisation constant that is not important for the tools we are going to use. The resulting distribution $p(\boldsymbol{\Theta}|d)$ is the *posterior probability* after considering the prior and the likelihood. $p(\boldsymbol{\Theta}|d)$ can be understood as the probability that $\boldsymbol{\Theta}$ gives the correct description of the measured data. In Bayesian statistics, the notion of probability is not that of an observed frequency but rather that of the possibility that an event is going to take place given also subjective expectations. In subsequent measurements, what has been the posterior before is promoted to the prior and a new posterior is gained with the new data.

Once the likelihood and the prior are defined, the posterior distribution can be explored with methods such as Markov Chain Monte Carlo. This is not an easy task, since $\boldsymbol{\Theta}$ can have from 9 to 17 dimensions in GR. In Bayesian statistics, one trades the intuitive notion of probability that is much closer to the human perception of reality for the fact that posterior probabilities are very expensive to compute.

To summarise, Bayesian statistics views the data as fixed and the underlying parameters as variable while frequentist statistics assumes that the underlying parameters are fixed and various experiments with a random component can be conducted. As Bayesian statistics requires a prior that shows the subjective expectation of an individual, different priors will lead to different posteriors. Hence it would be useful to check the robustness of acquired results by imposing different priors. It has to be emphasised that also a flat prior is a subjective prior.

The Bayesian viewpoint is more natural and intuitive than the frequentist viewpoint for GW astronomy. Yet it has been only recently that people started to incorporate Bayesian tools such as Markov Chain Monte Carlo algorithms, as we are just entering an era where computers and algorithms are getting fast enough to allow us to compute the desired probabilities in a reasonable time frame.

3.6 Bayesian inference for tests of GR

In Chapter 2.3 we introduced different alternatives to GR that are to date not ruled out using pulsar and solar system tests. Given some detector data d, how can we know if GR is the true underlying theory? Might it be that an alternative to it, giving rise to a modified waveform model, provides a better answer? In other words: What theory fits the data best while keeping the number of possible parameters to a minimum? A good answer to this problem can be provided by Bayesian inference. Although the methods mentioned in this section have not been used in the studies conducted for this thesis, for future reference, let us give a brief review of how one can test hypotheses with Bayesian inference, with emphasis on alternative theories. More in-depth reviews can be found in [36–38].

Let us consider two different hypotheses in the following:

- $\mathscr{H}_{\rm GR}$: GR is the true underlying theory and the GW signal is described with the waveform model $h_{\rm GR}(\boldsymbol{\Theta})$.
- $\mathscr{H}_{\rm NGR}$: Any parametrised deviation from GR is a better fundamental theory of gravity, implying a modified waveform model $h_{\rm NGR}(\boldsymbol{\Theta}, \boldsymbol{\lambda})$, where $\boldsymbol{\lambda}$ is a set of additional theory parameters.

In the remainder of this section, for simplicity, we will always use the vector $\boldsymbol{\Theta}$ for the parameter set of the waveform model, regardless whether $\boldsymbol{\Theta}$ consists just of binary system parameters (GR) or contains also additional theory parameters that allow for non-GR (NGR) theories.

Let us come back to the central question of this section: Given some detector data d, which of the above hypotheses is in favour and describes the detector data d better?

As in Section 3.5 we start with Bayes' theorem:

$$p(\mathscr{H}_i|d) = \frac{p(d|\mathscr{H}_i)\,p(\mathscr{H}_i)}{p(d)}. \tag{3.35}$$

Here, the posterior $p(\mathscr{H}_i|d)$, the probability that $\mathscr{H}_i$ is the true hypothesis describing the data, can be computed through the evaluation of the likelihood $p(d|\mathscr{H}_i)$, the prior $p(\mathscr{H}_i)$ that can be placed on the hypothesis and the evidence $p(d) = \sum_i p(d|\mathscr{H}_i)\,p(\mathscr{H}_i)$ that takes again the role of a normalisation constant. The likelihood is marginalised over the binary and theory parameters:

$$p(d|\mathscr{H}_i) = \int \mathrm{d}\boldsymbol{\Theta}\, p(d|\boldsymbol{\Theta}, \mathscr{H}_i)\, p(\boldsymbol{\Theta}|\mathscr{H}_i), \tag{3.36}$$

where $p(\boldsymbol{\Theta}|\mathscr{H}_i)$ are the priors that can be placed on the parameters in the specific case of where hypothesis $\mathscr{H}_i$ is assumed to be true. $p(d|\boldsymbol{\Theta}, \mathscr{H}_i)$ is the likelihood function discussed in Section 3.5 with a waveform model that assumes this particular hypothesis. If one aims to find the parameter set $\boldsymbol{\Theta}$ that describes the detector data best assuming that hypothesis $\mathscr{H}_i$ is true, it is straightforward to generalise Eq. (3.34) to

$$p(\boldsymbol{\Theta}|d, \mathscr{H}_i) = \frac{p(\boldsymbol{\Theta}|\mathscr{H}_i)\,p(d|\boldsymbol{\Theta}, \mathscr{H}_i)}{p(d|\mathscr{H}_i)}. \tag{3.37}$$

Once the waveform models are established for the different hypotheses, all the necessary quantities needed for Equation (3.35) are available. In practice, however, in order to compute the evidence $p(d)$, we would need to sum over all possible hypotheses (or theories); this is unfeasible because of the lack of our knowledge of all possible models. Yet we can compare different hypotheses and choose which one we are going to favour in the light of the measured data. A tool for such a comparison is the *odds ratio*

$$\mathscr{O}^{\rm NGR}_{\rm GR} = \frac{p(\mathscr{H}_{\rm NGR}|d)}{p(\mathscr{H}_{\rm GR}|d)} = \frac{p(\mathscr{H}_{\rm NGR})}{p(\mathscr{H}_{\rm GR})}\,\frac{p(d|\mathscr{H}_{\rm NGR})}{p(d|\mathscr{H}_{\rm GR})}, \tag{3.38}$$

which compares relative probabilities and represents the 'betting odds' for a certain hypothesis. The odds ratio has the advantage that the evidence $p(d)$ cancels out. More commonly, assuming flat prior odds, people use the *Bayes factor*

$$\mathrm{BF} = \frac{p(d|\mathscr{H}_{\rm NGR})}{p(d|\mathscr{H}_{\rm GR})}. \tag{3.39}$$

Large Bayes factors would thus imply a clear tendency towards an alternative theory describing the data much better than GR.

Chapter 4

Gravitational Wave Polarization Modes in $f(R)$ theories

R. Kausar, L. Philippoz, P. Jetzer

Published in Physical Review D, Volume **93***, 124071 (2016)*

Abstract

Many studies have been carried out in the literature to evaluate the number of polarization modes of gravitational waves in modified theories, in particular in $f(R)$ theories. In the latter ones, besides the usual two transverse-traceless tensor modes present in general relativity, there are two additional scalar ones: a massive longitudinal mode and a massless transverse mode (the so-called breathing mode). This last mode has often been overlooked in the literature, due to the assumption that the application of the Lorenz gauge implies transverse-traceless wave solutions. We however show that this is in general not possible and, in particular, that the traceless condition cannot be imposed due to the fact that we no longer have a Minkowski background metric. Our findings are in agreement with the results found using the Newman-Penrose formalism, and thus clarify the inconsistencies found so far in the literature.

4.1 Introduction

The questions about the concepts of dark matter and dark energy motivated the development of new gravity theories. Most of them are direct modifications of general relativity (GR), such as $f(R)$ theories where, in contrast to GR, the Einstein-Hilbert Lagrangian density is replaced by a nonlinear function $f(R)$. The nonlinearities lead to different sets of field equations according to the different variational approaches for the action [39].

The first variational approach is known as the metric formalism, where fourth-order field equations are derived by varying the action with respect to the metric tensor $g_{\mu\nu}$. In this case, connections are metric dependent and hence every field in the gravitational sector is coming from the metric tensor. The second type of variational approach leads to the Palatini formalism where the metric and the connections are assumed to be independent fields, and the action is this time varied with respect to both of them. The field equations remain of second order as is the case of the Einstein field equations. A third type is the metric-affine variational approach, which comes if one uses the Palatini variation but also includes torsion by assuming nonmetricity of the connections. This last approach is the most general case of $f(R)$ gravity.

The scalar-tensor theories proposed by Brans and Dicke [40] with the aim of making the theory of gravity compatible with Mach's principle can have a dynamical equivalence to $f(R)$ gravity, the metric formalism of $f(R)$ corresponding to the specific case $\omega_{\mathrm{BD}} = 0$ and the Palatini one to $\omega_{\mathrm{BD}} = -3/2$ (see e.g. [39] or [27]). Scalar-tensor theories are also of great interest since a coupling between a scalar field and gravity seems to be a generic outcome of the low-energy limit of string theories [41]. Another interest in the scalar-tensor models lies in the fact that the $f(R)$ theories can be written as the Einstein equations plus a scalar field, and thus we could in principle extend the same formalism applied for the scalar-tensor theories to the $f(R)$ field equations [42].

The recent detection of gravitational waves (GWs) by the LIGO Collaboration [43] is a milestone in GWs research and opens new perspectives in the study of general relativity and astrophysics. Moreover, future space-borne detectors will offer access to an unprecedented signal sensitivity [44]. It is thus worthwhile to explore GWs in alternative theories of gravity, especially in $f(R)$ and scalar-tensor theories. The observation of the polarization modes of GWs will be a key tool to obtain valuable information about the astronomical objects and physics of the early Universe; depending if additional polarizations are found or not in a detected signal, our knowledge of gravitation could have to be extended beyond GR, but we could in any case exclude some theoretical models according to which modes are actually detected. Note that even if the recent detection allows one to put contraints on the Compton wavelength of a massive graviton, it cannot exclude the existence of non-GR polarization yet, but this will be possible in the future using a network of detectors with different orientations [45].

Usually, the general procedure to evaluate the power spectrum of the cosmological GWs is to consider the linearized theory by making small metric perturbations around the Minkowski metric (e.g. [9]). The basic idea is to analyze all the physically relevant components of the Riemann tensor $R_{\lambda\mu\nu\rho}$, which cause relative acceleration between test particles. In linearized theory, the Riemann tensor can be split into six algebraically independent components. Assuming that GWs are propagating in the z direction, the six components can be classified into six polarizations modes, namely $+$, $\times$, b, l, x, and y denoting plus, cross, breathing, longitudinal, vector-x, and vector-y modes, respectively. According to the rotation symmetry around the propagation axis of the GWs, the $+$ and $\times$ modes can be identified with the tensor-type (spin 2) GWs, the x and y modes are vector-type (spin 1) GWs, and the b and l modes are scalar-type (spin 0) GWs.

In GR, the GWs present only two polarization states, the $+$ and $\times$ modes. However, when the framework of an alternative theory of gravity is considered, the number of non-null components of the Riemann tensor and hence of polarization modes can be greater than two. This is a direct consequence of the new field equations which can lead to the existence of additional radiative modes. Using a linearized approach, several studies investigated the additional polarization modes in all versions of $f(R)$ theories ([46–51], or more recently [52]) and scalar-tensor theories [53], and it has been shown that only one massive longitudinal mode exists along with the two usual tensorial modes of GR. In addition to the linearized approach, another powerful tool to study the properties of GWs in any metric theory is the Newman-Penrose (NP) approach developed by Eardley *et al.* [54, 55]. In their work, they used a null-tetrad basis in order to calculate the NP [56] quantities in terms of the irreducible parts of $R_{\lambda\mu\nu\rho}$, namely, the Weyl tensor, the traceless Ricci tensor and the Ricci scalar. They showed that six possible modes of GWs polarization can be represented by these non-null NP quantities. Applying this technique, Alves, Miranda and de Araujo [56, 57] found that scalar-tensor and $f(R)$ theories have, with respect to GR, two additional modes: a longitudinal and a breathing mode. Therefore, there seems to be a disagreement between the linearized and the NP approaches.

Adopting the linearized approach, we explore extra polarization modes of GWs in modified $f(R)$ theories. The outline of the paper is as follows: in Sec. 4.2, we consider the $f(R)$ model with a quadratic term and linearize the field equation for this model in the metric formalism. The solutions of GWs arising in this theory are found explicitly and we present how two more polarization modes appear in addition to the usual two coming from GR. In Sec. 4.3, we consider the Palatini formalism for $f(R)$ theories. A summary of our results is given in Sec. 4.4. In the Appendix, we briefly overview the NP formalism to show the consistency of our results.

4.2 Polarization Modes in Metric $f(R)$ Theory

In this section we closely follow the approach discussed in Ref. [58] and rederive the main results leading to the wave equations for GWs. In a generic $f(R)$ theory, the corresponding action with a generalized function of the Ricci scalar R can be written as

$$S = \frac{1}{2\kappa}\int d^4x\sqrt{-g}f(R), \tag{4.1}$$

where κ is the coupling constant and g is the determinant of the metric tensor. Varying this action with respect to $g_{\mu\nu}$ yields the following set of vacuum field equations for $f(R)$ gravity:

$$f'(R)R_{\mu\nu} - \frac{1}{2}f(R)g_{\mu\nu} - \nabla_\mu\nabla_\nu f'(R) + g_{\mu\nu}\Box f'(R) = 0, \tag{4.2}$$

where $\mu,\nu = 0,1,2,3$ and $\Box = \nabla^\mu\nabla_\mu$ with ∇_μ being the covariant derivative for $g_{\mu\nu}$. Taking the trace of the field equations, we get

$$f'(R)R + 3\Box f'(R) - 2f(R) = 0. \tag{4.3}$$

To study gravitational waves, we use the linearized framework as in GR. Considering the perturbation of the metric from flat Minkowski space such that

$$g_{\mu\nu} = \eta_{\mu\nu} + h_{\mu\nu}, \tag{4.4}$$
$$R = R^{(0)} + R^{(1)}, \tag{4.5}$$

with $R^{(0)} = 0$. The first-order Ricci tensor and Ricci scalar are given, respectively, by

$$R^{(1)}_{\mu\nu} = \frac{1}{2}(\partial_\mu\partial_\rho h^\rho_\nu + \partial_\nu\partial_\rho h^\rho_\mu - \partial_\mu\partial_\nu h - \Box h_{\mu\nu}), \tag{4.6}$$
$$R^{(1)} = \partial_\mu\partial_\rho h^{\rho\mu} - \Box h. \tag{4.7}$$

We first discuss the case where $f(R)$ is a polynomial and then the other cases.

Polynomial $f(R)$ Models

We shall first consider polynomial $f(R)$ models of the form

$$f(R) = R + \alpha R^2 + \beta R^3 + \dots . \tag{4.8}$$

For such cases up to first order in $R^{(1)}$, only terms up to R^2 contribute to the field equations (4.2) for which we get

$$R^{(1)}_{\mu\nu} - \frac{1}{2}R^{(1)}\eta_{\mu\nu} - 2\alpha\partial_\mu\partial_\nu R^{(1)} + 2\alpha\eta_{\mu\nu}\Box R^{(1)} = 0. \tag{4.9}$$

The trace equation can be written in the form of a Klein-Gordon equation:

$$\Box R^{(1)} + m^2 R^{(1)} = 0, \tag{4.10}$$

where $m^2 = -\frac{1}{6\alpha}$. Physically meaningful solutions require $m^2 > 0$ and thus negative values for α.

In GR, the linearized Einstein field equations can be reduced to the simple wave equation

$$\Box\bar{h}_{\mu\nu} = -\frac{16\pi G}{c^4}T_{\mu\nu} \tag{4.11}$$

if one defines the trace-reversed perturbation

$$\bar{h}_{\mu\nu} = h_{\mu\nu} - \frac{h}{2}\eta_{\mu\nu} \tag{4.12}$$

or equivalently

$$h_{\mu\nu} = \bar{h}_{\mu\nu} - \frac{\bar{h}}{2}\eta_{\mu\nu} \tag{4.13}$$

and then imposes the Lorenz gauge for $\bar{h}_{\mu\nu}$ [9, 59]:

$$\nabla^{\mu}\bar{h}_{\mu\nu} = 0. \tag{4.14}$$

We now want to apply this similar standard reasoning within the $f(R)$ framework and find a quantity $\bar{h}_{\mu\nu}$ that satisfies a wave equation when linearizing the field equations (4.2). It has been shown [58] that the appropriate transformation is given by

$$h_{\mu\nu} = \bar{h}_{\mu\nu} - \frac{\bar{h}}{2}\eta_{\mu\nu} - 2\alpha R^{(1)}\eta_{\mu\nu}. \tag{4.15}$$

By taking the trace, we get

$$h = -\bar{h} - 8\alpha R^{(1)}. \tag{4.16}$$

We then impose the Lorenz gauge (4.14), and after inserting equations (4.14) and (4.15) into (4.6) for the Ricci tensor, we obtain instead

$$R^{(1)}_{\mu\nu} = \frac{1}{2}\left[4\alpha\partial_{\mu}\partial_{\nu}R^{(1)} - \Box(\bar{h}_{\mu\nu} - \frac{\bar{h}}{2}\eta_{\mu\nu}) + 2\alpha\eta_{\mu\nu}\Box R^{(1)}\right]. \tag{4.17}$$

Substituting it into Eq. (4.9), we find

$$-\frac{1}{2}\Box\bar{h}_{\mu\nu} + \frac{1}{4}\eta_{\mu\nu}\Box\bar{h} + 3\alpha\eta_{\mu\nu}\Box R^{(1)} - \frac{1}{2}\eta_{\mu\nu}R^{(1)} = 0. \tag{4.18}$$

Using Eq. (4.15) and the Lorenz gauge given by Eq. (4.14), Eq. (4.7) becomes

$$R^{(1)} = 6\alpha\Box R^{(1)} + \frac{1}{2}\Box\bar{h} \tag{4.19}$$

or

$$\Box R^{(1)} + m^2 R^{(1)} = \frac{1}{2}m^2\Box\bar{h}. \tag{4.20}$$

Comparing this equation with Eq. (4.10) it follows that $\Box\bar{h} = 0$ has to be fulfilled as well. Inserting $\Box\bar{h}$ as from Eq. (4.20) into Eq. (4.18) we finally get

$$\frac{1}{2}\Box\bar{h}_{\mu\nu} = 0. \tag{4.21}$$

In GR this wave equation is then solved using the Lorenz gauge, which implies transverse wave solutions, and the vanishing of the trace $\bar{h}$. The latter quantity being a scalar in GR and thus invariant under coordinate transformations, both $h_{\mu\nu}$ and $\bar{h}_{\mu\nu}$ can be traceless at the same time. However, in $f(R)$ theories, as can be seen from Eq. (4.16), by imposing $\bar{h} = 0$ one cannot obtain $h = 0$, since the trace does no longer behave as a scalar under coordinate transformations, due to the additional coupled scalar equation for $R^{(1)}$. It has been argued that nonetheless it is possible to perform a gauge transformation such that $\bar{h} = 0$, in which case the solution of the wave equation (4.21) would thus be the same as in GR, with no additional polarization mode, in particular the breathing mode. However, we show in the following that, in $f(R)$ theories, one cannot preserve transversality and the traceless condition at the same time. The main point being that when considering a gauge transformation in order to get a vanishing $\bar{h} = 0$ one has to take into account that the background metric is no longer just Minkowski, but due to the fact that $R^{(1)}$ is nonzero, as clearly has to be the case due to Eq. (4.10), the metric is $\bar{g}_{\mu\nu}$ as induced by $R^{(1)}$.

Let us consider a gauge transformation generated by ξ_{μ}, in which case $\bar{h}_{\mu\nu}$ becomes

$$\bar{h}_{\mu\nu} \to \bar{h}'_{\mu\nu} = \bar{h}_{\mu\nu} + \xi_{\nu;\mu} + \xi_{\mu;\nu} - \bar{g}_{\mu\nu}\xi^{;\lambda}_{\lambda}, \tag{4.22}$$

where a semicolon denotes the covariant derivative with respect to the background metric $\bar{g}_{\mu\nu}$, which is thus used for raising and lowering indices. Taking the trace of this equation by contracting with $\bar{g}_{\mu\nu}$, we get

$$\bar{h}' = \bar{h} - 2\xi^{;\lambda}_{\ \lambda} \tag{4.23}$$

Applying $\Box$ on the above equation, we obtain a condition that ξ_λ has to fulfill if we require that $\bar{h}'$ is traceless:

$$\begin{aligned} \Box\bar{h}' = 0 \quad &\Leftrightarrow \quad \Box(\bar{h} - 2\xi^{;\lambda}_{\ \lambda}) = 0, \\ &\Leftrightarrow \quad \Box\xi^{;\lambda}_{\ \lambda} = 0 \Leftrightarrow (\Box\xi_\lambda)^{;\lambda} = 0 \\ &\Leftrightarrow \quad \Box\xi_\lambda = 0 \text{ or constant.} \end{aligned} \tag{4.24}$$

In the second step, we used the fact that $\Box\bar{h} = 0$. Now, requiring the Lorenz gauge condition and using the Ricci identity (see e.g. [8])

$$\xi^i_{\ ;l;k} - \xi^i_{\ ;k;l} = R^i_{\ jkl}\xi^j, \tag{4.25}$$

we get from the above transformation (4.22)

$$\bar{h}_{\mu\nu}^{\ \ ;\nu} \to \bar{h}'_{\mu\nu}^{\ \ ;\nu} = \bar{h}_{\mu\nu}^{\ \ ;\nu} + \xi_{\mu;\nu}^{\ \ ;\nu} + \bar{R}^{(1)}_{\mu\nu}\xi^\nu, \tag{4.26}$$

where $\bar{R}^{(1)}_{\mu\nu}$ is the Ricci tensor of the background metric. Since $\bar{h}_\mu^{\ \nu}_{\ ;\nu} = 0$ due to the Lorenz gauge condition, hence $\bar{h}'_\mu^{\ \ \nu}_{\ ;\nu}$ can be zero if and only if $\xi_\mu^{\ ;\nu}_{\ ;\nu} + \bar{R}^{(1)}_{\mu\nu}\xi^\nu = 0$; however, one has that $\Box\xi_\mu = -\bar{R}^{(1)}_{\mu\nu}\xi^\nu \neq 0$ or constant. This contradicts Eq. (4.24) and tells us that it is in general not possible to achieve both conditions of vanishing trace and transversality at the same time.

Solutions

Next, we discuss the solutions corresponding to waves in vacuum of the wave equations given by Eq. (4.10) and Eq. (4.21), respectively. We make the usual plane wave ansatz, corresponding to a standard Fourier decomposition, and we get for Eq. (4.21)

$$\bar{h}_{\mu\nu} = \hat{h}_{\mu\nu}(k^\rho)\exp(ik_\rho x^\rho), \tag{4.27}$$

where k is a four vector. We assume that the wave is traveling along the z axis, and due to the Lorenz gauge, from which it follows that the wave is transverse with respect to the z axis,

$$k^\mu \quad = \quad \omega(1,0,0,1), \tag{4.28}$$

where ω is the angular frequency. Due to the Lorenz gauge condition, we have

$$k^\mu\hat{h}_{\mu\nu} = 0, \tag{4.29}$$

$$\Rightarrow \qquad \hat{h}_{0\nu} + \hat{h}_{3\nu} = 0. \tag{4.30}$$

Assuming $\hat{h}_{0\nu} = 0$, implies $\hat{h}_{3\nu} = 0$. The only nonzero components of $\hat{h}_{\mu\nu}$ are therefore $\hat{h}_{11}$, $\hat{h}_{12}$, $\hat{h}_{21}$ and $\hat{h}_{22}$, so in general we can write

$$\hat{h}_{\mu\nu} = \begin{pmatrix} 0 & 0 & 0 & 0 \\ 0 & \hat{h}^b_{11} + \hat{h}^+_{11} & \hat{h}^\times_{12} & 0 \\ 0 & \hat{h}^\times_{21} & \hat{h}^b_{22} - \hat{h}^+_{22} & 0 \\ 0 & 0 & 0 & 0 \end{pmatrix}, \tag{4.31}$$

where the superscript $+$, $\times$ and b denote the plus, the cross and the breathing polarizations modes of the gravitational radiations, respectively. Note that we have $\hat{h}^b_{11} = \hat{h}^b_{22} \equiv \hat{h}^b$, $\hat{h}^+_{11} = \hat{h}^+_{22} \equiv \hat{h}^+$, and $\hat{h}^\times_{12} = \hat{h}^\times_{21} \equiv \hat{h}^\times$. These modes are transverse to the direction of propagation, with the two $+, \times$ representing quadrupolar deformations and b representing a monopolar breathing deformation. In GR, the breathing polarization mode vanishes due to the traceless condition of $\hat{h}_{\mu\nu}$, and only the two usual $+$ and $\times$ polarizations remain.

The solution of the second wave equation (4.10) can be written as

$$R^{(1)} = \hat{R}(q^\rho)\exp(iq_\rho x^\rho), \tag{4.32}$$

where q^ρ is a four vector. Considering a wave traveling along the z axis and taking Ω as its angular frequency, we can write

$$q^\mu = (\Omega, 0, 0, \sqrt{\Omega^2 - m^2}). \tag{4.33}$$

Thus Eq. (4.32) yields the massive scalar longitudinal mode in the z direction. By analogy with our previous notation, the corresponding amplitude $\hat{R}$ can be written as

$$\hat{R} \equiv \hat{h}^l, \tag{4.34}$$

where the superscript l denotes the longitudinal mode. However, the longitudinal mode does not travel with the speed of light c, but instead has a group velocity [46, 58]

$$v(\Omega) = \frac{\sqrt{\Omega^2 - m^2}}{\Omega}\ , \tag{4.35}$$

which for $m^2 > 0$ leads to $v < c$ and for $\Omega < m$ the wave is decaying.

General $f(R)$ Model

To find the polarization modes for a general $f(R)$ function, including in particular also $f(R) = \frac{1}{R}$ models, we define a scalar field $\phi = f'(R)$ and an effective potential

$$V = f(R) - Rf'(R) \tag{4.36}$$

such that $f''(R) \neq 0$ and $f'(R)$ is invertible. Then the field equations (4.2) can be written as

$$R_{\mu\nu} - \frac{1}{2}Rg_{\mu\nu} = \frac{1}{\phi}\left(\frac{1}{2}g_{\mu\nu}V(\phi) + \nabla_\mu\nabla_\nu\phi - g_{\mu\nu}\Box\phi\right). \tag{4.37}$$

Next, we consider small perturbations from Minkowski background equation (4.4) in the metric tensor and in the scalar field ϕ_0, i.e., around the constant scalar curvature, such that

$$\phi = \phi_0 + \delta\phi. \tag{4.38}$$

Here, we also assume ϕ_0 to be a steady minimum for the effective potential V, say that is V_0. As the effective scalar field and the effective potential arise directly from the prime derivative $f'(R)$ of the spacetime curvature, hence the potential presents a square (i.e., parabolic) trend, in a function of the effective scalar field, near the minimum V_0, i.e.,

$$V \simeq V_0 + \frac{1}{2}a\delta\phi^2 \Rightarrow \frac{dV}{d\phi} \simeq a\delta\phi, \tag{4.39}$$

where a is a constant (see [60] for more details on this argument). The linearized field equations up to first order in $h_{\mu\nu}$ and $\delta\phi$ become [46]

$$R^{(1)}_{\mu\nu} - \frac{1}{2}R^{(1)}\eta_{\mu\nu} = \partial_\mu\partial_\nu h_f - \eta_{\mu\nu}\Box h_f, \tag{4.40}$$

where $h_f = \frac{\delta\phi}{\phi_0}$. Modifying Eq. (4.15) for a general function, h_f, we have

$$h_{\mu\nu} \quad = \quad \bar{h}_{\mu\nu} - \frac{\bar{h}}{2}\eta_{\mu\nu} - h_f\eta_{\mu\nu}. \tag{4.41}$$

Using Eqs. (4.6) and (4.7) along with the above transformation and imposing the Lorenz gauge condition, the linearized field equations become

$$\Box\bar{h}_{\mu\nu} = 0. \tag{4.42}$$

This equation is identical to Eq. (4.21); it can thus be solved in a similar manner and the solution—thus the number of polarizations—is identical to the one found for a polynomial model. Hence, we have the +, × and breathing modes in this case, too.

For the massive mode, taking the trace of the Eq. (4.37), we have

$$-R = -\frac{3}{\phi}\Box\phi + \frac{2}{\phi}V(\phi). \tag{4.43}$$

Differentiating Eq. (4.36) with respect to ϕ, we obtain

$$R = -V'(\phi). \tag{4.44}$$

Using this equation in Eq. (4.43), we get

$$3\Box\phi - 2V(\phi) + \phi V'(\phi) = 0. \tag{4.45}$$

In linearized approximation, applying Eqs. (4.38) and (4.39) and assuming $V_0 = 0$, we finally get

$$\Box h_f + m^2 h_f = 0, \tag{4.46}$$

where $m^2 = \frac{a\phi_0}{3}$. The solution to this equation yields the longitudinal mode in the same way as discussed in the previous section.

In conclusion, any metric formulation of $f(R)$ leads to the existence of four polarization modes: two tensor modes and two scalar ones.

4.3 Polarization Modes in Palatini Formalism

In this formalism, the action can be defined as [47]

$$S(g,\Gamma) = \frac{1}{2\kappa}\int d^4x\sqrt{-g}f(R) + L_m, \tag{4.47}$$

where L_m is the Lagrangian for the matter field. In this approach, the connection Γ is nonmetric (i.e., the connection and the metric are considered as independent) but with vanishing torsion. Assuming that the matter Lagrangian does not depend on the dynamical connection, the field equations can be achieved by varying the action independently with respect to $g_{\mu\nu}$ and $\Gamma^{\lambda}_{\mu\nu}$ and are given by

$$f'(R)R_{\mu\nu} - \frac{1}{2}f(R)g_{\mu\nu} = kT_{\mu\nu}, \tag{4.48}$$

$$\nabla_\alpha(\sqrt{-g}f'(R)g^{\mu\nu}) = 0, \tag{4.49}$$

with ∇_α the covariant derivative with respect to Γ.

In order to study the propagation of GWs, we first assume the vacuum case, i.e., $T = g^{\mu\nu}T_{\mu\nu} = 0$. The trace of Eq. (4.48) leads then to the constraint

$$f'(R)R - 2f(R) = 0. \tag{4.50}$$

If $f(R) \neq \alpha R^2$, it can be shown that the associated theory actually corresponds to GR with a cosmological constant [61], which yields the two usual tensorial polarization modes + and × [62].

However, if $f(R) = \alpha R^2$ [which identically satisfies Eq. (4.50)], one cannot reduce this function to a usual expansion of the form "$R+$ corrections" which would be physically meaningful. However, using the approach of [56], one can nevertheless show that the Newman-Penrose quantities ψ_2, ψ_3 and ϕ_{22} vanish, and no additional polarization mode would arise (see the Appendix).

4.4 Conclusion

In this paper we have discussed GWs polarization modes in $f(R)$ theories. Using the weak-field approximation, we have explicitly shown that in the polynomial case of $f(R)$ theories, two scalar modes arise in addition to the two

ordinary tensorial modes from standard GR. One of these extra modes is a massive longitudinal one, whereas the second one is a massless breathing mode. Extending the discussion to a general function $f(R)$, one finds that the field equations are similar to the polynomial case where our argument can be applied once again, thus leading to the existence of the two additional scalar modes.

As previously mentioned, one can also check that scalar-tensor theories have the same number of polarization modes since $f(R)$ theories are equivalent under simple transformations [42]. However, the mass is in this case $m^2 = \frac{a\phi_0}{2\omega+3}$, where ω is the transforming parameter.

Moreover, in Brans-Dicke theory, one generally finds four modes [especially in the case ω_{BD} which is equivalent to the $f(R)$ metric formalism], but should the scalar field be massless ($m^2 = 0$), then only one scalar mode remains, namely the massless breathing mode [63, 64]. In the specific case $\omega_{\mathrm{BD}} = -3/2$, the theory however reduces to the Palatini formalism, where the vacuum field equations only produce the two usual tensor modes since this formulation is equivalent to GR, up to a cosmological constant.

In Table 1 we summarize our results.

Table 4.1: *Additional polarizations found in various theories. +, ×, b, l denote the plus, cross, breathing and longitudinal modes, respectively.*

Theories	Polarization modes
Metric $f(R)$ gravity	$+,\ \times,\ b,\ l$
Palatini $f(R)$ gravity	$+,\ \times$
Scalar-tensor theory (massive)	$+,\ \times,\ b,\ l$
Brans-Dicke theory (massive)	$+,\ \times,\ b,\ l$
Brans-Dicke theory (massless)	$+,\ \times,\ b$

We would like to mention that our work is in agreement with the results obtained by Alves, Miranda et de Araujo [56, 57] where they use the Newman-Penrose approach. In the Appendix, we shortly summarize the related formalism. Additionally, GWs polarizations have also recently been studied in $f(R, T)$ models—where T is the trace of the energy momentum tensor—again in the NP formalism [65]. Since one needs to examine the theory in a region far from the source of GWs, where $T = 0$, the number of polarization modes is again the same as in $f(R)$ theories, i.e., four modes.

Recent studies have shown that in some extensions of $f(R)$ theories, the polarization content can greatly vary. For instance, in the so-called $F(T)$ theories (where T is the torsion scalar in teleparallelism), there is an equivalence with GR, and thus no additional GWs modes [66]. On the other hand, a detailed study of the GWs solutions of fourth-order gravity has shown that, in general, besides the two usual massless solutions, there are two further massive modes with finite-distance interaction [67].

Finally, we note that if GWs present nontensorial polarization modes as discussed in this paper, a measured signal, for instance a stochastic cosmological background of GWs, would consist of a mixture of all those modes. Through the analysis of such a signal, the existence of scalar and/or vector modes could help to discriminate between the possible theories of gravity beyond GR or to set some bounds on the respective intensity of each mode if only tensorial polarizations are present.

4.4 Acknowledgments

H.R.K was supported by a Swiss Government Excellence Scholarship for the academic year 2014-2015 and L.P and P.J thank the Swiss National Foundation for support. We also thank the referee for the useful comments.

4.5 Appendix

Newman-Penrose Formalism: Overview

In this section, we give a short overview of the Newman-Penrose (NP) formalism to find extra polarization modes; more details can be found in the appropriate references [54, 56, 57].

To define the NP quantities which corresponds to the six polarization modes of GWs, one can define a system of four linearly independent vectors $(e_t,\ e_x,\ e_y,\ e_z)$ at any point of space, which are called tetrads. From this system one can introduce a particular tetrad, known as the NP tetrad, denoted as $k,\ l,\ m,\ \bar{m}$ [54]. The first two of these vectors are real null vectors defined as

$$k = \frac{1}{\sqrt{2}}(e_t + e_z), \quad l = \frac{1}{\sqrt{2}}(e_t - e_z), \tag{4.51}$$

whereas the other two null vectors m and $\bar{m}$ are complex conjugates of each other and defined as

$$m = \frac{1}{\sqrt{2}}(e_x + ie_y), \quad \bar{m} = \frac{1}{\sqrt{2}}(e_x - ie_y). \tag{4.52}$$

The so-defined tetrad vectors obey the following relations:

$$-k.l = m.\bar{m} = 1, \quad k.m = k.\bar{m} = l.m = l.\bar{m} = 0. \tag{4.53}$$

The Riemann tensor $R_{\lambda\mu\nu\rho}$ can be split into irreducible parts: a ten-component Weyl tensor (ψ's), a nine-component traceless Ricci tensor (ϕ's) and a curvature scalar (Λ). The total number of independent components can however be reduced to six [55] by assuming nearly plane wave and making use of the properties of the Riemann tensor. In order to describe a wave in a generic metric theory in a null frame, one can associate those six independent components to the following quantities: ψ_2, ϕ_{22}, ψ_3 and ψ_4. ψ_3 and ψ_4 are complex, and thus each one corresponds to two independent polarizations. These NP quantities are related to the following components of the Riemann tensor in the null tetrad basis:

$$\psi_2 = -\frac{1}{6}R_{lklk} \quad \sim \quad \text{longitudinal scalar mode,} \tag{4.54}$$

$$\psi_3 = -\frac{1}{2}R_{lkl\bar{m}} \quad \sim \quad \text{vector-}x\text{ and }y\text{ modes,} \tag{4.55}$$

$$\psi_4 = -R_{l\bar{m}l\bar{m}} \quad \sim \quad +,\times \text{ tensorial modes,} \tag{4.56}$$

$$\phi_{22} = -R_{lml\bar{m}} \quad \sim \quad \text{breathing scalar mode.} \tag{4.57}$$

$$\tag{4.58}$$

The following relations for the Ricci tensor and the Ricci scalar hold:

$$R_{lk} = R_{lklk}, \tag{4.59}$$

$$R_{ll} = 2R_{lml\bar{m}}, \tag{4.60}$$

$$R_{lm} = R_{lklm}, \tag{4.61}$$

$$R_{l\bar{m}} = R_{lkl\bar{m}}, \tag{4.62}$$

$$R = -2R_{lk} = -2R_{lklk}. \tag{4.63}$$

The field equations (4.2) and (4.3) can be written in the following form:

$$R_{\mu\nu} = \frac{1}{f'(R)}\left[\frac{1}{2}f(R)g_{\mu\nu} + \nabla_\mu\nabla_\nu f'(R) - g_{\mu\nu}\Box f'(R)\right], \tag{4.64}$$

$$R = \frac{2f(R) - 3\Box f'(R)}{f'(R)}. \tag{4.65}$$

In this approach, one first determines the Ricci scalar (4.65) (by considering the trace of the field equation) and then substitutes it into Eq. (4.64). By writing the coordinates of the Ricci tensor in the NP tetrad, one can finally determine the possible polarization modes with the help of the previously described Newton-Penrose quantities. For instance for the model $f(R) = R + \alpha R^2$ studied in Sec. 4.2.1, Eq. (4.64) and its solution correspond to our previous Eq. (4.10) and Eq. (4.32). Hence substituting the solution given in Eq. (4.32) into Eq. (4.64), we finally get the following nonzero components for the Ricci tensor [56]:

$$R_{tt} = \frac{-1}{2}(4\alpha q^2 + 1)R, \tag{4.66}$$

$$R_{tz} = 2\alpha q\sqrt{q^2 + \frac{1}{6\alpha}R}, \tag{4.67}$$

$$R_{zz} = \frac{1}{6}(-12\alpha q^2 + 1)R. \tag{4.68}$$

Using Eqs. (4.54)-(4.63), one finds the following NP quantities:

$$\psi_2 \neq 0, \quad \psi_3 = 0, \quad \psi_4 \neq 0, \quad \phi_{22} \neq 0. \tag{4.69}$$

Thus we get four polarization modes for the GWs: $+$, $\times$, b and l.

Case $f(R) = \alpha R^2$ in Palatini

We give here the proof that the case $f(R) = \alpha R^2$ also does not give rise to additional polarization modes. First considering a theory of the form $f(R) = \alpha R^{-\beta}$, one finds

$$R_{\mu\nu} = -\frac{1}{2\beta}Rg_{\mu\nu}, \tag{4.70}$$

$$R = -\frac{2}{\beta}R, \tag{4.71}$$

similarly to Eqs. (4.64) and (4.65). If $\beta \neq -2$, the theory reduces to GR with $R = 0$, $R_{\mu\nu} = 0$, and hence two tensor polarization modes. Otherwise, the field equation reads

$$R_{\mu\nu} = \frac{1}{4}Rg_{\mu\nu}, \tag{4.72}$$

which implies that the following Newman-Penrose parameters must be zero:

$$\psi_2 = \psi_3 = \phi_{22} = 0. \tag{4.73}$$

This, once again, corresponds to the two tensor modes $+$ and $\times$.

Chapter 5

Gravitational Wave Polarization from Combined Earth-space Detectors

L. Philippoz, A. Boîtier, P. Jetzer

Published in Physical Review D, Volume **98***, 044025 (2018)*

Abstract

In this paper, we investigate the sensitivity to additional gravitational wave polarization modes of future detectors. We first look at the upcoming Einstein Telescope and its combination with existing or planned Earth-based detectors in the case of a stochastic gravitational wave background. We then study its correlation with a possible future space-borne detector sensitive to high-frequencies, like DECIGO. Finally, we adapt those results for a single GW source and establish the sensitivity of the modes, as well as the localization on the sky.

5.1 Introduction

Since the first detection of gravitational waves (GW) by the LIGO collaboration, a total of 5 black hole mergers[43, 68–71] has been observed so far[1], as well as a neutron star merger visible through gravitational waves and all accessible frequency bands of the electromagnetic spectrum [72, 73]. The results matched with Einstein's theory of general relativity (GR) up to measurement precision.

Until now, many tests of general relativity have been performed (e.g. the perihelion precession of Mercury, the geodetic precession and the Lense-Thirring effect by Gravity Probe B [74] or the weak equivalence principle by MICROSCOPE [75] to name only a few) and so far, they all agree with general relativity. Modifications to GR have been constrained by experiments, but there are still some possibilities which cannot be excluded, see Will [11] to get an overview. As we will discuss in the next part, one could for example modify GR by adding a scalar or a vector field which only couple to the metric and therefore act as correction to GR. These fields would allow additional polarizations to the two tensor polarizations, + (plus) and × (cross), predicted by GR. The scalar field would create the breathing (b) and the longitudinal (l) and the vector field the x and y polarizations.

The standard model of cosmology describes the creation of the universe as an exponentially fast expansion of a quantum state. In quantum mechanics, no field or degree of freedom can be zero. If one now expands the universe, the quantum fluctuations of the fields get macroscopic and create a homogeneous and isotropic background where all polarizations are excited equally.

Using the electromagnetic spectrum we can only observe events as far back as the cosmic microwave background (CMB). The neutrinos decouple a bit earlier and would allow us to see further back in time, given we would figure out how to measure low energy particles, which almost never interact. If we could however measure a gravitational wave background (GWB), then we could test cosmological models way further back in time. One expects that the gravitational waves decouple at the Planck time due to the weak coupling of the metric to the other fields. This might allow us to get information about quantum gravity and thus an energy scale which is far out of reach of modern particle colliders. Since one expects all polarizations to be excited in the GWB, this would serve as a test for GR or allow to put constrains on alternative theories of gravity by checking the presence or absence of additional polarization modes in a given signal.

The second-generation ground-based detectors advanced LIGO and advanced VIRGO can detect GW from binary black holes (BBH) and binary neutron stars (BNS) [72]. A similar detector is being built in Japan (KAGRA) [76] and another advanced LIGO is planned in the near future in India (IndIGO) [77]. With the Einstein Telescope (ET) [78], a cluster of three detectors arranged in an equilateral triangle with an arm length of 10 km, one plans to build a third-generation detector in Europe which is supposed to be about 10 times more sensitive to a GW signal than the current generation.

Space-borne detectors are also on their way. LISA pathfinder was a success [79], which is very promising for LISA [80], a cluster of three satellites planned to be launched as the next ESA L3 mission. LISA will be put on a heliocentric orbit, at about 20° behind the Earth. DECIGO [81, 82] was originally planned to consist of 4 clusters distributed in Earth-orbit around the Sun, each forming a 1000 km equilateral triangle with three satellites. A recent paper [83] proposes a scaled down version (100 km), B-DECIGO (basic), as a first generation of deci-Hz detectors. It is planned to revolve around the Earth at an altitude of 2000 km.

The ground-based detectors of the second generation are not capable of detecting the gravitational wave background on their own and it is unlikely that an improvement of about one order of magnitude in sensitivity would be sufficient. But if we combine the signals of all the detectors which are built to measure BBH and BNS anyway, then one could enhance the sensitivity by three to four orders of magnitude and thus get more restrictive constraints on the GWB or even detect it.

With its high and low frequency interferometers, ET is designed to measure in a frequency range from 1.5 Hz to 10 kHz. It therefore makes perfect sense to cross correlate its signals with the ones of any second-generation ground-based detector, or even DECIGO. The correlation between ET and DECIGO has the advantage that their noises are very different, since ET is Earth-based and DECIGO is in space and therefore does not have any seismic noise for instance. A correlation of ET or DECIGO with LISA would however be difficult since the designed sensitivity of the

[1]The current state of the detections by the LIGO/VIRGO Collaboration can be found on: `https://www.ligo.caltech.edu/page/detection-companion-papers`

latter lies within the range 10^{-4} Hz to about 1 Hz, out of the frequency band considered for ET/DECIGO.

Testing GR by using the gravitational wave background can be of interest due to its constant and isotropic nature. One does not have to extract complex waveforms in a combination of all the 6 possible polarizations from the strain, which may differ according to the modified theory considered. Note that because of the isotropy of the GWB, one cannot distinguish between + and × tensor polarizations, or x and y vector polarizations, but it is nevertheless possible to separate the three modes (tensor T, vector V and scalar S), which can already give us information on the involved fields.

In the case of point sources, one can additionally determine the direction of the incoming GW on the sky, as well as distinguishing between the polarizations. However, this makes the calculation more complicated since we have to deal with 8 degrees of freedom instead of 3.

This paper is outlined as follows: in section 5.2 we recall some theoretical basics about polarization and summarize the derivation of the signal to noise ratio (SNR) for a polarization mode when combining multiple detectors in the case of a GWB, as done in Nishizawa et al. [84, 85]. We also derive the general expression of the power spectral density and the overlap reduction functions for detectors having arbitrary opening angles. In section 5.3, we apply those results in the case of ET and consider its correlation with ground-based detectors. In section 5.4, we introduce DECIGO in the detector network and investigate how the time dependent sensitivity of a cross correlation between DECIGO and Earth detectors can be used to distinguish the three polarization modes, as an alternative method to the maximum likelihood method on all detector pairs. Finally, we consider the case of point sources and derive the SNR for a single polarization and the variance on the incoming direction of the GW in section 5.5.

5.2 Theory and Methods

In this section, we introduce the techniques used to calculate the sensitivities to GW-polarizations of various combinations of detectors. We first give a short overview of GW and the notion of polarization in GR or alternative theories of gravitation, as well as the detection principle. We continue by extracting the signal of a correlation between two detectors. Then, we take multiple detector pairs and combine their signals in an optimal way to distinguish the polarizations and enhance the sensitivity.

The sensitivity is dependent on the noise power spectrum of the detector and geometry factors, which in the case of a gravitational wave background are the overlap reduction functions (ORFs). To calculate the sensitivity for a collection of detectors including ET or DECIGO we need to generalize the formula for the noise power spectral density to arbitrary opening angles and we can simplify the expression for the ORFs for ground-based detectors which comes in handy since many of the detectors we consider here are ground based.

Polarizations of Gravitational Waves

The linearization of the Einstein field equations leads to a linear wave equation for perturbations in the metric. Since the metric is required to be symmetric, the degrees of freedom of a 4-dimensional tensor of rank 2 are reduced from 16 to 10. The Einstein equations are invariant under a change of reference frame, while the linearized version is only invariant under an infinitesimal change of coordinates, which reduces the degrees of freedom to 6. By choosing an orthonormal basis $(\hat{m}, \hat{n}, \hat{\Omega})$, where $\hat{\Omega} \parallel \boldsymbol{k}$ is the direction of travel [84], we can write a general solution as:

$$h_{ij}(t,\boldsymbol{x}) = \begin{pmatrix} h_{11} & h_{12} & h_{13} \\ h_{12} & h_{22} & h_{23} \\ h_{13} & h_{23} & h_{33} \end{pmatrix} e^{2\pi i f\left(t-\frac{\hat{\Omega}\cdot\boldsymbol{x}}{c}\right)} + c.c. = \sum_A h_A(t,\boldsymbol{x}) e^A_{ij} e^{2\pi i f\left(t-\frac{\hat{\Omega}\cdot\boldsymbol{x}_I}{c}\right)} + c.c., \tag{5.1}$$

where the e^A are the basis tensors of the possible polarizations we describe afterwards, and h_A is the amplitude of the GW in the polarization A.

Therefore, we can have at most 6 polarizations. Since this is a vacuum equation in the case of unmodified GR, the equation is invariant under a gauge transformation on the fields $h_{\mu\nu} \mapsto h'_{\mu\nu} = h_{\mu\nu} - \epsilon_{\mu,\nu} - \epsilon_{\nu,\mu}$, with $\Box\epsilon^\mu = 0$. This further reduces the degrees of freedom to the 2 tensor polarizations + and ×. They are purely transversal waves, which enlarge distances in one direction and squeeze space in the orthogonal direction. The basis tensors of the tensor mode are given by:

$$e^+ = \hat{m} \otimes \hat{m} - \hat{n} \otimes \hat{n}, \qquad e^\times = \hat{m} \otimes \hat{n} + \hat{n} \otimes \hat{m}. \tag{5.2}$$

We will now look at two representative examples of modifications of GR and their consequences on gravitational waves. Adding a scalar field to the Lagrangian is one possibility to modify GR [11]. A general scalar-tensor action can be written as:

$$S[g,\phi] = \frac{1}{16\pi G} \int \left[R - 2g^{\mu\nu}\partial_\mu\phi\,\partial_\nu\phi - U(\phi)\right]\sqrt{-g}d^4x. \tag{5.3}$$

This leads to the two scalar polarizations called the breathing mode b, since it stretches and squeezes space simultaneously in all transversal directions, and the longitudinal mode l, which is a purely longitudinal wave. Their basis tensors are given by:

$$e^b = \hat{m} \otimes \hat{m} + \hat{n} \otimes \hat{n}, \qquad e^l = \sqrt{2}\hat{\Omega} \otimes \hat{\Omega}. \tag{5.4}$$

Another possibility would be to add a vector field Lagrangian as follows:

$$S[g,V] = \frac{1}{16\pi G} \int \left[(1 + \omega V_\mu V^\mu)R - K^{\mu\nu}_{\rho\sigma}\nabla_\mu V^\rho \nabla_\nu V\sigma + \lambda(V_\mu V^\mu + 1)\right]\sqrt{-g}\; d^4x \tag{5.5}$$

with

$$K^{\mu\nu}_{\rho\sigma} = c_1 g^{\mu\nu}g_{\rho\sigma} + c_2\delta^\mu_\rho\delta^\nu_\sigma + c_3\delta^\mu_\sigma\delta^\nu_\rho - c_4 V^\mu V^\nu g_{\rho\sigma}, \tag{5.6}$$

where the c_i are coefficients which would have to be determined by experiments. This modification generates the two vector polarizations x and y which oscillate in direction of travel and in one orthogonal to it. Their respective basis tensors are given by:

$$e^x = \hat{m} \otimes \hat{\Omega} + \hat{\Omega} \otimes \hat{m}, \qquad e^y = \hat{n} \otimes \hat{\Omega} + \hat{\Omega} \otimes \hat{n}. \tag{5.7}$$

We can finally express a general solution in terms of all six polarizations:

$$h_{ij}(t,\boldsymbol{x}) = \begin{pmatrix} h_b + h_+ & h_\times & h_x \\ h_\times & h_b - h_+ & h_y \\ h_x & h_y & h_l \end{pmatrix} e^{2\pi i f\left(t - \frac{\hat{\Omega}\cdot\boldsymbol{x}}{c}\right)} + c.c. \tag{5.8}$$

When a gravitational wave stretches or squeezes an arm of a Michelson interferometer, then one can observe a phase shift. This phase shift is larger if the amplitude of the wave is larger and if the detector arms are optimally aligned given an incoming wave with a certain polarization. So the signal in the detector can be written as:

$$h_{ij}(t,\boldsymbol{x}) = D^{ij}\sum_A h_A(t,\boldsymbol{x})e^A_{ij}e^{2\pi i f\left(t - \frac{\hat{\Omega}\cdot\boldsymbol{x}}{c}\right)}. \tag{5.9}$$

The detector tensor $D = \frac{1}{2}(\hat{u}\otimes\hat{u} - \hat{v}\otimes\hat{v})$ describes the orientations of the interferometer arms, given by the unit vectors $\hat{u}$, $\hat{v}$, and the polarization of the wave can be written as a linear combination of the basis tensors e^A described above. If we contract the two tensors, we get a scalar quantity, the angular pattern function, which describes the geometric dependence of the signal:

$$F^A := D^{ij}e^A_{ij}. \tag{5.10}$$

A GW thus produces one scalar signal in each detector, which means that we need to combine at least 6 detectors to distinguish them. In the case of a gravitational background however, we expect a direction independent signal.

Therefore, one can only distinguish between the three modes: tensor, vector and scalar; three independent signals are thus sufficient, but more signals would of course improve the sensitivity.

By using the matched filtering method, one can calculate the signal to noise ratio of a given signal. Since the ET project has declared a signal to noise ratio of at least 8 as their condition to accept an event as an actual signal[78], we set the SNR to 8 and calculate the minimal amplitude a gravitational wave needs to have to be recognized as a true signal by a certain collection of detectors and use this as a measure of their combined sensitivity.
The SNR is related to the false alarm rate α and detection rate γ by [86]:

$$SNR \geqslant \sqrt{\frac{2}{n}}\left(\mathrm{erfc}^{-1}(2\alpha) - \mathrm{erfc}^{-1}(2\gamma)\right) \tag{5.11}$$

Once one has chosen a minimal signal to noise ratio, one has to choose either a false alarm or a detection rate. If we would split our observation time ($T = 1\,\mathrm{yr}$ would be a realistic choice for a GWB observation) into small time intervals of for example 4 s and do statistical tests on them, then one false alarm in 27 000 yr would be equivalent to a false alarm rate of $\alpha = \frac{4\,s}{27\,000\,\mathrm{yr}} = 4.8 \cdot 10^{-12}$. This would give us about $n = 7.8 \cdot 10^6$ time splits and result in a detection rate $\gamma \approx 1$ under the assumption of a SNR of 8. The detection rate is related to the false dismissal rate β by $\gamma = 1 - \beta$ which gives us a false dismissal rate of $\beta = 3.3 \cdot 10^{-18}$.

We will now derive an expression for the SNR in terms of the GW signal and the detector noise.

Combined Sensitivity of Multiple Detectors

Since the signal of a GW is usually smaller than the noise, one can rely on two different techniques in order to get rid of the noise. First, we can multiply the Fourier transform of the signal with a suitable filter function, which turns out to be proportional to the signal, and integrate over all frequencies. This method is called matched filtering. Secondly, we can cross correlate the strains $s_{I,J} = h_{I,J} + n_{I,J}$ of two detectors I and J. Since the noises $n_{I,J}$ of the two detectors are not correlated between them and also not correlated to the signals $h_{I,J}$, we can get rid of the noise by taking the expectation of the Fourier transform (FT) of the complex conjugated strain $\tilde{s}_I^*$ of detector I multiplied with the FT of the strain $\tilde{s}_J$ of detector J:

$$\mathbb{E}[\tilde{s}_I^* \tilde{s}_J] = \mathbb{E}[\tilde{h}_I^* \tilde{h}_J] + \underbrace{\mathbb{E}[\tilde{h}_I^* \tilde{n}_J]}_{=0} + \underbrace{\mathbb{E}[\tilde{n}_I^* \tilde{h}_J]}_{=0} + \underbrace{\mathbb{E}[\tilde{n}_I^* \tilde{n}_J]}_{=0}. \tag{5.12}$$

Nishizawa et al. [84] used the matched filtering method on a cross correlated signal and derived the SNR for a detector pair (I, J), and we now shortly remind the result.

The energy density parameter Ω_{GW} of the GWB can be written as a sum over all modes M, where each mode has two polarizations M_1 and M_2 as discussed previously:

$$\begin{aligned} \Omega_{GW}(f) &= \sum_M \Omega_{GW}^M = \sum_M \left(\Omega_{GW}^{M_1} + \Omega_{GW}^{M_2}\right), \\ M = \begin{pmatrix} M_1 \\ M_2 \end{pmatrix} &\in \left\{ T = \begin{pmatrix} + \\ \times \end{pmatrix},\ V = \begin{pmatrix} x \\ y \end{pmatrix},\ S = \begin{pmatrix} b \\ l \end{pmatrix} \right\}. \end{aligned} \tag{5.13}$$

The power spectral density $S_h^{M_i}$ of the polarization M_i is related to its energy density parameter by:

$$\Omega_{GW}^{M_i}(f) = \frac{2\pi^2}{3H_0^2} f^3 S_h^{M_i}(f). \tag{5.14}$$

By assuming that only one mode M is excited and using the ansatz $S_h^{M_i}(f) = h_{0,M_i}^2 \delta(f' - f)$, where h_{0,M_i} is the

amplitude of the polarization M_i, we get the sensitivity of the detector pair (I,J) to the specific mode M:

$$\begin{aligned}(SNR^M_{IJ})^2 &= \frac{3H_0^2}{10\pi^2}\sqrt{T\int_{-\infty}^{\infty}\frac{(\Omega^M_{GW}(|f'|)\gamma^M_{IJ}(|f'|))^2}{f^6 P_I(|f'|)P_J(|f'|)}df'} \\ &= \frac{1}{5}\sqrt{T\int_{-\infty}^{\infty}\frac{(S^M_h(|f'|)\gamma^M_{IJ}(|f'|))^2}{P_I(|f'|)P_J(|f'|)}df'} \\ &= \frac{T}{5}\frac{(h^2_{0,M_1}+h^2_{0,M_2})\gamma^M_{IJ}(f)}{\sqrt{P_I(f)P_J(f)}},\end{aligned} \tag{5.15}$$

where H_0 is the Hubble constant, T the observation time, $P_{I,J}$ are the noise power spectral densities of the detectors I and J and γ^M_{IJ} is the overlap reduction function defined by:

$$\begin{aligned}\gamma^M_{IJ}(f) &\coloneqq \frac{5}{2}\int_{\mathbb{S}^2}(F_I^{M_1}F_J^{M_1}+F_I^{M_2}F_J^{M_2})e^{\frac{2\pi i f}{c}\hat{\Omega}_0\cdot\Delta\boldsymbol{x}_{IJ}}\frac{d\hat{\Omega}}{4\pi} \\ &= \rho_1^M(\alpha)D_I^{ij}D^J_{ij}+\rho_2^M(\alpha)D^i_{I,k}D_J^{kj}\hat{d}_i\hat{d}_j+\rho_3^M(\alpha)D_I^{ij}D_J^{kl}\hat{d}_i\hat{d}_j\hat{d}_k\hat{d}_l,\end{aligned} \tag{5.16}$$

with $\alpha(f)\coloneqq\frac{2\pi f|\Delta\boldsymbol{x}_{IJ}|}{c}$ and where the ρ_i^M are linear combinations of the zeroth, second and fourth spherical Bessel functions.

By requiring again $SNR\overset{!}{\geqslant}8$ for a GW with mode M to be considered a true signal, we can rewrite (5.15) to get the minimal amplitude a GW would need to be detected as such:

$$|h_0^M(f)|_{min} = 8\sqrt{\frac{5}{T}}\left(\frac{\sqrt{P_I(f)P_J(f)}}{|\gamma^M_{IJ}(f)|}\right)^{1/2}. \tag{5.17}$$

If we have more than two detectors we can use the maximum likelihood method to distinguish the polarizations. We then get a SNR with which we recognize a mode M, as derived by Nishizawa et al. [85]:

$$\begin{aligned}(SNR^M)^2 &= \frac{3H_0^2}{10\pi^2}\sqrt{T\int_{-\infty}^{\infty}\frac{(\Omega^M_{GW}(f))^2\det\mathbf{F}(f)}{f^6\mathscr{F}_M(f)}df} \\ &= \frac{1}{5}\sqrt{T\int_{-\infty}^{\infty}\frac{S^M_h(f)^2\det\mathbf{F}(f)}{\mathscr{F}_M(f)}df}.\end{aligned} \tag{5.18}$$

Using the same ansatz as above, we get the minimal amplitude we require to not only detect a GW with mode M, but also distinguish its polarization, with a SNR of at least 8:

$$|h_0^M(f)|_{min} = 8\sqrt{\frac{5}{T}}\left(\frac{\mathscr{F}_M}{\det\mathbf{F}}\right)^{1/4}, \tag{5.19}$$

where the Fisher matrix $\mathbf{F}$ is obtained by summing over the Fisher matrices of all detector pairs (I,J)

$$F_{MM'}(f) = \sum_{(I,J)}\int_0^{T_{obs}}\frac{\gamma^M_{IJ}(t,f)\gamma^{M'}_{IJ}(t,f)}{P_I(f)P_J(f)}dt \tag{5.20}$$

and $\mathscr{F}_M$ is the determinant of the minor one gets by removing the M-th row and column from $\mathbf{F}$.

Optical Read-out Noise

The quantum fluctuations of the laser cause a fundamental noise source in each detector which is statistically independent from the other detectors. The fluctuation in the number density of photons arriving at the detector causes a random fluctuation in the measured power and a fluctuation in the light pressure on the mirror which causes the mirror to vibrate randomly. By increasing the laser power, the fluctuation in the number density increase in total but

is less compared to the average, which causes the relative fluctuations in the measured laser power to decrease, but the pressure and therefore the fluctuations in the position of the mirror increases. One therefore needs to balance one effect against the other, which causes an uncertainty relation similar to the one arising from quantum mechanics. We are now going to derive the optical read-out noise based on [9], but for an arbitrary opening angle between the detector arms.

A Michelson interferometer with a Fabry-Perot cavity catches an additional term dependant on the frequency f of the measured gravitational wave and on a pole frequency f_p which is a characteristic of the cavity. The power recycling C appears as a higher effective power, and the detector efficiency η as a lower one, and we modifiy the input power P_0 as $P_0 \mapsto \eta C P_0$.

The phase shift of a Fabry-Perot interferometer $\Delta\phi_{FP}$ is related to the one of a Michelson interferometer without cavity $\Delta\phi_{Mich}$ by:

$$|\Delta\phi_{FP}| = \frac{2\mathscr{F}}{\pi} \frac{|\Delta\phi_{Mich}|}{\sqrt{1+\left(\frac{f}{f_p}\right)^2}}, \tag{5.21}$$

$$|\Delta\phi_{Mich}| := \Delta\phi_u - \Delta\phi_v, \tag{5.22}$$

where $\mathscr{F}$ is the finesse of the Fabry-Perot cavity, L the arm length of the detector, $\Delta\phi_u$ and $\Delta\phi_v$ are the phase shifts in the arms u and v respectively, and f_p the pole frequency of the cavity is given by:

$$f_p \approx \frac{c}{4\mathscr{F}L}. \tag{5.23}$$

To calculate the phase shift of a Michelson interferometer with opening angle θ, we consider an incoming GW with a + polarization:

$$h^+_{\mu\nu} = h_+ \begin{pmatrix} 0 & 0 & 0 & 0 \\ 0 & 1 & 0 & 0 \\ 0 & 0 & -1 & 0 \\ 0 & 0 & 0 & 0 \end{pmatrix} \cos(\omega_{GW} t). \tag{5.24}$$

The GW effectively stretches space in x-direction and squeezes it in y-direction, as depicted in Fig. 5.1, by a factor $h_+(t - \frac{L}{c})$, using the approximation $\frac{\omega_{GW} L}{c} << 1$. In this choice of reference frame we can write $\boldsymbol{v}$ as:

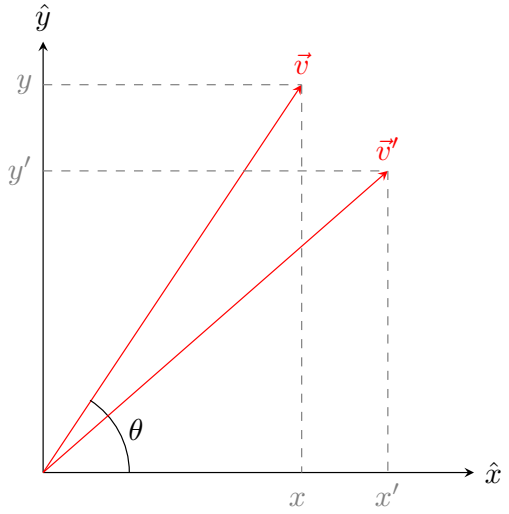

Figure 5.1: *The detector arm $\boldsymbol{v}$ of a detector with opening angle θ gets deformed to $\boldsymbol{v}'$ under the influence of a gravitational wave with + polarization. The other detector arm $\boldsymbol{u}$ lies on the x-axis.*

$$\boldsymbol{v} = \begin{pmatrix} x \\ y \end{pmatrix} = L \begin{pmatrix} \cos\theta \\ \\ \sin\theta \end{pmatrix}, \quad |\boldsymbol{v}| = L. \tag{5.25}$$

Using the previous approximation, we can write down the components of the deformed arm $\boldsymbol{v}'$ and express the change in the coordinates as:

$$x' = \sqrt{x^2 + h_+ x^2} \approx \left[1 + \frac{1}{2}h_+\right] x \;\Rightarrow\; \Delta x = \frac{1}{2}h_+ x, \tag{5.26}$$

$$y' = \sqrt{y^2 - h_+ y^2} \approx \left[1 - \frac{1}{2}h_+\right] y \;\Rightarrow\; \Delta y = -\frac{1}{2}h_+ y, \tag{5.27}$$

where we used the short notation h_+ for $h_+(t - \frac{L}{c})$ and expanded to first order. The total change in the length of the detector arm is then given by:

$$\begin{aligned} \Delta v &= |\boldsymbol{v}'| - |\boldsymbol{v}| = \sqrt{x'^2 + y'^2} - \sqrt{x^2 + y^2} \\ &= \frac{1}{2}\frac{2x}{\sqrt{x^2+y^2}}\Delta x + \frac{1}{2}\frac{2y}{\sqrt{x^2+y^2}}\Delta y + \mathcal{O}(\Delta^2) \\ &\approx \frac{\cos\theta L}{L}\Delta x + \frac{\sin\theta L}{L}\Delta y \\ &= \frac{1}{2}h_+ L(\cos^2\theta - \sin^2\theta) \end{aligned} \tag{5.28}$$

Since the light bounces back and forth, the phase shift catches a factor of two: $\Delta\phi_u = 2k_L\Delta u$ and $\Delta\phi_v = 2k_L\Delta v$.

With those results, we can calculate the amplitude of the Michelson phase shift:

$$\begin{aligned} |\Delta\phi_{Mich}| &= |\Delta\phi_u - \Delta\phi_v| \\ &= \left| k_L h_+ \left(t - \frac{L}{c}\right) L \right. \\ &\quad \left. - k_L h_+ \left(t - \frac{L}{c}\right) L(\cos^2\theta - \sin^2\theta) \right| \\ &= \frac{4\pi}{\lambda_L}\sin^2\theta L h_+, \end{aligned} \tag{5.29}$$

with the wave number k_L and wave length λ_L of the laser: $k_L = \frac{2\pi}{\lambda_L}$. The change in the pathlength of a photon due to the incoming GW is given by:

$$\Delta L = 2(\Delta u - \Delta v) = \sin^2\theta L h_+ \tag{5.30}$$

Therefore the transfer function (change in pathlength per GW amplitude) is $\sin^2\theta L$.

By inserting $|\Delta\phi_{Mich}|$ and the transfer function for a general opening angle θ of the detector arms into the equations (9.220), (9.234) and (9.122) of [9] and neglecting the efficiency of the photodetector $\eta \approx 1$ we get the shot-noise

$$\sqrt{S_n(f)}\Big|_{shot} = \frac{1}{4\mathcal{F}\sin^2\theta L}\sqrt{\frac{\pi\hbar\lambda_L c}{CP_0}}\sqrt{1 + \left(\frac{f}{f_p}\right)^2}, \tag{5.31}$$

the radiation pressure

$$\sqrt{S_n(f)}\Big|_{rad} = \frac{16\mathcal{F}}{M\sin^2\theta L}\sqrt{\frac{\hbar C P_0}{\pi\lambda_L c}}\frac{1}{(2\pi f)^2\sqrt{1 + \left(\frac{f}{f_p}\right)^2}}, \tag{5.32}$$

and the optical read-out noise is thus given by:

$$S_n(f)|_{opt} = S_n(f)|_{shot} + S_n(f)|_{rad}. \tag{5.33}$$

We will use this last result as the main component of the total noise, for an opening angle θ ($\pi/3$ for ET and $\pi/2$ for LIGO-like detectors).

Each ET detector consists of a high- (HF) and a low- (LF) frequency detector which are then used as one to broaden the frequency range. The detector characteristics of these two detectors are listed in Tab. 5.1 and will be used throughout this paper. The values we are using for advanced LIGO are summarized in Tab. 5.2.

Quantity	ET-HF	ET-LF
Input power (after IMC) P_0	500 W	3 W
Laser wavelength λ_L	1064 nm	1550 nm
Arm length L	10 km	10 km
Mirror mass M	200 kg	211 kg
Finesse $\mathscr{F}$	880	880
Recycling gain C	21.6	21.6

Table 5.1: *Detector characteristics of the high- (HF) and the low- (LF) frequency detectors, taken from the Einstein Telescope proposal [78], section 5.1*

Quantity	aLIGO
Input power (at PRM) P_0	up to 125 W
Laser wavelength λ_L	1064 nm
Arm length L	4 km
Mirror mass M	40 kg
Finesse $\mathscr{F}$	450
Recycling gain C	38

Table 5.2: *Detector characteristics of the aLIGO detectors, taken from [87], and C from [88]*

Overlap Reduction Functions $\gamma^M_{I,J}(f)$

The angular dependence of the pattern functions $F_A(\hat{\Omega})$ can be split into the relative orientation of the detectors towards each other and the orientation of an incoming GW with respect to the two-detector cluster. The overlap reduction functions (ORF) account for the relative orientation of the two detectors.
We consider a pair (I,J) of Michelson interferometers on Earth with opening angles ϕ_I and ϕ_J. We denote the direction vectors of the detector arms as $\hat{u}_{I,J}, \hat{v}_{I,J}$ such that $(\hat{u}_{I,J}, \hat{v}_{I,J}, \hat{z}_{I,J})$, with $\hat{z}_{I,J}$ being the direction pointing to the sky, forms a positively oriented frame, as shown in Fig. 5.2. The relative orientation of the detectors can be described by the angles $\sigma_{I,J}$ between the detector arms $\hat{u}_{I,J}$ and the separation vector $\Delta\boldsymbol{x}$, which points from detector I to J.

The direction vectors of the detector arms in the cluster frame are given by:

$$\hat{u}_I = \begin{pmatrix} \cos\sigma_I \\ \sin\sigma_I \\ 0 \end{pmatrix}, \; \hat{v}_I = \begin{pmatrix} \cos(\sigma_I + \phi_I) \\ \sin(\sigma_I + \phi_I) \\ 0 \end{pmatrix}, \; \hat{d} = \frac{1}{\sqrt{2(1-\cos\beta)}} \begin{pmatrix} \sin\beta \\ 0 \\ \cos\beta - 1 \end{pmatrix},$$
$$\hat{u}_J = \begin{pmatrix} \cos\beta\cos\sigma_J \\ \sin\sigma_J \\ -\sin\beta\cos\sigma_J \end{pmatrix}, \; \hat{v}_J = \begin{pmatrix} \cos\beta\cos(\sigma_J + \phi_J) \\ \sin(\sigma_J + \phi_J) \\ -\sin\beta\cos(\sigma_J + \phi_J) \end{pmatrix} \tag{5.34}$$

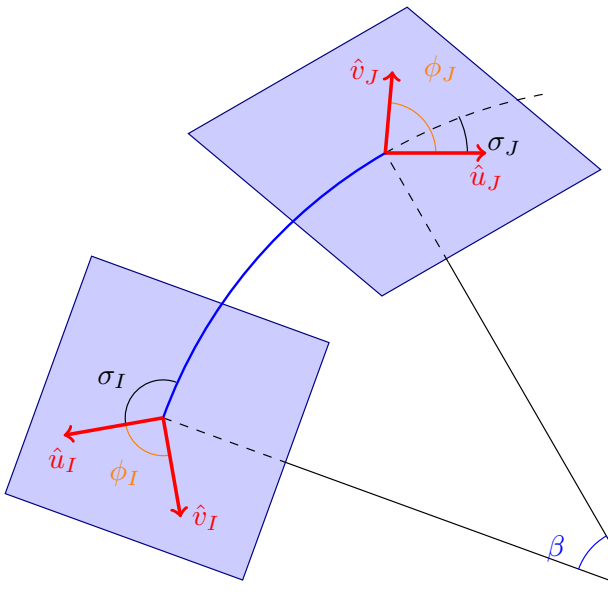

Figure 5.2: *Depiction of the unit vectors of the detector arms $\hat{u}_I, \hat{v}_I, \hat{u}_J, \hat{v}_J$ (red), the opening angles ϕ_I, ϕ_J (orange) and the angles σ_I, σ_J between $\hat{u}_{I,J}$ and the great circle (blue) between the detectors I and J*

The contractions of the two detector tensors are then given by:

$$\begin{aligned}
D_I^{ij} D_{ij}^J &= \frac{1}{2}(\hat{u}_I^i \hat{u}_I^j - \hat{v}_I^i \hat{v}_I^j)\frac{1}{2}(\hat{u}_i^J \hat{u}_j^J - \hat{v}_i^J \hat{v}_j^J) \\
&= \frac{1}{4}\left[(\hat{u}_I \cdot \hat{u}_J)^2 - (\hat{v}_I \cdot \hat{u}_J)^2 - (\hat{u}_I \cdot \hat{v}_J)^2 + (\hat{v}_I \cdot \hat{v}_J)^2\right] \\
&= \frac{1}{4}\Big[(\sin^2\sigma_I - \sin^2(\sigma_I + \phi_I))(\sin^2\sigma_J - \sin^2(\sigma_I + \phi_J)) \\
&\quad + 2\cos\beta(\sin\sigma_I\cos\sigma_I - \sin(\sigma_I + \phi_I)\cos(\sigma_I + \phi_I)) \cdot (\sin\sigma_J\cos\sigma_J - \sin(\sigma_J + \phi_J)\cos(\sigma_J + \phi_J)) \\
&\quad + \cos^2\beta(\cos^2\sigma_I - \cos^2(\sigma_I + \phi_I))(\cos^2\sigma_J - \cos^2(\sigma_J + \phi_J))\Big] \\
&= \frac{1}{4}\Big[(\sin^2\sigma_{1+} - \sin^2\sigma_{1-})(\sin^2\sigma_{2+} - \sin^2\sigma_{2-}) \\
&\quad + \frac{1}{2}\cos\beta(\sin(2\sigma_{1+}) - \sin(2\sigma_{1-}))(\sin(2\sigma_{2+}) - \sin(2\sigma_{2-})) \\
&\quad + \cos^2\beta(\cos^2\sigma_{1+} - \cos^2\sigma_{1-})(\cos^2\sigma_{1+} - \cos^2\sigma_{1-})\Big],
\end{aligned} \tag{5.35}$$

$$\begin{aligned}
D_{I,k}^i D_J^{kj} \hat{d}_i \hat{d}_j &= \frac{1}{4}\left((\hat{u}_I \cdot \hat{d})\hat{u}_I - (\hat{v}_I \cdot \hat{d})\hat{v}_I\right) \cdot \left((\hat{u}_J \cdot \hat{d})\hat{u}_J - (\hat{v}_J \cdot \hat{d})\hat{v}_J\right) \\
&= \frac{1 + \cos\beta}{8}\Big[\frac{1}{4}(\sin(2\sigma_{1+}) - \sin(2\sigma_{1-}))(\sin(2\sigma_{2+}) - \sin(2\sigma_{2-})) \\
&\qquad + \cos\beta(\cos^2\sigma_{1+} - \cos^2\sigma_{1-})(\cos^2\sigma_{2+} - \cos^2\sigma_{2-})\Big],
\end{aligned} \tag{5.36}$$

$$\begin{aligned}
D_I^{ij} D_J^{kl} \hat{d}_i \hat{d}_j \hat{d}_k \hat{d}_l &= \frac{1}{4}\left((\hat{u}_I \cdot \hat{d})^2 - (\hat{v}_I \cdot \hat{d})^2\right)\left((\hat{u}_J \cdot \hat{d})^2 - (\hat{v}_J \cdot \hat{d})^2\right) \\
&= \frac{(1 + \cos\beta)^2}{16}(\cos^2\sigma_{1+} - \cos^2\sigma_{1-})(\cos^2\sigma_{2+} - \cos^2\sigma_{2-}),
\end{aligned} \tag{5.37}$$

with $\sigma_{1+} \coloneqq \sigma_I + \phi_I$, $\sigma_{1-} \coloneqq \sigma_I$, $\sigma_{2+} \coloneqq \sigma_J + \phi_J$ and $\sigma_{2-} \coloneqq \sigma_J$.

Nishizawa et al. [84] have used a different definition of the angles $\sigma_{1,2}$, which is related to our notation by: $\sigma_{1+} = \sigma_1 + \frac{\phi_I}{2}$, $\sigma_{1-} = \sigma_2 - \frac{\phi_I}{2}$, $\sigma_{2+} = \sigma_2 + \frac{\phi_J}{2}$ and $\sigma_{2-} = \sigma_2 - \frac{\phi_J}{2}$.

Finally we get the following expression for the ORF γ_{IJ}^M of the detectors I and J for the polarization M:

$$\begin{aligned}
\gamma_{IJ}^M(f) &= \rho_1^M(\alpha) D_I^{ij} D_{ij}^J + \rho_2^M(\alpha) D_{I,k}^i D_J^{kj} \hat{d}_i \hat{d}_j + \rho_3^M(\alpha) D_I^{ij} D_J^{kl} \hat{d}_i \hat{d}_j \hat{d}_k \hat{d}_l \\
&= \frac{1}{16}\Big\{4\rho_1^M(\sin^2\sigma_{1+} - \sin^2\sigma_{1-})(\sin^2\sigma_{2+} - \sin^2\sigma_{2-}) \\
&+ \left(2\rho_1^M\cos\beta + \rho_2^M\frac{1 + \cos\beta}{2}\right) \cdot (\sin(2\sigma_{1+}) - \sin(2\sigma_{1-}))(\sin(2\sigma_{2+}) - \sin(2\sigma_{2-})) \\
&+ \left(4\rho_1^M\cos^2\beta + 2\rho_2^M(1 + \cos\beta)\cos\beta + \rho_3^M(1 + \cos\beta)^2\right)\} \cdot (\cos^2\sigma_{1+} - \cos^2\sigma_{1-})(\cos^2\sigma_{2+} - \cos^2\sigma_{2-})\Big\},
\end{aligned} \tag{5.38}$$

where we defined the argument α and the relation between the arclength β and the distance $|\boldsymbol{d}|$ by:

$$\alpha(f) \coloneqq \frac{2\pi f |\boldsymbol{d}|}{c}, \quad |\boldsymbol{d}| = 2R_E \sin\frac{\beta}{2}. \tag{5.39}$$

5.3 Einstein Telescope and Earth-based Detectors

As mentionned in the introduction, the Einstein Telescope is going to be part of the third generation of Earth-based detectors, and we thus want to consider several ground based networks involving ET, in order to figure out how

ET can affect the overall sensitivity. The estimation of the maximal achievable sensitivity could be of use for future detector designs and expectations in the constraint of cosmological parameters. In particular, we want to investigate the polarizations of the gravitational background and ET's capability of measuring it.

Symmetry of the Einstein Telescope

Since ET consists of three detectors, one can form three detector pairs which can be used to cross correlate the signal. With the resulting three noise-free signals, one could in principle (as we will see below, for ET those three signals are not independent) solve for the fraction of the power in each polarization mode (tensor T, vector V, scalar S) by using the ORFs.

The fraction in Eq. (5.18) can be rewritten as:

$$\frac{\det \mathbf{F}}{\mathscr{F}_T} = \frac{\begin{vmatrix} F_{TT} & F_{TV} & F_{TS} \\ F_{VT} & F_{VV} & F_{VS} \\ F_{ST} & F_{SV} & F_{SS} \end{vmatrix}}{\begin{vmatrix} F_{VV} & F_{VS} \\ F_{SV} & F_{SS} \end{vmatrix}} = F_{TT} - \frac{F_{VV}F_{TS}^2 - 2F_{VS}F_{TS}F_{TV} + F_{SS}F_{TV}^2}{F_{VV}F_{SS} - F_{VS}^2}. \tag{5.40}$$

This formula was derived via a maximum likelihood method for more than 3 detectors to find 3 modes and is therefore not well defined for 2 detectors, which can be seen by writing out the expression for $\mathscr{F}_T$:

$$\begin{aligned} \mathscr{F}_T &= \sum_{(I,J)} \sum_{(I',J')} \int_0^{T_{obs}} \frac{\gamma_{IJ}^V(t)^2 \gamma_{I'J'}^S(t')^2 - \gamma_{IJ}^V(t)\gamma_{IJ}^S(t)\gamma_{I'J'}^V(t')\gamma_{I'J'}^S(t')}{P_I P_J P_{I'} P_{J'}} dt'dt \\ &= \int_0^{T_{obs}} \frac{\gamma_{IJ}^V(t)^2 \gamma_{IJ}^S(t')^2 - \gamma_{IJ}^V(t)\gamma_{IJ}^S(t)\gamma_{IJ}^V(t')\gamma_{IJ}^S(t')}{P_I^2 P_J^2} dt'dt \quad = 0, \end{aligned} \tag{5.41}$$

where we used that in our case the ORFs are time independent: $\gamma_{IJ}^M(t) = \gamma_{IJ}^M(0)$.

Neglecting for the moment factors of $\frac{T_{obs}}{P_I P_J}$, we find:

$$\begin{aligned} \sqrt{F_{VV}F_{SS}} &\sim \sqrt{\sum_{(I,J)} \sum_{(I',J')} (\gamma_{IJ}^V)^2 (\gamma_{I'J'}^S)^2} = \sqrt{(\gamma_{IJ}^V \gamma_{IJ}^S)^2} = \gamma_{IJ}^V \gamma_{IJ}^S \sim F_{VS} \\ \Rightarrow \frac{\det \mathbf{F}}{\mathscr{F}_T} &= F_{TT} - \frac{(\sqrt{F_{VV}}F_{TS} - \sqrt{F_{SS}}F_{TV})^2}{F_{VV}F_{SS} - F_{VS}^2} \\ &= \frac{T_{obs}}{P_I P_J} \left[(\gamma_{IJ}^T)^2 \quad - \frac{(\gamma_{IJ}^V \gamma_{IJ}^T \gamma_{IJ}^S - \gamma_{IJ}^S \gamma_{IJ}^T \gamma_{IJ}^V)^2}{(\gamma_{IJ}^V)^2 (\gamma_{IJ}^S)^2 - (\gamma_{IJ}^V \gamma_{IJ}^S)^2} \right]. \end{aligned} \tag{5.42}$$

This expression is not well defined since the denominator is zero. In order to see whether the vanishing numerator helps, one has to carefully take the limit of a slightly non-degenerate case. Even if one uses the formula for more than 3 detectors, one should be careful, since the fraction is ill defined as soon as the $\sum_{(I,J)} \gamma_{I,J}^M$ commute, which happens for the 3 ET-detectors due to the fact that they are three identical detectors and their symmetric arrangement leads

to ($P_I = P_J =: P$ for every pair (I,J)):

$$\begin{aligned}
&\gamma_{12}^M = \gamma_{23}^M = \gamma_{31}^M \quad \forall M \in \{T,V,S\} \\
&\Rightarrow\ F_{MM'} = T_{obs}\frac{\gamma_M \gamma_{M'}}{P^2} \qquad (5.43)\\
&\Rightarrow\ \sum_{(I,J)}(\gamma_{IJ}^M)^2 \sum_{(I,J)}(\gamma_{IJ}^{M'})^2 = 9(\gamma_{IJ}^M)^2(\gamma_{IJ}^{M'})^2 \\
&= (\sum_{(I,J)}\gamma_{IJ}^M \gamma_{IJ}^{M'})^2. \qquad (5.44)
\end{aligned}$$

To use the formula for the ET-detector we have to break the symmetry by changing the ORF of one detector pair by a small amount $\epsilon(f)$ and then take the limit:

$$\epsilon(f) \to 0 \quad \forall f.$$

Without loss of generality, we can for example consider the case $M = T$, and we perturb one of the ORFs:

$$\gamma_{12}^M = \gamma_{23}^M = \gamma_{31}^M - \epsilon_M =: \gamma_M \quad \forall M \in \{T,V,S\};$$

When we plug this into the denominator and numerator of the fraction in the right-hand side of Eq. (5.40) we get:

$$\begin{aligned}
\mathscr{F}_T &= F_{VV}F_{SS} - F_{VS}^2 \\
&= \left(\frac{T_{obs}}{P^2}\right)^2 \left(\sum_{(I,J)}(\gamma_{IJ}^V)^2 \sum_{(I,J)}(\gamma_{IJ}^S)^2 - (\sum_{(I,J)}\gamma_{IJ}^V \gamma_{IJ}^S)^2\right) \\
&= 2\left(\frac{T_{obs}}{P^2}\right)^2 (\epsilon_V \gamma_S - \epsilon_S \gamma_V)^2 \qquad (5.45)
\end{aligned}$$

and similarly for the numerator. Plugging these expressions into Eq. (5.40) and taking the limit we arrive at:

$$\begin{aligned}
\frac{\det \mathbf{F}}{\mathscr{F}_T} &= F_{TT} - \frac{F_{VV}F_{TS}^2 - 2F_{VS}F_{TS}F_{TV} + F_{SS}F_{TV}^2}{F_{VV}F_{SS} - F_{VS}^2} \\
&= \frac{T_{obs}}{P^2}\left(\frac{3}{2}\gamma_T\epsilon_T + \frac{3}{2}\gamma_V\gamma_S\epsilon_T\frac{\epsilon_T(\gamma_V\epsilon_S + \gamma_S\epsilon_V)}{(\gamma_V\epsilon_S - \gamma_S\epsilon_V)^2} + 3\gamma_T\gamma_V\gamma_S\epsilon_T\frac{\epsilon_V\epsilon_S}{(\gamma_V\epsilon_S - \gamma_S\epsilon_V)^2}\right) \\
&\quad + \mathscr{O}(\epsilon^2) \ \xrightarrow{\epsilon\to 0}\ 0. \qquad (5.46)
\end{aligned}$$

Due to the symmetry of the Einstein Telescope it is thus impossible to separate the modes out of the signal. The ORFs of each detector pair are the same, since they only depend on their relative orientation. Therefore, the detector correlation matrix Π has a vanishing determinant and the relation between the cross-correlated signals and the modes of the gravitational wave background cannot be inverted:

$$\det\Pi = \begin{vmatrix} \gamma_{12}^T & \gamma_{12}^V & \gamma_{12}^S \\ \gamma_{23}^T & \gamma_{23}^V & \gamma_{23}^S \\ \gamma_{31}^T & \gamma_{31}^V & \gamma_{31}^S \end{vmatrix} = \begin{vmatrix} \gamma_T & \gamma_V & \gamma_S \\ \gamma_T & \gamma_V & \gamma_S \\ \gamma_T & \gamma_V & \gamma_S \end{vmatrix} = 0. \qquad (5.47)$$

Note that even by perturbing the symmetry of ET (slightly changing the arm length or tilting the detector plane), the induced changes are negligible and do not allow the use of ET alone to distinguish between the polarization modes. A detailed calculation of the symmetry breakings can be found in the appendix 5.7.1.

Cross Correlation of Future Earth-based Detectors

We now turn our attention to combinations of ET with other detectors, which are already existing (LIGO, Virgo) or under construction (KAGRA). By adding two additional signals to the ET-cluster we break the symmetry and the

problem mentionned in the previous section is solved. We add the two advanced LIGO detectors in Livingston (LL) and Hanford (LH) to our set of detectors, which results in 6 correlation signals out of which 4 (ET-ET, ET-LL, ET-LH, LL-LH) are independent. This allows us to distinguish the polarization modes, even if one of the detectors could not be used for some reason.

In Fig. 5.3 we compare the noise power spectral densities of ET, LIGO, Virgo and KAGRA and show their combined sensitivity for the polarization modes of a GW signal.

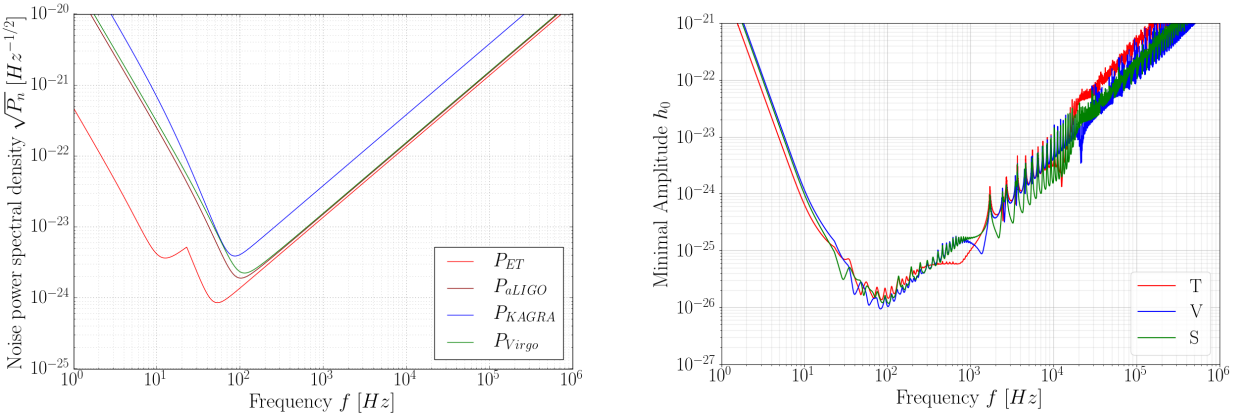

Figure 5.3: *The noise power spectral densities of all involved detectors (left) and the sensitivity of all existing and near future Earth detectors combined (ET, LIGO, Virgo and KAGRA) (right). The minimal achievable sensitivity is considered for a SNR of 8.*

Note that all ET detectors lie in the same plane and are on the scale of Earth at the same position. Should one of the three ET detectors be taken out of the network for any reason, the directions in which its arms were pointing are still covered by the neighbouring detectors. This is why the sensitivity would not be significantly affected.

Moreover, by considering the addition of Virgo and KAGRA to the network, beside ET and LIGO, we gain slightly gain sensitivity for frequencies above 100 Hz.

5.4 DECIGO and Correlation with Earth Detectors

After having considered the combined sensitivity of a strictly Earth-based network of detectors, we can now investigate the consequences of a future space-borne detector. As already mentionned in the introduction, we focus on the DECIGO project, since the LISA sensitivity lies in a lower frequency range than the Earth detectors, and not overlap of their respective frequency bands would be possible.

Earth-space Network Sensitivity

DECIGO is a space-based experiment, and therefore there is no noise due to vibrations of the ground. Since its sensitive region and the one of ET and LIGO overlap in the frequency range between 10 Hz and 100 Hz, it makes sense to cross correlate their signal to get a higher precision and confidence for the separation of the signal into the three different polarization modes.

The DECIGO experiment consists of four detector clusters. Each cluster is made up by three satellites which form three independent identical Michelson interferometers. One can for example arrange the four clusters in the C3 configuration [81, 82] where two clusters are located at the same position near the Earth (about 1 AU behind the Earth, on the same orbit around the Sun) and form a star shape, and the remaining two form a triangle together with the star-cluster, which has the Sun at its centre. In Fig. 5.4 we compare the noise power spectrum of DECIGO to the ones of ET and LIGO and plot the sensitivity of DECIGO in the C3 configuration.

DECIGO is much more sensitive in the low frequencies than all detectors on Earth combined and is even slightly more sensitive around 10 Hz, which comes in handy when we combine it with Earth detectors. When we add ET and then LIGO to the set of detectors and sum over all combinations of cross-correlations, we get the plots shown in Fig. 5.5.

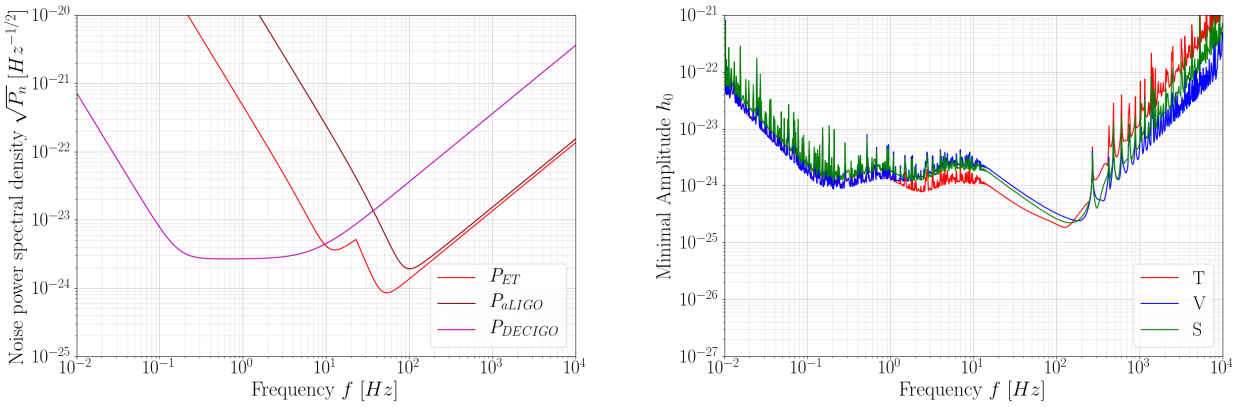

Figure 5.4: *Noise power spectra of a DECIGO, ET and advanced LIGO detector (left) and the sensitivity of DECIGO alone in its C3 configuration (right).*

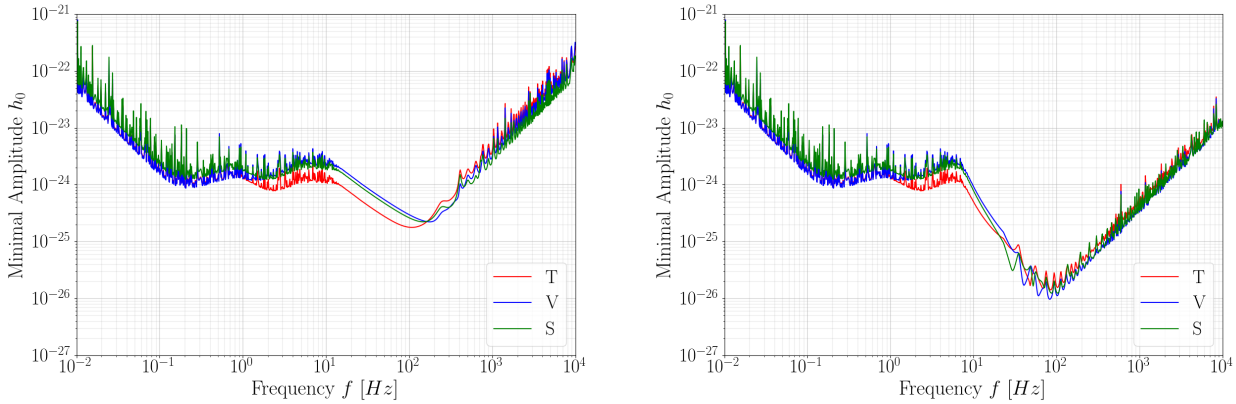

Figure 5.5: *ET and all DECIGO detectors in C3 configuration (left) and together with both LIGO detectors (right), averaged over a total measurement time of one year. The addition of the LIGO detectors significantly improve the sensitivity around* 100 Hz. *Virgo and KAGRA were not included, since the effect is negligible.*

As we can see, ET drags the curves down around 10 Hz and mostly above 100 Hz. In particular, the tensor and scalar modes are affected and become about as sensitive as the vector mode. Together with LIGO the sensitivity is enhanced by one order of magnitude at LIGO's most sensitive frequency range around 100 Hz.

Time-dependent Sensitivity

In the planned C3-configuration of DECIGO we used previously, each cluster rotates around its own axis perpendicular to the detector plane as it rotates around the Sun, such that it returns to its original position after one year. A detector on Earth follows Earth rotation and therefore a relatively quick oscillation of one day superposed to a slow oscillation of one year. This combined change in the orientations of the detectors in a DECIGO-cluster relative to detectors on Earth leads to a time varying sensitivity, which is different for each mode, as can be seen in Fig. 5.6. The time dependence of the sensitivity is independent of the frequency. We plot the sensitivities at 100 Hz, where the DECIGO-Earth detector pairs are most sensitive.

The variation of the sensitivity with time is different if we form the pair with a DECIGO detector close to the Earth or one far away from it. The location of the peaks is also different for DECIGO-Earth pairs, formed with different DECIGO detectors. Changing the detector on Earth however does not matter, since they are almost at the same place viewed on the solar system scale and oscillate much faster, and therefore do not influence the trend on a monthly scale.

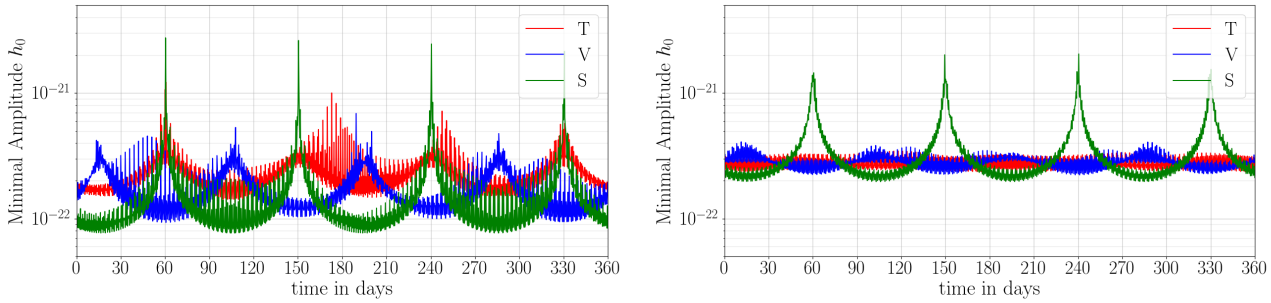

Figure 5.6: *Left: There are two DECIGO detectors in the star cluster, which show the same time dependence when cross correlated with an Earth detector. We take all correlations between those two and all ET and LIGO detectors. Right: In a square configuration, where the four DECIGO clusters are put on a square around the Sun, there is one detector in each of the three clusters which are far away from the Earth, which have the same time dependence when we correlate them with Earth detectors. We form all pairs of these three with ET and LIGO. Both plots correspond to a frequency of* 100 Hz.

We now optimize the sensitivity by combining all detector pairs with a similar time-dependence and average over an integration time of 5 days in order not to lose to much of the variation. For this purpose, we can always form all pairs with the Earth detectors, but we have to be careful which space detectors we pick. If we want to be able to clearly separate the vector mode from the other two, then it makes sense to pick the C3 configuration, because it has many detectors close to Earth. For two of the detectors in the star cluster the correlation with any Earth detector has almost the same time-dependence since their orientation only differs by 30°. In Fig. 5.7 we use all those pairs and integrate over 5 days to increase the sensitivity. Due to the fact that the vector modes time-dependence is phase-shifted with respect to the other two modes, we can easily separate it from the other two in this case.

However, if we rather want to identify the scalar mode, then it makes more sense to move more clusters further away from Earth and at best on the opposite side of the orbit around the Sun, because for detectors which are far away from Earth the scalar mode has large peaks which correspond to blind spots. In this case we could arrange the four DECIGO clusters in a square around the Sun, such that only one cluster is close to Earth, and one is on the opposite side of Earth orbit. We can then arrange the initial orientation of the clusters, such that the peaks for one detector of each of the three clusters far from Earth coincide. Their combined time dependent sensitivity is shown in Fig. 5.8.

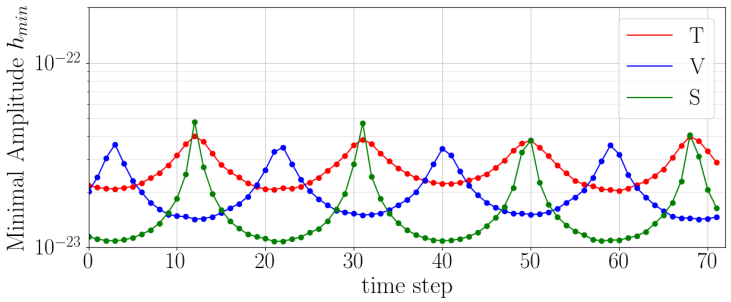

Figure 5.7: *Combined sensitivity of the detector pairs with one of two neighbouring detectors in the star cluster and all ground-based detectors with an integration time of 5 days at a frequency of* 100 Hz *for one year.*

By using the same detectors as previously and combining the data differently, one gets an alternative method to the maximum likelihood method for distinguishing the polarization modes. This can help to check the results and gives a higher confidence on a test of GR, without having to build another experiment.

Note that we performed the samed analysis for a scaled-down version of DECIGO closer to the Earth, B-DECIGO[83]. Although the sensitivity curves are a bit similar as the DECIGO ones, the results of the time dependent sensitivities does not appear to provide good enough differences between the modes. All the details regarding B-DECIGO can be found in the Appendix 5.7.2.

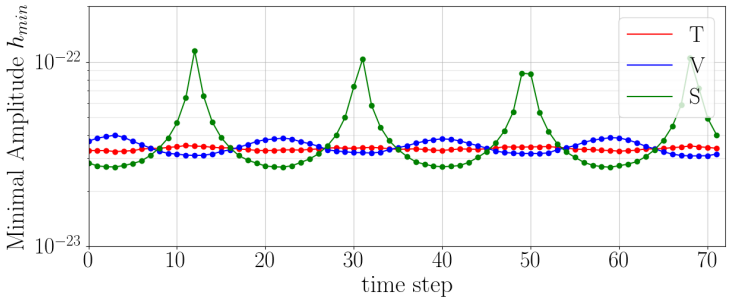

Figure 5.8: *Time dependent sensitivity of detector pairs with one of each of the three clusters far from Earth in the square configuration with all Earth detectors, binned in time with steps of 5 days at a frequency of* 100 Hz *for one year.*

5.5 Gravitational Waves from Point-sources

Until now we have calculated the sensitivity of various combinations of GW-detectors to an isotropic gravitational wave background. Now we attempt to do the same for point sources. Since the signal of a point source is coming from a specific direction, we do not average over all solid angles and our sensitivity becomes direction dependent.

Sensitivity

The derivation of the expression for the signal to noise ratio works in analogy to what we have done in section 5.2. The metric perturbation field at the location of the detector $\boldsymbol{x}_I$ can be described as the sum of all gravitational waves, incident on the detector I, coming from all directions:

$$\begin{aligned} h_{ij}(t,\boldsymbol{x}_I) &= \sum_A \int_{\mathbb{S}^2} h_A(t,\boldsymbol{x}_I,\hat{\Omega}) e^A_{ij}(\hat{\Omega}) d\hat{\Omega} \\ &= \sum_A \int \int_{\mathbb{S}^2} \tilde{h}_A(f,\hat{\Omega}) e^{2\pi i f\left(t-\frac{\hat{\Omega}\cdot\boldsymbol{x}_I}{c}\right)} e^A_{ij}(\hat{\Omega}) d\hat{\Omega} df. \end{aligned} \tag{5.48}$$

For a gravitational wave coming from a point source located at $\hat{\Omega}_0$ in the sky, the frequency-space amplitude takes the form:

$$\tilde{h}_A(f,\hat{\Omega}) = \hat{h}_A(f)\delta(\hat{\Omega}-\hat{\Omega}_0). \tag{5.49}$$

The response of the detector I to an incoming gravitational wave is described by the so called pattern functions F^A_I, which are defined by contracting the basis tensors e^A of the metric perturbations due to GW's for the polarizations $A \in \{+,\times,x,y,b,l\}$ with the detector tensor D_I:

$$F^A_I(\hat{\Omega}) := e^A_{ij}(\hat{\Omega}) D^{ij}_I. \tag{5.50}$$

Therefore, the Fourier transform of the signal is given by:

$$\tilde{h}_I(f) = \sum_A \tilde{h}_A(f) e^{-2\pi i f \frac{\hat{\Omega}_0\cdot\boldsymbol{x}_I}{c}} F^A_I(\hat{\Omega}_0). \tag{5.51}$$

By cross correlating two strains of different detectors (s_I, s_J) we get rid of the noise as seen in Eq. (5.12). Thus, the expectation of the Fourier transform of the two strains is:

$$\mathbb{E}[\tilde{h}^*_I(f)\tilde{h}_J(f')] = \tilde{h}^*_A(f)\tilde{h}_{A'}(f') e^{-\frac{2\pi i}{c}\hat{\Omega}_0\cdot(f\boldsymbol{x}_I - f'\boldsymbol{x}_J)} \cdot F^A_I(\hat{\Omega}_0) F^{A'}_J(\hat{\Omega}_0). \tag{5.52}$$

To maximize the signal to noise ratio, we filter this cross correlated strain with a filter function $\tilde{Q}$:

$$\begin{aligned}\mu &:= \mathbb{E}[Y] = \int \delta_T(f-f')\mathbb{E}[\tilde{h}_I^*(f)\tilde{h}_J(f')]\tilde{Q}(f')df'df \\ &= \int \tilde{h}_A^*(f)\tilde{h}_{A'}(f)e^{-\frac{2\pi i f}{c}\hat{\Omega}_0\cdot(\boldsymbol{x}_I-\boldsymbol{x}_J)}\cdot F_I^A(\hat{\Omega}_0)F_J^{A'}(\hat{\Omega}_0)\tilde{Q}(f)df, \end{aligned} \tag{5.53}$$

where Y is the cross correlated signal:

$$Y := \int_{-\infty}^{\infty}\int_{-\infty}^{\infty}\delta_T(f-f')\tilde{s}_I^*(f)\tilde{s}_J(f')\tilde{Q}(f-f')df'df. \tag{5.54}$$

To find the optimal filter function $\tilde{Q}$ we define a scalar product on the space of smooth complex valued functions $C^\infty(\mathbb{C})$:

$$(A,B) := \int A^*(f)B(f)P_I(|f|)P_J(|f|)df. \tag{5.55}$$

Since the noise power spectra diverge algebraically at the origin and at infinity, we have to restrict our functions A and B to the Schwartz-space $\mathscr{S}(\mathbb{C})$.

We can express the expectation of the correlated signal and its variance in terms of this scalar product:

$$\mu = \left(\tilde{Q}, \frac{\tilde{h}_A^*\tilde{h}_{A'}e^{-\frac{2\pi i f}{c}\hat{\Omega}_0\cdot\Delta\boldsymbol{x}}F_I^AF_J^{A'}}{P_IP_J}\right), \tag{5.56}$$

$$\sigma^2 := \mathbb{V}[Y] = \mathbb{E}[Y^2]-\mathbb{E}[Y]^2 \approx \mathbb{E}[Y^2] = \frac{T}{4}(\tilde{Q},\tilde{Q}), \tag{5.57}$$

where $\Delta\boldsymbol{x} := \boldsymbol{x}_I - \boldsymbol{x}_J$ is the distance vector between the detectors I and J.
The signal to noise ratio is therefore given by:

$$SNR = \frac{\mu}{\sigma} = \frac{\left(\tilde{Q}, \frac{\tilde{h}_A^*\tilde{h}_{A'}e^{-\frac{2\pi i f}{c}\hat{\Omega}_0\cdot\Delta\boldsymbol{x}}F_I^AF_J^{A'}}{P_IP_J}\right)}{\sqrt{\frac{T}{4}(\tilde{Q},\tilde{Q})}}. \tag{5.58}$$

This can be maximized, by choosing the filter function $\tilde{Q}$ parallell to the correlated signal with respect to our scalar product.

$$\tilde{Q} \propto \frac{\tilde{h}_A^*\tilde{h}_{A'}e^{-\frac{2\pi i f}{c}\hat{\Omega}_0\cdot\Delta\boldsymbol{x}}F_I^AF_J^{A'}}{P_IP_J} =: \langle h_I h_J\rangle. \tag{5.59}$$

With a proportionality constant K we get:

$$\begin{aligned} SNR &= \sqrt{\frac{4}{T}}\frac{(K\langle h_Ih_J\rangle, \langle h_Ih_J\rangle)}{\sqrt{(K\langle h_Ih_J\rangle, K\langle h_Ih_J\rangle)}} \\ &= 2\sqrt{T(\langle h_Ih_J\rangle, \langle h_Ih_J\rangle)}. \end{aligned} \tag{5.60}$$

Without loss of generality we can therefore choose $\tilde{Q} = \langle h_Ih_J\rangle$. Finally, we can calculate the maximal possible signal to noise ratio, with this choice of optimal filter function.

$$\begin{aligned} SNR &= 2\sqrt{\frac{1}{T}(\tilde{Q},\tilde{Q})} \\ &= 2\sqrt{\frac{1}{T}\int\frac{(\tilde{h}_A(f)\tilde{h}_{A'}(f)F_I^A(\hat{\Omega}_0)F_J^{A'}(\hat{\Omega}_0))^2}{P_I(|f|)P_J(|f|)}df}. \end{aligned} \tag{5.61}$$

To extract the frequency dependence and the polarization we insert a harmonic wave with amplitude h_0, frequency f and polarization A.

$$\tilde{h}(f) \stackrel{!}{=} h_0 \delta_T(f - f_0)\delta_{A'A}; \tag{5.62}$$

$$\begin{aligned} SNR &= 2\sqrt{T^2 \frac{(|h_0|^2 F_I^A(\hat{\Omega}_0) F_J^A \hat{\Omega}_0)^2}{P_I(|f|)P_J(|f|)}} \\ &= 2T \frac{|h_0|^2 F_I^A(\hat{\Omega}_0) F_J^A(\hat{\Omega}_0)}{\sqrt{P_I(|f|)P_J(|f|)}}. \end{aligned} \tag{5.63}$$

So, we get the minimal amplitude required to detect a gravitational wave with polarization A and at a SNR of at least 8.

$$|h_0^A(f)|_{min} = \sqrt{32} \frac{\sqrt[4]{P_I(|f|)P_J(|f|)}}{\sqrt{T F_I^A(\hat{\Omega}_0) F_J^A(\hat{\Omega}_0)}} \tag{5.64}$$

Determination of Location and Polarizations of Point Sources

If one has more than 8 detector pairs (I, J) (DECIGO would do for example), one can solve for the direction $\hat{\Omega} \simeq (\theta, \phi)$ and all 6 possible polarizations $A \in \{+, \times, x, y, b, l\}$ of an incoming gravitational wave from a point source. We determine the SNR for each quantity under the assumption that the maximum likelihood method is used to calculate them from the at least 8 cross-correlated signals μ_{IJ}. The derivation is analogue to the one given in Nishizawa et al. [85].

The true parameters are denoted by $\boldsymbol{\theta}_{true} = (Y, s_A, \hat{\omega})$:

$$Y_{IJ}(f) = T^{3/2} \left| \sum_A \tilde{s}_A(f) F_I^A(\hat{\omega}) \sum_{A'} \tilde{s}_{A'}(f) F_J^{A'}(\hat{\omega}) \right|. \tag{5.65}$$

The estimated values are $\mu = \langle Y \rangle, h_A = \langle s_A \rangle, \hat{\Omega} = \langle \hat{\omega} \rangle$.

$$\begin{aligned} \mu_{IJ}(f) &= Y_{IJ}(f) + n_{IJ}(f) \\ &= T^{3/2} \left| \sum_A \tilde{h}_A(f) F_I^A(\hat{\Omega}) \sum_{A'} \tilde{h}_{A'}(f) F_J^{A'}(\hat{\Omega}) \right|, \end{aligned} \tag{5.66}$$

where the noise $n_{IJ}(f)$ satisfies:

$$\mathbb{E}[n_{IJ}(f)] = 0\,, \tag{5.67a}$$

$$\mathbb{V}[n_{IJ}(f)] = \frac{T}{4} P_I(f) P_J(f) =: \mathcal{N}_{IJ}(f) \tag{5.67b}$$

Our likelihood function is given by:

$$L(\mu_{IJ}|\boldsymbol{\theta}) = \exp\left[-\sum_{(I,J)} \frac{(Y_{IJ} - \mu_{IJ})^2}{2\mathcal{N}_{IJ}} \right], \tag{5.68}$$

with the parameters $\boldsymbol{\theta} = (\theta, \phi, +, \times, x, y, b, l)$.

The Fisher information matrix can then be calculated as follows:

$$F_{ij} = \mathbb{E}\Big[\big(\partial_{\theta_i} \ln L(\mu_{IJ}|\boldsymbol{\theta})\big) \big(\partial_{\theta_j} \ln L(\mu_{IJ}|\boldsymbol{\theta})\big) \Big], \tag{5.69}$$

$$\mathbf{F} = \begin{pmatrix} F_{\theta\theta} & F_{\theta\phi} & F_{\theta A'} \\ F_{\phi\theta} & F_{\phi\phi} & F_{\phi A'} \\ F_{A\theta} & F_{A\phi} & F_{AA'} \end{pmatrix}. \tag{5.70}$$

To simplify the notation, we define: $\alpha' \coloneqq \frac{2\pi f}{c}$. We now calculate the $\theta\theta$- and the θA-components for a GW with polarization A_0:

$$\begin{aligned} F_{\theta\theta}|_{h=h_{A_0}} &= \mathbb{E}\big[(\partial_\theta \ln L)^2\big]\big|_{h=h_{A_0}} = \mathbb{E}\left[\left(\sum_{(I,J)} \frac{1}{\mathscr{N}_{IJ}}(Y_{IJ}-\mu_{IJ})T^3|\tilde{h}_{A_0}|^2\partial_\theta F_I^{A_0}F_J^{A_0}\right)^2\right] \\ &= \sum_{(I,J)} \frac{1}{\mathscr{N}_{IJ}^2}\underbrace{\mathbb{E}\big[(Y_{IJ}-\mu_{IJ})^2\big]}_{=\mathscr{N}_{IJ}} T^3\left(|\tilde{h}_{A_0}|^2\partial_\theta F_I^{A_0}F_J^{A_0}\right)^2 \\ &\quad + \sum_{(I,J)\neq(I',J')} \frac{1}{\mathscr{N}_{IJ}\mathscr{N}_{I'J'}}\underbrace{\mathbb{E}[(Y_{IJ}-\mu_{IJ})(Y_{I'J'}-\mu_{I'J'})]}_{=0} T^3\left(|\tilde{h}_{A_0}|^2\partial_\theta F_I^{A_0}F_J^{A_0}\right)\left(|\tilde{h}_{A_0}|^2\partial_\theta F_{I'}^{A_0}F_{J'}^{A_0}\right) \\ &= \sum_{(I,J)} \frac{T^3}{\mathscr{N}_{IJ}}\left(|\tilde{h}_{A_0}|^2\partial_\theta F_I^{A_0}F_J^{A_0}\right)^2, \end{aligned} \tag{5.71}$$

$$\begin{aligned} F_{\theta A}|_{h=h_{A_0}} &= \mathbb{E}\big[(\partial_\theta \ln L)\big(\partial_{|\tilde{h}_A|^2}\ln L\big)\big]\Big|_{h=h_{A_0}} \\ &= \mathbb{E}\left[\left(\sum_{(I,J)} \frac{1}{\mathscr{N}_{IJ}}(Y_{IJ}-\mu_{IJ})T^{\frac{3}{2}}|\tilde{h}_{A_0}|^2\partial_\theta F_I^{A_0}F_J^{A_0}\right)\left(\sum_{(I,J)} \frac{1}{\mathscr{N}_{IJ}}(Y_{IJ}-\mu_{IJ})T^{\frac{3}{2}}\partial_{|h_A|^2}|\tilde{h}_I\tilde{h}_J|\right)\right|_{h=h_{A_0}}\Bigg] \\ &= \sum_{(I,J)} \frac{T^3}{\mathscr{N}_{IJ}}\left(F_I^AF_J^A + (1-\delta_{AA_0})\frac{1}{2}\left[\frac{(F_I^A)^2F_J^{A_0}}{F_I^{A_0}} + \frac{(F_J^A)^2F_IA_0}{F_J^{A_0}}\right]\right)|\tilde{h}_{A_0}|^2\partial_\theta F_I^{A_0}F_J^{A_0}. \end{aligned} \tag{5.72}$$

A detailed calculation of the matrix elements for the more general case, where we have different integration times for different detectors, can be found in Appendix 5.7.4. We list here the rest of the components again for an A_0 polarization wave:

$$\begin{aligned} F_{\phi\phi} &= \sum_{(I,J)} \frac{T^3}{\mathscr{N}_{IJ}}\left(|\tilde{h}_{A_0}|^2\partial_\phi F_I^{A_0}F_J^{A_0}\right)^2, \\ F_{\theta\phi} &= \sum_{(I,J)} \frac{T^3}{\mathscr{N}_{IJ}}(|\tilde{h}_{A_0}|^2)^2\left(\partial_\theta F_I^{A_0}F_J^{A_0}\right)\left(\partial_\phi F_I^{A_0}F_J^{A_0}\right), \\ F_{\phi A} &= \sum_{(I,J)} \frac{T^3}{\mathscr{N}_{IJ}}\left(F_I^AF_J^A + (1-\delta_{AA_0})\frac{1}{2}\left[\frac{(F_I^A)^2F_J^{A_0}}{F_I^{A_0}} + \frac{(F_J^A)^2F_I^{A_0}}{F_J^{A_0}}\right]\right)|\tilde{h}_{A_0}|^2\partial_\phi F_I^{A_0}F_J^{A_0}, \\ F_{AA'} &= \sum_{(I,J)} \frac{T^3}{\mathscr{N}_{IJ}}\left(F_I^AF_J^A + (1-\delta_{AA_0})\frac{1}{2}\left[\frac{(F_I^A)^2F_J^{A_0}}{F_I^{A_0}} + \frac{(F_J^A)^2F_I^{A_0}}{F_J^{A_0}}\right]\right) \\ &\qquad \cdot\left(F_I^{A'}F_J^{A'} + (1-\delta_{A'A_0})\frac{1}{2}\left[\frac{(F_I^{A'})^2F_J^{A_0}}{F_I^{A_0}} + \frac{(F_J^{A'})^2F_I^{A_0}}{F_J^{A_0}}\right]\right). \end{aligned} \tag{5.73}$$

The inverse of the Fisher matrix is the covariance matrix, which has the variance of θ_i in the i-th diagonal entry. So, the square of the *SNR* for measuring polarization A is given by:

$$\begin{aligned} SNR_A^2 &\coloneqq \frac{(|\tilde{h}_A|^2)^2}{\sigma_A^2}\bigg|_{h=h_A} = \frac{(|\tilde{h}_A|^2)^2}{(\mathbf{F}^{-1})_{AA}}\bigg|_{h=h_A} \\ &= \frac{(|\tilde{h}_A|^2)^2\det\mathbf{F}}{\mathscr{F}_A}\bigg|_{h=h_A}, \end{aligned} \tag{5.74}$$

where $\mathscr{F}_{\theta_i}$ is the determinant of the minor one gets from removing the i-th row and column from the Fisher matrix $\mathbf{F}$. The SNR of the cross correlation is related to the one of amplitude by:

$$SNR[\mu] = SNR[h^2] = SNR^2[h]. \tag{5.75}$$

Again, demanding an $SNR[h]$ of at least 8 gives us the minimal amplitude. We can read off the prefactors by comparing with the result for one detector pair above:

$$|\tilde{h}_A|_{min} = \sqrt{\frac{32}{T}} \sqrt[4]{\left|\frac{\mathscr{F}_A}{\det \mathbf{F}}\right|_{h=h_A}}. \tag{5.76}$$

The variance of the position in the sky is given by:

$$\mathbb{V}[\theta] = (\mathbf{F}^{-1})_{\theta\theta} = \frac{\mathscr{F}_\theta}{\det \mathbf{F}}, \tag{5.77a}$$

$$\mathbb{V}[\phi] = (\mathbf{F}^{-1})_{\phi\phi} = \frac{\mathscr{F}_\phi}{\det \mathbf{F}}. \tag{5.77b}$$

It turns out that the angular pattern functions of the breathing and the longitudinal modes are proportional to each other: $F_I^l = -\sqrt{2}F_I^b$. Therefore it is impossible to distinguish these two with laser interferometry, and we therefore focus on the distinction between the 4 tensor and vector polarizations and the scalar mode. From now on we use the polarization A as:

$$A \in \{+, \times, x, y, S\}. \tag{5.78}$$

In our calculations, we only use one cluster out of all the DECIGO clusters, namely the one closest to Earth ($\phi = -20°$ from the Earth position, on its orbit around the Sun). We keep including ET and the already existing LIGO detectors. We use the HEALPix pixelization scheme to evenly distribute n points on the sky and then average over the h_{min} values for each f and obtain the frequency dependant behaviour of the average sensitivity of ET, LIGO and DECIGO in Fig. 5.9.

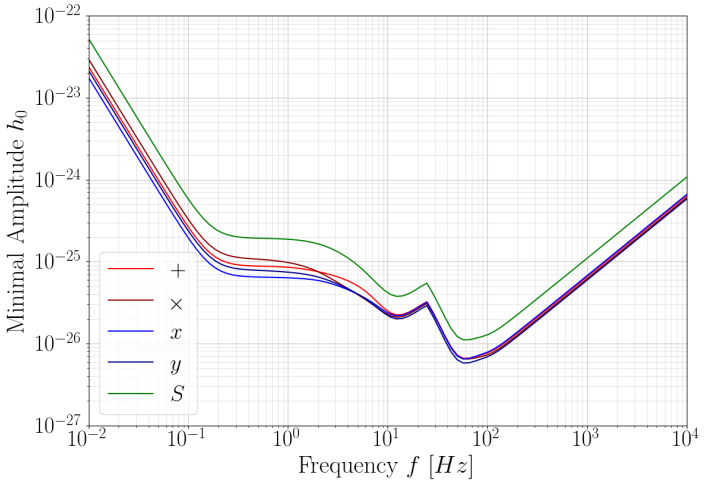

Figure 5.9: *Frequency dependent sensitivity of ET, LIGO and DECIGO towards the polarizations $A \in \{+, \times, x, y, S\}$.*

There are two aspects of the frequency dependent standard deviation of θ and ϕ. One is that if one measures a signal with a certain amplitude, then we can measure the position of the source more precisely if it emits GW in frequencies in which we are more sensitive. We plot this in Fig. 5.10. The other aspect is that the standard deviations vary with the frequency, relative to the sensitivity at that frequency. This means that if we consider for instance a wave which has twice the minimal amplitude for each frequency, we still get frequency dependence. In Fig. 5.10 (below) we take $h = 2|h_S|_{min}(f)$ since it is always higher than the other polarizations and we can therefore detect it, no matter which

polarization we choose and for any fixed frequency we have the same amplitude for all polarizations. This allows us to compare the polarizations with each other.

In Fig.5.11, we give the direction dependent sensitivities using Eq. (5.76), along with the angular resolution for waves with these polarizations by taking the square root of Eqs.(5.77a)-(5.77b) at a frequency of 100 Hz, where our set of detectors is most sensitive. We do a similar procedure at 10 Hz and 1 Hz, and the results are given in Fig. 5.12 and 5.13. Note that the purple zones correspond to true poles.

5.6 Conclusion

The Einstein Telescope alone cannot be used to distinguish between GW polarization modes, and small changes in its geometry lead to no almost no difference. However, by combining ET with second generation detectors such as LIGO, VIRGO and KAGRA, one can detect a GW background with a strain amplitude down to 10^{-26} and distinguish its polarization modes around a frequency of 100 Hz. One can enhance the sensitivity for lower frequencies by cross correlating the network with the DECIGO detector, especially in its C3 configuration. In that case, the observation window is enhanced and allow measurement of strains below 10^{-23}, down to 10^{-26}, in a frequency band from 0.1 Hz to 10 kHz.

It is possible to use an alternative method to distinguish the modes by using the time dependence of the signals. Using the right detector pairs, one can then clearly distinguish the scalar and vector modes by the blind spots. The effect is quite significant over a time period of one year for a ground-space network of detectors involving DECIGO, ET and LIGO. In the case of a scaled-down B-DECIGO detector, the time dependence is however very chaotic, due to the angular frequency around Earth which is then an irrational fraction of Earth rotation, and the distance to Earth detectors, which is varying significantly. The sensitivities of the different modes are too close together, whenever the detectors are too close to Earth. This can be resolved however if one chooses an orbit on a higher altitude such that it circles the Earth once a day. In that case the method becomes more complicated than with the original DECIGO, but is still feasible.

We have thus showed that second and third generation detectors, combined with space-detectors, can provide two different methods to test GR or contrain alternative theories by measuring the polarization of a GW background.

In a future project, one could investigate the possibilities of detecting inhomogeneities in the GW background, analogue to the ones in the cosmic microwave background. Up to now we only calculated the minimal strain of a GW to be detected, but to find out how large the deviation from the mean would have to be to detect them, we would have to deal with the variance of the parameter estimation. It would be interesting to find out what angular resolution one could get with various detector combinations.

Gravitational waves should travel undisturbed since Planck time, which would make it possible to measure properties of the early quantum gravitational universe directly. This could give us valuable hints on the search of a unifying theory. This advantage of GW over the electromagnetic ones also has its disadvantages. Due to the enormous density of the early universe, many emissions of GW would be expected from different epochs after the Big Bang, and the difficulty would be to distinguish a signal of an earlier epoch from a later one. Overcoming that problem could however allow to establish a complete gravitational map of the beginning of our universe.

5.6 Acknowledgments

L.P. was supported by the UZH research grant FK-17-097. P.J. thanks the Swiss National Foundation for support.

5.7 Appendix

ET Perturbations

We have seen in section 5.3 that one cannot distinguish between the three polarization modes with the ET alone, although we have three signals, because of the symmetric arrangement of the three interferometers composing ET.

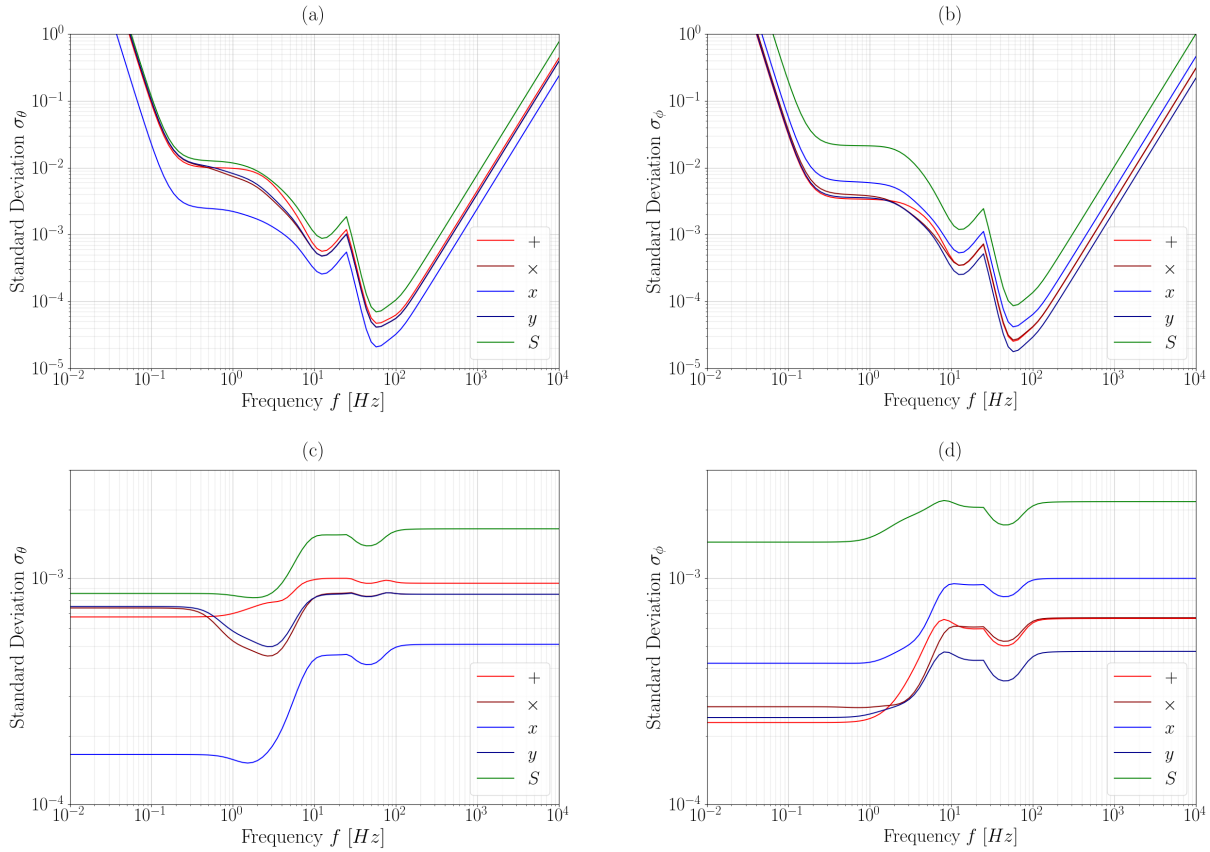

Figure 5.10: *Frequency dependent standard deviation of θ and ϕ for (a)-(b): a GW with amplitude $h = 10^{-25}$ and (c)-(d): for twice the minimal amplitude of the scalar mode $h = 2|h_S|_{min}$, see Fig. 5.9.*

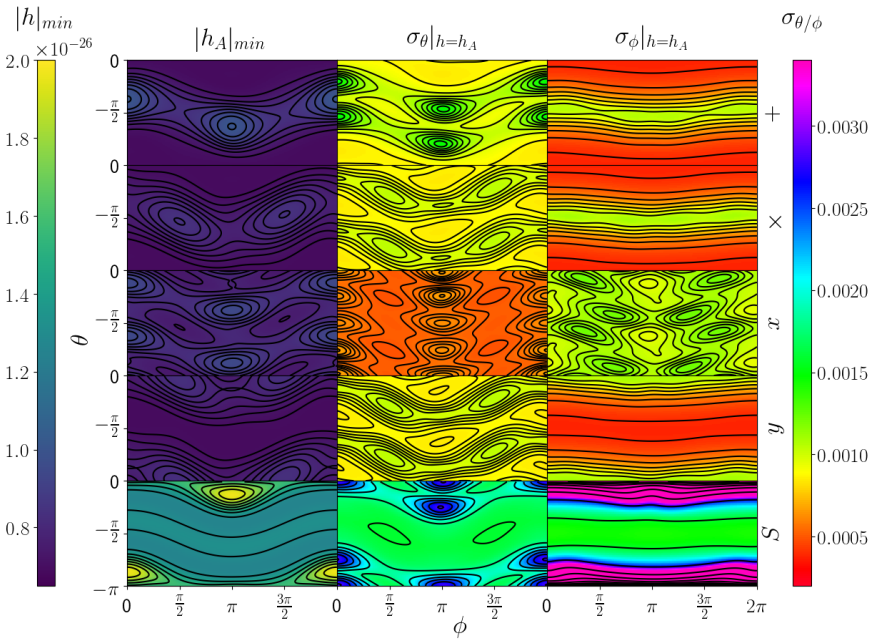

Figure 5.11: *Sensitivity of ET, LIGO and DECIGO at* 100 Hz *towards the polarizations $A \in \{+, \times, x, y, S\}$ in the left column. Standard deviation of the θ and ϕ angle for a GW with polarization A and amplitude of $h_A = 2.6 \cdot 10^{-26}$ in the middle and right column respectively.*

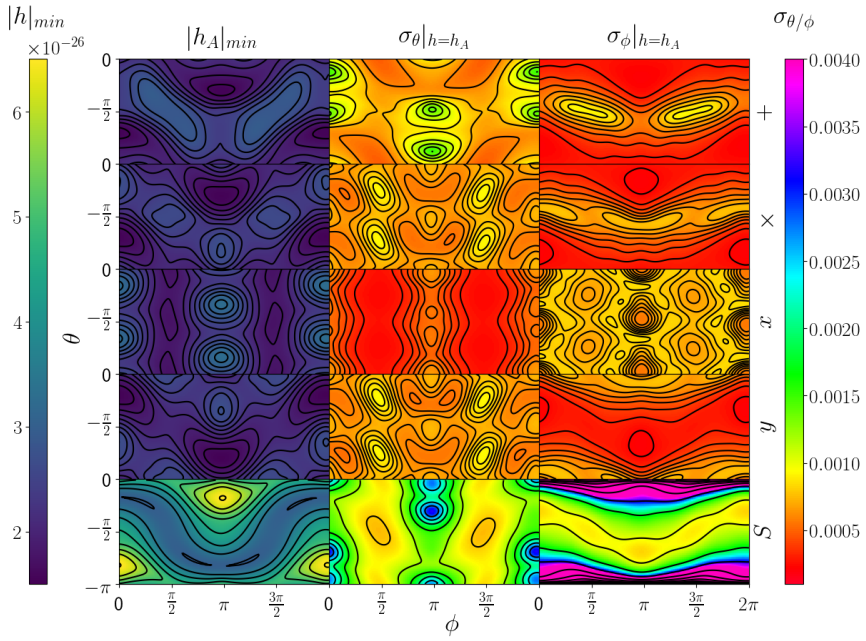

Figure 5.12: *Sensitivity of ET, LIGO and DECIGO at* 10 Hz *towards the polarizations* $A \in \{+, \times, x, y, S\}$ *in the left column. Standard deviation of the* θ *and* ϕ *angle for a GW with polarization A and amplitude of* $h_A = 8.9 \cdot 10^{-26}$ *in the middle and right column respectively.*

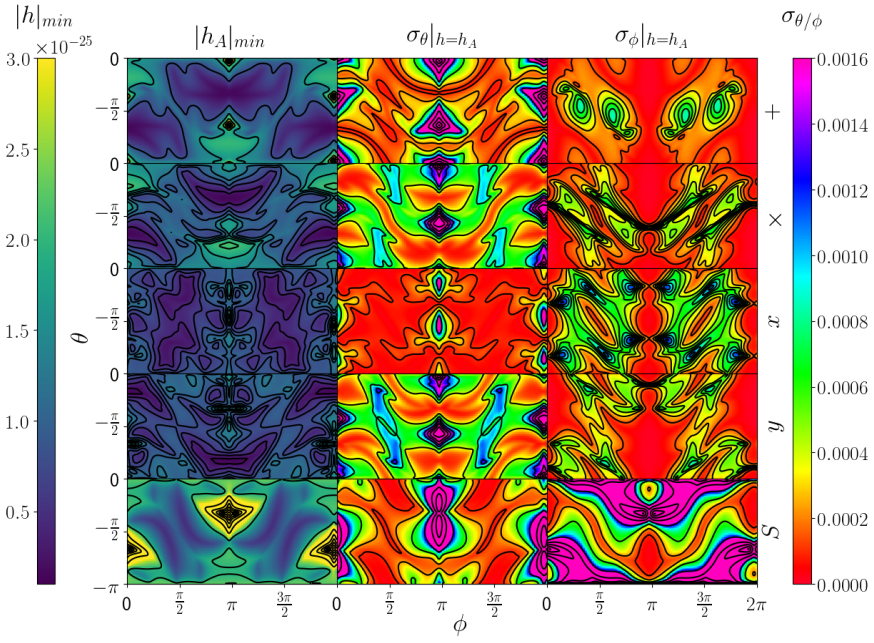

Figure 5.13: *Sensitivity of ET, LIGO and DECIGO at* 1 Hz *towards the polarizations* $A \in \{+, \times, x, y, S\}$ *in the left column. Standard deviation of the* θ *and* ϕ *angle for a GW with polarization A and amplitude of* $h_A = 3.8 \cdot 10^{-25}$ *in the middle and right column respectively.*

One has thus to break the symmetry in order to make the three rows in the detector correlation matrix independent. We are going to consider two ways of doing that perturbatively and use the framework of the previous section to determine their impact on the sensitivity, which will allow us to compare both methods.

Irregular Triangle

We make one opening angle smaller by a small angle ϵ_ϕ and make another angle bigger by the same amount, which leaves the third angle unchanged. We now have a completely irregular triangle with three different angles and therefore the ORFs of all three detector pairs become different, and the detector correlation matrix becomes invertible.

Changing the angles will also change the arm lengths and therefore the distance between a detector pair. We use the sine-law to determine the impact of a change in the angles on the change in the distance δ. To estimate the order of magnitude of effect of the perturbation on the detector correlation matrix, we calculate the change in the ORF of the detector pair $(1,2)$, when we shrink the angle ϕ_3 and enlarge ϕ_1 by ϵ_ϕ, which leaves ϕ_2 unchanged but shortens d_{12}:

$$\frac{d-\delta}{\sin(\phi_3)} = \frac{d}{\sin(\phi_1)}\,,\;\; \phi_3 = \phi - \epsilon_\phi\,,\;\; \phi_1 = \phi + \epsilon_\phi \tag{5.79}$$

for $\phi = \pi/3$. To first order we get:

$$\delta \approx \sqrt{3} d \epsilon_\phi. \tag{5.80}$$

With that expression, we can relate the effects of a change in the distance to the change in the angles:

$$\rho_i^M \mapsto (\rho_i^M)^{(0)} - \sqrt{3}\alpha(\rho_i^M)'\epsilon_\phi, \tag{5.81}$$

$$\cos\beta \mapsto \cos\beta^{(0)} + \sqrt{3}\frac{d^2}{R_E^2}\epsilon_\phi. \tag{5.82}$$

The only coordinate angle that changes is σ_{1+}. Therefore, we insert the values of the other angles:

$$\sigma_{1-} = 0\,,\quad \sigma_{1+} \mapsto \sigma_{1+}^{(0)} + \epsilon_\phi\,,\quad \sigma_{1+}^{(0)} = \frac{\pi}{3}, \tag{5.83}$$

$$\sigma_{2-} = \frac{2\pi}{3}\,,\quad \sigma_{2+} = \pi; \tag{5.84}$$

in Eq. (5.38) to get the new ORF:

$$\begin{aligned}
\gamma_{12}^M = \frac{1}{16}\Bigg\{ & -3\rho_1^M \sin^2\sigma_{1+} + \frac{\sqrt{3}}{2}\left[2\rho_1^M\cos\beta + \rho_2^M\frac{1+\cos\beta}{2}\right]\sin(2\sigma_{1+}) \\
& + \frac{3}{4}\left[4\rho_1^M\cos^2\beta + 2\rho_2^M(1+\cos\beta)\cos\beta + \rho_3^M(1+\cos\beta)^2\right](\cos^2\sigma_{1+} - 1)\Bigg\} \\
\mapsto \frac{1}{16}\Bigg\{ & -3\left((\rho_1^M)^{(0)} - \sqrt{3}\alpha(\rho_1^M)'\epsilon_\phi\right)\left(\sin^2\sigma_{1+}^{(0)} + 2\sin\sigma_{1+}^{(0)}\cos\sigma_{1+}^{(0)}\epsilon_\phi\right) \\
& + \frac{\sqrt{3}}{2}\Bigg[2\left((\rho_1^M)^{(0)} - \sqrt{3}\alpha(\rho_1^M)'\epsilon_\phi\right)\left(\cos\beta^{(0)} + \sqrt{3}\frac{d^2}{R_E^2}\epsilon_\phi\right) \\
& + \frac{1}{2}\left((\rho_2^M)^{(0)} - \sqrt{3}\alpha(\rho_2^M)'\epsilon_\phi\right)\left(1 + \cos\beta^{(0)} + \sqrt{3}\frac{d^2}{R_E^2}\epsilon_\phi\right)\Bigg]\left(\sin(2\sigma_{1+}^{(0)}) + 2\cos(2\sigma_{1+}^{(0)})\epsilon_\phi\right) \\
& + \frac{3}{4}\Bigg[4\left((\rho_1^M)^{(0)} - \sqrt{3}\alpha(\rho_1^M)'\epsilon_\phi\right)\left(\cos\beta^{(0)} + \sqrt{3}\frac{d^2}{R_E^2}\epsilon_\phi\right)^2 \\
& + 2\left((\rho_2^M)^{(0)} - \sqrt{3}\alpha(\rho_2^M)'\epsilon_\phi\right)\left(1 + \cos\beta^{(0)} + \sqrt{3}\frac{d^2}{R_E^2}\epsilon_\phi\right)\left(\cos\beta^{(0)} + \sqrt{3}\frac{d^2}{R_E^2}\epsilon_\phi\right) \\
& + \left((\rho_3^M)^{(0)} - \sqrt{3}\alpha(\rho_3^M)'\epsilon_\phi\right)\left(1 + \cos\beta^{(0)} + \sqrt{3}\frac{d^2}{R_E^2}\epsilon_\phi\right)^2\Bigg]\left(\cos^2\sigma_{1+}^{(0)} - 2\cos\sigma_{1+}^{(0)}\sin\sigma_{1+}^{(0)}\epsilon_\phi - 1\right)\Bigg\}.
\end{aligned} \tag{5.85}$$

We can simplify this expression, by plugging in the values for $\sigma_{1+}^{(0)}$ and approximating $\cos\beta^{(0)}$, using the fact that $\frac{d^2}{R_E^2} = 2.5 \cdot 10^{-6} \ll 1$:

$$\cos\beta^{(0)} = 1 - \frac{d^2}{2R_E^2} \approx 1. \tag{5.86}$$

To first order in ϵ_ϕ we get:

$$\begin{aligned}\epsilon_M &\approx \frac{1}{16}\left\{-\frac{3\sqrt{3}}{2}\left[(\rho_1^M)^{(0)} - \frac{3}{2}\alpha(\rho_1^M)'\right] - \frac{\sqrt{3}}{2}\left[2(\rho_1^M)^{(0)} + 3\alpha(\rho_1^M)' + (\rho_2^M)^{(0)} + \frac{3}{2}\alpha(\rho_2^M)'\right]\right. \\ &\quad \left. -\frac{3\sqrt{3}}{4}\left[2\left((\rho_1^M)^{(0)} + (\rho_2^M)^{(0)} + (\rho_3^M)^{(0)}\right) - 3\alpha\left((\rho_1^M)' + (\rho_2^M)' + (\rho_3^M)'\right)\right]\right\}\epsilon_\phi \\ &\approx -\frac{\sqrt{3}}{32}\left\{8(\rho_1^M)^{(0)} + 4(\rho_2^M)^{(0)} + 3(\rho_3^M)^{(0)} - 3\alpha\left(2(\rho_1^M)' + (\rho_2^M)' + \frac{3}{2}(\rho_3^M)'\right)\right\}\epsilon_\phi. \end{aligned} \tag{5.87}$$

In Fig. 5.14 we plot the response factor, which multiplies to ϵ_ϕ to get the change in the ORF ϵ_M.

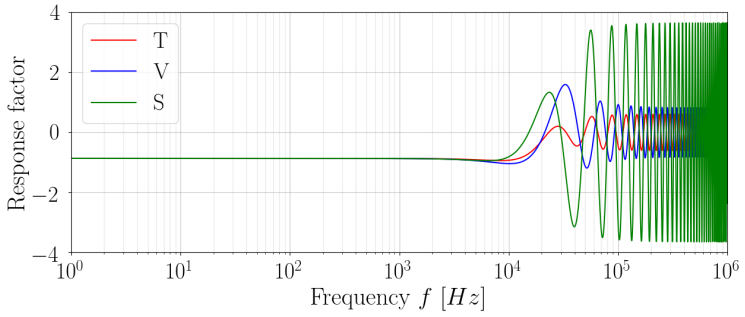

Figure 5.14: *The factor with which the ORF responds to a small change in the detector angles.*

The response factor stays almost constant at a value of -0.87, since $\alpha \ll 1$ until we get close to the critical frequency $f_{crit} = 3 \times 10^4$ Hz, defined over $\frac{f_{crit} d}{c} := 1$.

Tilted Detector Planes

Now we leave the angles and the arm-lengths of the three Michelson-interferometers invariant but tilt the plane in which one of the three detectors lies. We tilt the plane of detector 1, such that $\hat{u}_1$ gets tilted in negative z-direction. The other detector arms stay unchanged ($\hat{u}_J = \hat{u}_J^{(0)}$ for $J \neq 1$ and $\hat{v}_J = \hat{v}_J^{(0)}$ for all J), and we can write the perturbation as:

$$\hat{u}_1 \mapsto \hat{u}_1^{(0)} + \delta\hat{u}_1\,, \quad \delta\hat{u}_1 = \begin{pmatrix} 0 \\ 0 \\ -\delta u \end{pmatrix}. \tag{5.88}$$

The angle α by which $\hat{u}_1$ is rotated can be approximated by:

$$\alpha \approx \sin\alpha \approx \delta u. \tag{5.89}$$

We calculate the contractions of the perturbed detector tensors, analogue to Eqs. (5.35)-(5.37) to first order in δu:

$$\begin{aligned} D_1^{ij} D_{ij}^2 &= \frac{1}{4}\left[(\hat{u}_1^{(0)} \cdot \hat{u}_2 + \delta\hat{u}_1 \cdot \hat{u}_2)^2 - (\hat{v}_1 \cdot \hat{u}_2)^2 - (\hat{u}_1^{(0)} \cdot \hat{v}_2 + \delta\hat{u}_1 \cdot \hat{v}_2)^2 + (\hat{v}_1 \cdot \hat{v}_2)^2\right] \\ &\approx \frac{1}{4}(D_1^{ij} D_{ij}^2)^{(0)} + \frac{1}{2}\left[(\hat{u}_1^{(0)} \cdot \hat{u}_2)(\delta\hat{u}_1 \cdot \hat{u}_2) - (\hat{u}_1^{(0)} \cdot \hat{v}_2)(\delta\hat{u}_1 \cdot \hat{v}_2)\right]. \end{aligned}$$

Using the angles for ET as in Eq. (5.84) we get:

$$\begin{aligned}
\delta(D_1^{ij}D_{ij}^2) &= \frac{1}{2}\left[(\cos\beta\cos\sigma_{1-}\cos\sigma_{2-}+\sin\sigma_{1-}\sin\sigma_{2-})\delta u\sin\beta\cos\sigma_{2-}\right.\\
&\quad\left.-(\cos\beta\cos\sigma_{1-}\cos\sigma_{2+}+\sin\sigma_{1-}\sin\sigma_{2+})\delta u\sin\beta\cos\sigma_{2+}\right]\\
&= \frac{1}{2}\cos\beta\sin\beta(\cos^2\sigma_{2-}-1)\delta u = -\frac{3}{8}\cos\beta\sin\beta\delta u, \qquad (5.90)\\
D_{1,k}^i D_2^{kj}\hat{d}_i\hat{d}_j &= \frac{1}{4}\left((\hat{u}_1^{(0)}\cdot\hat{d}+\delta\hat{u}_1\cdot\hat{d})(\hat{u}_1^{(0)}+\delta\hat{u}_1)-(\hat{v}_1\cdot\hat{d})\hat{v}_1\right)\cdot\left((\hat{u}_2\cdot\hat{d})\hat{u}_2-(\hat{v}_2\cdot\hat{d})\hat{v}_2\right)\\
&\approx (D_{1,k}^i D_2^{kj}\hat{d}_i\hat{d}_j)^{(0)}+\frac{1}{4}\left((\delta\hat{u}_1\cdot\hat{d})\hat{u}_1^{(0)}+(\hat{u}_1^{(0)}\cdot\hat{d})\delta\hat{u}_1\right)\cdot\left((\hat{u}_2\cdot\hat{d})\hat{u}_2-(\hat{v}_2\cdot\hat{d})\cdot\hat{v}_2\right),\\
\delta(D_{1,k}^i D_2^{kj}\hat{d}_i\hat{d}_j) &= \frac{1}{8(1-\cos\beta)}\left(\delta u(1-\cos\beta)\hat{u}_1^{(0)}+\cos\sigma_{1-}\sin\beta\delta\hat{u}_1\right)\cdot(\sin\beta\cos\sigma_{2-}\hat{u}_2-\sin\beta\cos\sigma_{2+}\hat{v}_2)\\
&= \frac{\sin\beta}{8}\left(\cos\sigma_{2-}\underbrace{\cos\beta\cos\sigma_{2-}}_{\hat{u}_1^{(0)}\cdot\hat{u}_2}-\underbrace{\cos\beta}_{\hat{u}_1^{(0)}\cdot\hat{v}_2}\right)\delta u+\frac{1+\cos\beta}{8}\left(\cos\sigma_{2-}\underbrace{\delta u\sin\beta\cos\sigma_{2-}}_{\delta\hat{u}_1\cdot\hat{u}_2}-\underbrace{\delta u\sin\beta}_{\delta\hat{u}_1\cdot\hat{v}_2}\right)\\
&= \frac{\sin\beta}{8}\left[\cos\beta(\cos^2\sigma_{2-}-1)+(1+\cos\beta)(\cos^2\sigma_{2-}-1)\right]\delta u\\
&= -\frac{\sin\beta}{8}(1+2\cos\beta)\sin^2\sigma_{2-}\delta u = -\frac{3}{4}\frac{\sin\beta}{8}(1+2\cos\beta)\delta u, \qquad (5.91)\\
D_1^{ij}D_2^{kl}\hat{d}_i\hat{d}_j\hat{d}_k\hat{d}_l &= \frac{1}{4}\left((\hat{u}_1^{(0)}\cdot\hat{d}+\delta\hat{u}_1\cdot\hat{d})^2-(\hat{v}_1\cdot\hat{d})^2\right)\left((\hat{u}_2\cdot\hat{d})^2-(\hat{v}_2\cdot\hat{d})^2\right)\\
&= (D_1^{ij}D_2^{kl}\hat{d}_i\hat{d}_j\hat{d}_k\hat{d}_l)^{(0)}+\frac{1}{2}\left((\hat{u}_1^{(0)}\cdot\hat{d})(\delta\hat{u}_1\cdot\hat{d})\right)\left((\hat{u}_2\cdot\hat{d})^2-(\hat{v}_2\cdot\hat{d})^2\right),\\
\delta(D_1^{ij}D_2^{kl}\hat{d}_i\hat{d}_j\hat{d}_k\hat{d}_l) &= \frac{1}{8(1-\cos\beta)^2}\cos\sigma_{1-}\sin\beta\delta u(1-\cos\beta)\left(\sin^2\beta\cos^2\sigma_{2-}-\sin^2\beta\cos^2\sigma_{2+}\right)\\
&= \frac{1+\cos\beta}{8}\sin\beta\left(\cos^2\sigma_{2-}-1\right)\delta u = -\frac{3}{4}\frac{1+\cos\beta}{8}\sin\beta\delta u. \qquad (5.92)
\end{aligned}$$

Finally, we can patch all terms together in order to calculate the perturbation ϵ_M:

$$\begin{aligned}
\epsilon_M &= \rho_1^M\delta(D_1^{ij}D_{ij}^2)+\rho_2^M\delta(D_{1,k}^i D_2^{kj}\hat{d}_i\hat{d}_j)+\rho_3^M\delta(D_1^{ij}D_2^{kl}\hat{d}_i\hat{d}_j\hat{d}_k\hat{d}_l)\\
&= -\frac{3}{8}\sin\beta\left\{\rho_1^M\cos\beta+\frac{1}{4}\rho_2^M(1+2\cos\beta)+\frac{1}{4}\rho_3^M(1+\cos\beta)\right\}\delta u. \qquad (5.93)
\end{aligned}$$

Again, we find that ϵ_M is almost independent of f, but the effect is three orders of magnitude smaller if we tilt one plane, instead of deforming the equilateral triangle.

$$\epsilon_M = 1.2\cdot 10^{-3}\delta u \qquad (5.94)$$

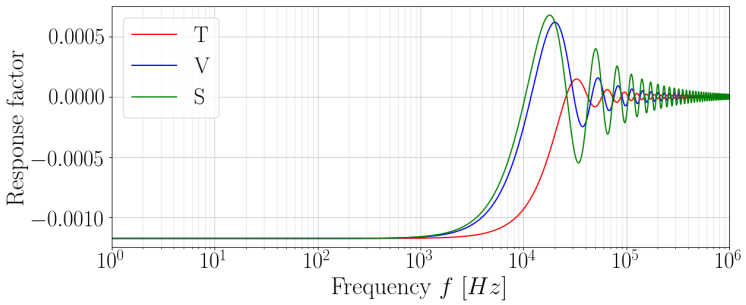

Figure 5.15: *Factor with which the ORF responds to a small tilt of one of the detector planes.*

The response factor for the tilted plane, shown in Fig. 5.15, stays at about -0.001 for frequencies far below f_{crit} and oscillates ever closer around zero for increasing frequencies above 10^5 Hz. Since ET is designed to measure in a frequency range from 1.5 Hz to 10 kHz the oscillations are not relevant. We find that the response to the same small change in the tilt angle is three orders of magnitude smaller than that of the change in the opening angle.

The effect of a perturbation is at best as small as the angle by which we change ET's geometry, in the case of the irregular triangle. As we will argue in the next section, the problem is resolved if one adds additional detectors, for example LIGO, which exists already anyway, and changing the geometry of ET is therefore not worth the effort.

B-DECIGO

The scaled-down detector B-DECIGO[83] orbits around the Earth on an altitude of 2000 km which is on the same order of magnitude as the radius of the Earth (6371 km). If we replace DECIGO by this smalle version, we can see in Fig. 5.16 that the sensitivity gets worse below 10 Hz for all polarizations, as compared to DECIGO.

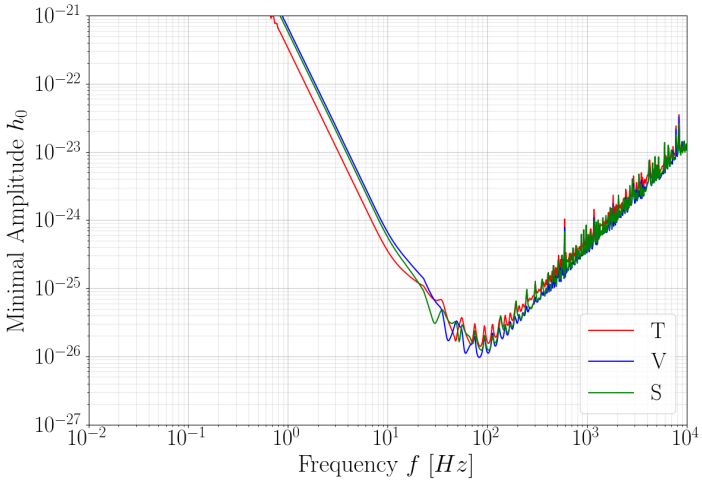

Figure 5.16: *Combined sensitivity of B-DECIGO, ET and both advanced LIGO detectors.*

B-DECIGO circles the Earth in a Sun-synchronous dusk-dawn orbit with an angular frequency of about $8.2 \times 10^{-4}\,s^{-1}$ while Earth rotation corresponds to $7.3 \times 10^{-5}\,s^{-1}$. This leads to rapidly varying distances and directions of the detector arms and the irrational ratio between the two angular velocities leads to a chaotic behaviour, which makes the use of the time dependent sensitivity very complicated. Additionally one can observe that the sensitivities for the different modes get closer together as one moves a space detector closer to Earth.

If one would instead let B-DECIGO take the same type of orbit but on a higher altitude (35 867 km), such that it would circle Earth in one day, one would get almost the same signal every day over a period of about a week, because the change would now be on the time-scale of a year. The detectors would also be far enough from Earth to get relevantly different sensitivity curves for the different modes. The procedure would be more complicated than in the case of DECIGO, but one could still use certain blind spots or other characteristics that only one mode shows. A large disadvantage to DECIGO would also be that one would have to spot those characteristics in a model in advance, since the sensitivities are not periodic.

We compare the time dependent sensitivities of both versions (original B-DECIGO and higher altitude) for time-span of one day in Fig. 5.17.

In Fig. 5.18 we plot the frequency dependent sensitivity of B-DECIGO together with ET and LIGO in the case of point sources. The behaviour is very similar to the one with DECIGO, except that the plateau around 1 Hz is missing. Since B-DECIGO is not as sensitive as DECIGO, it can only increase the sensitivity there a bit.

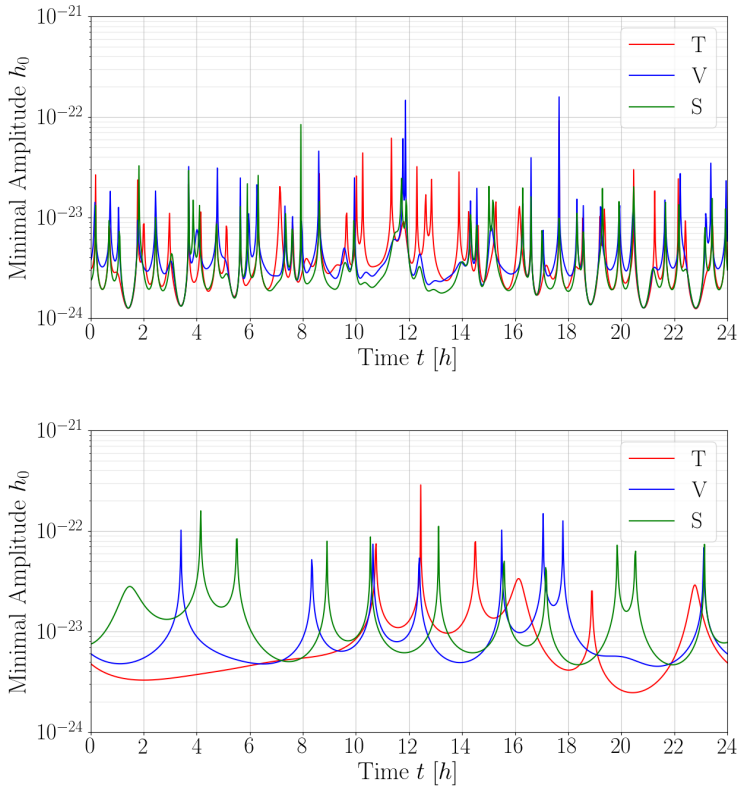

Figure 5.17: *Time dependence of the sensitivity for B-DECIGO for one day (above) and for a higher altitude of* 35 867 km *(below) for a frequency of* 100 Hz.

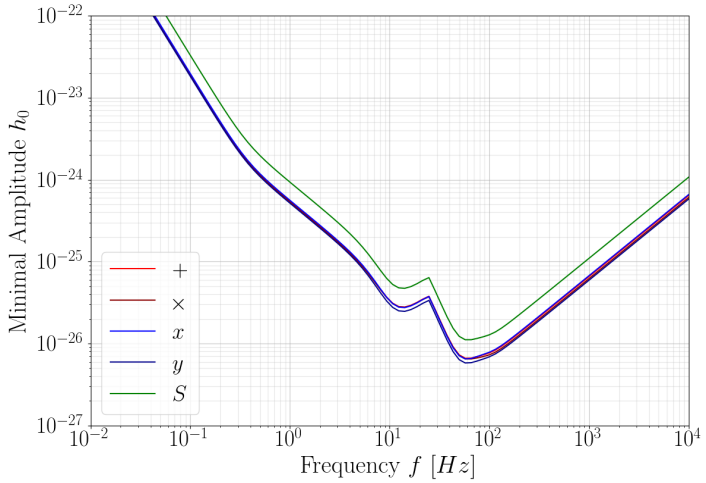

Figure 5.18: *Frequency dependent sensitivity of ET, LIGO and B-DECIGO.*

Delta Distribution Approximation

In this Appendix we give a detailed derivation of the signal to noise ratio for a merger by focusing on the approximations of the Dirac delta distribution and the Fourier transforms. We first use a scalar signal, measured by two detectors, to simplify the calculation and then generalize to a wave with arbitrary polarizations measured by multiple detectors.
In future all GW detectors together could be sensitive enough to measure the in spiral of a binary Black Hole or

neutron star merger, months before the merger event happens. In this case detectors with different distances from the source would have different observation times. This would help to measure the position of the source in the sky:

$$c\Delta T = \hat{\Omega}\cdot\Delta\boldsymbol{x}_{IJ}, \qquad \Delta T = T_I - T_J, \qquad \Delta\boldsymbol{x}_{IJ} = \boldsymbol{x}_I - \boldsymbol{x}_J, \tag{5.95}$$

where T_I and T_J are the observation times of the detectors I and J, $\boldsymbol{x}_I$ and $\boldsymbol{x}_J$ their position vectors and $\hat{\Omega}$ is the direction of travel of the GW.

We define the cross correlated and filtered strain amplitude of the detector pair (I,J) by:

$$Y := \int_{-T_I/2}^{T_I/2}\int_{-T_J/2}^{T_J/2} s_I(t)s_J(t')Q(t-t')dt'dt, \tag{5.96}$$

where Q is the filter function and s_I, s_J are the strains measured by the detectors I,J, which are the sum of the signal h_I and the noise n_I in detector I:

$$s_I(t) = h_I(t) + n_I(t). \tag{5.97}$$

By taking the ensemble average we get rid of the noise terms:

$$\begin{aligned}
\mu &:= \mathbb{E}[Y] \\
&= \int_{-T_I/2}^{T_I/2}\int_{-T_J/2}^{T_J/2} \left\{\mathbb{E}[h_I(t)h_J(t')] + \mathbb{E}[h_I(t)n_J(t')] + \mathbb{E}[n_I(t)h_J(t')] + \mathbb{E}[n_I(t)n_J(t')]\right\} Q(t-t')dt'dt \\
&= \int_{-T_I/2}^{T_I/2}\int_{-T_J/2}^{T_J/2}\int \tilde{h}_I^*(f)e^{2\pi i f\left(t-\frac{\hat{\Omega}\cdot\boldsymbol{x}_I}{c}\right)}df \int \tilde{h}_J(f')e^{-2\pi i f'\left(t'-\frac{\hat{\Omega}\cdot\boldsymbol{x}_J}{c}\right)}df' Q(t-t')dt'dt \\
&= \int \tilde{h}_I^*(f)\tilde{h}_J(f')e^{-\frac{2\pi i}{c}\hat{\Omega}\cdot(f\boldsymbol{x}_I - f'\boldsymbol{x}_J)}\int_{-T_I/2}^{T_I/2}\int_{-T_J/2}^{T_J/2} Q(t-t')e^{-2\pi i(f't'-ft)}dt'dtdf'df,
\end{aligned} \tag{5.98}$$

where we replaced the signal by its Fourier transform: $h_I(t) = \int \tilde{h}_I(f)e^{-2\pi i f\left(t-\frac{\hat{\Omega}\cdot\boldsymbol{x}_I}{c}\right)}df$.

We apply the following substitution to the integral over t': $\tau = t - t'$, $d\tau = dt$,

$$\mu = \int \tilde{h}_I^*(f)\tilde{h}_J(f')e^{-\frac{2\pi i}{c}\hat{\Omega}\cdot(f\boldsymbol{x}_I - f'\boldsymbol{x}_J)}\int_{-T_J/2}^{T_J/2}\int_{-T_I/2-t'}^{T_I/2-t'} Q(\tau)e^{2\pi i f\tau}d\tau e^{-2\pi i(f'-f)t'}dt'df'df. \tag{5.99}$$

Then we approximate the integral over τ with the Fourier transform of the filter function Q:

$$\int_{-T_I/2-t'}^{T_I/2-t'} Q(\tau)e^{2\pi i f\tau}d\tau \approx \tilde{Q}(f). \tag{5.100}$$

If we shift a wave packed in time, it is still composed of the same frequencies. Therefore, we can ignore the time shift in the integration volume by $-t$.

We pull this out of the t integral and get:

$$\begin{aligned}
\int_{-T_J/2}^{T_J/2} e^{-2\pi i(f'-f)t'}dt' &= -\frac{1}{\pi\Delta f}\frac{1}{2i}\left(e^{-\pi i\Delta f T_J} - e^{\pi i\Delta f T_J}\right) \\
&= \frac{\sin(\pi\Delta f T_J)}{\pi\Delta f} =: \delta_{T_J}(f'-f).
\end{aligned} \tag{5.101}$$

If $\Delta f = f' - f$ approaches zero, we get: $\lim_{\Delta f\to 0}\delta_{T_J}(\Delta f) = \lim_{\Delta f\to 0}\frac{1}{\pi\Delta f}(0 + \pi T_J\Delta f + \mathcal{O}(\Delta f^2)) = T_J$ and for big Δf, δ_{T_J} gets small:

$$\left|\frac{\sin(\pi\Delta f T_J)}{\pi\Delta f}\right| \leqslant \frac{1}{\pi\Delta f} \overset{\Delta f\to\infty}{\longrightarrow} 0. \tag{5.102}$$

By approximating $\delta_{T_J}(f'-f) \approx \delta(f'-f)$ with the Dirac delta distribution we can evaluate the integral over f'.

$$\begin{aligned}\mu &\approx \int \tilde{h}_I^*(f)\tilde{h}_J(f')e^{-\frac{2\pi i}{c}\hat{\Omega}\cdot(f\boldsymbol{x}_I - f'\boldsymbol{x}_J)}\tilde{Q}(f')\delta(f'-f)df'df \\ &= \int \tilde{h}_I^*(f)\tilde{h}_J(f)\tilde{Q}(f)e^{-2\pi i f\frac{\hat{\Omega}\cdot\Delta\boldsymbol{x}_{IJ}}{c}}df. \end{aligned} \tag{5.103}$$

We now have an expression for the signal. To calculate the signal to noise ratio we need to deal with noise which is the square root of the variance in absence of a signal:

$$\begin{aligned}\sigma^2 &\coloneqq \mathbb{V}[Y]|_{h=0} = \mathbb{E}[Y^2] - \mathbb{E}[Y]^2|_{h=0} = \mathbb{E}[Y^2]|_{h=0} \\ &= \int_{-T_I/2}^{T_I/2}\int_{-T_I/2}^{T_I/2}\int_{-T_J/2}^{T_J/2}\int_{-T_J/2}^{T_J/2}\mathbb{E}[s_I(t)s_I(t')s_J(\tau)s_J(\tau')]Q(t-\tau)Q(t'-\tau')d\tau' d\tau dt' dt|_{h=0} \\ &= \int_{-T_I/2}^{T_I/2}\int_{-T_I/2}^{T_I/2}\int_{-T_J/2}^{T_J/2}\int_{-T_J/2}^{T_J/2}\mathbb{E}[n_I(t)n_I(t')]\mathbb{E}[n_J(\tau)n_J(\tau')]Q(t-\tau)Q(t'-\tau')d\tau' d\tau dt' dt. \end{aligned} \tag{5.104}$$

Since the noises of the two detectors are independent of each other, we can take their expectation separately. We then insert the Fourier transformation (FT) of the noise, in the time interval in which the measurement is taken:

$$n_I(t) = \int \tilde{n}_I(f)e^{-2\pi i f t}df, \tag{5.105}$$

And then swap the time and frequency integrals and approximate the FT of the filter function and the delta distribution as before:

$$\begin{aligned}\sigma^2 &= \int \mathbb{E}[\tilde{n}_I^*(f)\tilde{n}_I(f')]\mathbb{E}[\tilde{n}_J(\nu)\tilde{n}_J^*(\nu')]\tilde{Q}(\nu)\delta(\nu-f)\tilde{Q}^*(\nu')\delta(\nu'-f')d\nu' d\nu df' df \\ &= \int \mathbb{E}[\tilde{n}_I^*(f)\tilde{n}_I(f')]\mathbb{E}[\tilde{n}_J(f)\tilde{n}_J^*(f')]\tilde{Q}(f)\tilde{Q}^*(f')df' df. \end{aligned} \tag{5.106}$$

Now we use that different frequencies in the noise are not correlated to each other and the definition of the two sided noise power spectral density:

$$\mathbb{E}[\tilde{n}_I^*(f)\tilde{n}_I(f')] =: \frac{1}{2}P_I(|f'|)\delta(f'-f). \tag{5.107}$$

If we would carelessly plug in this identity, we would get a multiplication of two delta distributions, which is not definable. But we cannot take the expectation of the noise squared over an infinite time integral anyway. So, the delta distribution is actually a δ_{T_I}. This is a smooth function and not a distribution and can therefore be multiplied with another δ_{T_J}.

$$\begin{aligned}\sigma^2 &= \frac{1}{4}\int P_I(|f'|)P_J(|f'|)\tilde{Q}(f)\tilde{Q}^*(f')\cdot\int_{-T_I/2}^{T_I/2}e^{-2\pi i(f'-f)t}dt\int_{-T_J/2}^{T_J/2}e^{2\pi i(f'-f)t'}dt' df' df \\ &= \frac{1}{4}\int P_I(|f'|)P_J(|f'|)\tilde{Q}(f)\tilde{Q}^*(f')\cdot\int_{-T_I/2}^{T_I/2}\int_{-T_J/2}^{T_J/2}e^{2\pi i(f'-f)(t'-t)}dt' dt df' df. \end{aligned} \tag{5.108}$$

To evaluate the time integrals we have to split the integration domain into three regions as depicted in Fig. 5.19, since we need an integration region which is symmetric around $t'-t=0$, where we can use Eq. (5.101). The rest can be evaluated separately.

Let $T_I < T_J$, $\Delta T = T_J - T_I$ and $\Delta f = f'-f$, then the time integrals read:

$$\delta_{T_I}\delta_{T_J} = \int_{-T_I/2}^{T_I/2}\int_{-T_J/2}^{-T_I/2}e^{-2\pi i\Delta f(t'-t)}dt' + \int_{-T_I/2}^{T_I/2}e^{-2\pi i\Delta f(t'-t)}dt' + \int_{T_I/2}^{T_J/2}e^{-2\pi i\Delta f(t'-t)}dt' dt.$$

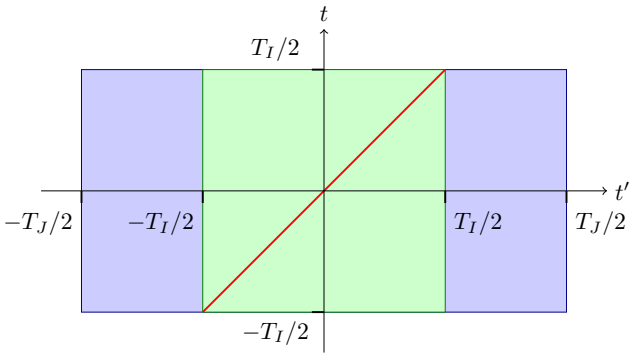

Figure 5.19: *The green region is symmetric around $t'-t=0$ (red line). The blue rectangle marks the entire integration region.*

We substitute $\eta = -t'$ in the first integral over t', to bring it into the same form as the third one.

$$\begin{aligned}
\delta_{T_I}\delta_{T_J} &= \int_{-T_I/2}^{T_I/2} - \int_{T_J/2}^{T_I/2} e^{2\pi i\Delta f(\eta+t)}d\eta + \int_{T_I/2}^{T_J/2} e^{-2\pi i\Delta f(t'-t)}dt'dt + \int_{-T_I/2}^{T_I/2}\int_{-T_I/2}^{T_I/2} e^{-2\pi i\Delta f(t'-t)}dt'dt \\
&= \int_{-T_I/2}^{T_I/2} e^{2\pi i\Delta f t}\int_{T_I/2}^{T_J/2} e^{2\pi i\Delta f t'} + e^{-2\pi i\Delta f t'}dt'dt + \delta^2_{T_I}(\Delta f) \\
&= \int_{-T_I/2}^{T_I/2} e^{2\pi i\Delta f t}dt \int_{T_I/2}^{T_J/2} 2\cos(2\pi\Delta f t')dt' + \delta^2_{T_I}(\Delta f) \\
&= \delta_{T_I}(\Delta f)\left(\frac{\sin(\pi\Delta f T_J)-\sin(\pi\Delta f T_I)}{\pi\Delta f} + \delta_{T_I}(\Delta f)\right) \\
&\approx \delta(f'-f)\left(\frac{\sin(\pi\Delta f T_I)+\pi\Delta f\Delta T+\mathcal{O}((\pi\Delta f\Delta T)^2)-\sin(\pi\Delta f T_I)}{\pi\Delta f} + \delta_{T_I}(\Delta f)\right),
\end{aligned} \tag{5.109}$$

where we assumed, that $\Delta T \ll T_I$.

This approximated distribution acts on functions as:

$$\begin{aligned}
\int g(f')\delta_{T_I}\delta_{T_J}(\Delta f)df' &\approx \int g(f')\left(\Delta T + \mathcal{O}(f'-f) + \delta_{T_I}(f'-f)\right)\delta(f'-f)df \\
&= g(f)(T_I+\Delta T),\ \forall g \in C^\infty(\mathbb{C}).
\end{aligned} \tag{5.110}$$

Inserting this into the variance and integrating over f' we get:

$$\begin{aligned}
\sigma^2 &= \frac{1}{4}\int P_I(|f'|)P_J(|f'|)\tilde{Q}(f)\tilde{Q}^*(f')\delta_{T_I}\delta_{T_J}(f'-f)df'df \\
&= \frac{T_I+\Delta T}{4}\int P_I(|f|)P_J(|f|)|\tilde{Q}(f)|^2 df.
\end{aligned} \tag{5.111}$$

Using matched filtering with the scalar product: $(\tilde{A},\tilde{B}) \coloneqq \int \tilde{A}^*(f)\tilde{B}(f)P_I(|f|)P_J(|f|)df$,
leads us to a filter function:

$$\tilde{Q}(f) = \frac{\tilde{h}_I^*(f)\tilde{h}_J(f)e^{2\pi i f\frac{\hat{\Omega}\cdot\Delta\mathbf{x}_{IJ}}{c}}}{P_I(|f|)P_J(|f|)}. \tag{5.112}$$

We can write the signal and noise in terms of the filter function and arrive at the signal to noise ratio:

$$\begin{aligned}
SNR = \frac{\mu}{\sigma} &= \frac{(\tilde{Q},\tilde{Q})}{\sqrt{\frac{T_I+\Delta T}{4}(\tilde{Q},\tilde{Q})}} \\
&= 2\sqrt{\frac{1}{T_I+\Delta T}\int \frac{|\tilde{h}_I(f)\tilde{h}_J(f)|^2}{P_I(|f|)P_J(|f|)}df}.
\end{aligned} \tag{5.113}$$

We now model the merger as a periodic source, which stops radiating at the end of the merging event at its time coordinate t_0. Under the assumption that the detectors are far away from the source, we can model the incoming wave as a plane wave with amplitude h_0 and frequency f_0, traveling in direction $\hat{\Omega}$:

$$h(t) = h_0 e^{2\pi i f_0 (t - \frac{\hat{\Omega}\cdot\boldsymbol{x}}{c})} \theta\left(t_0 - \frac{\hat{\Omega}\cdot\boldsymbol{x}}{c} - t\right). \tag{5.114}$$

The detector I will measure the signal over a time period T_I and the Fourier transform of the measured signal is therefore:

$$\begin{aligned}\tilde{h}_I(f) &= \int_{-T_I/2}^{T_I/2} h_0 e^{2\pi i f_0 (t - \frac{\hat{\Omega}\cdot\boldsymbol{x}}{c})} e^{-2\pi i f t} dt \\ &= h_0 e^{-2\pi i f_0 \frac{\hat{\Omega}\cdot\boldsymbol{x}}{c}} \int_{-T_I/2}^{T_I/2} e^{-2\pi i (f - f_0) t} dt\end{aligned} \tag{5.115}$$

Again, we cannot approximate this with a delta distribution, otherwise we would get a δ^4 for the $|\tilde{h}_I \tilde{h}_J|^2$ term.

$$|\tilde{h}_I(f)\tilde{h}_J(f)|^2 = h_0^4 \int_{-T_I/2}^{T_I/2}\int_{-T_I/2}^{T_I/2}\int_{-T_J/2}^{T_J/2}\int_{-T_J/2}^{T_J/2} e^{-2\pi i (f-f_0)(t'-t+\tau'-\tau)} d\tau' d\tau dt' dt. \tag{5.116}$$

We do the same splitting of the T_J interval as above, under the assumption $T_I < T_J$ and using the short hand $\rho = t' - t + \tau' - \tau$:

$$\begin{aligned}|\tilde{h}_I\tilde{h}_J|^2 \propto \delta_{T_I}^2 \delta_{T_J}^2 &= \int_{-T_I/2}^{T_I/2}\int_{-T_J/2}^{T_J/2} e^{-2\pi i (f'-f)(t'-t+\tau'-\tau)} d\tau' d\tau dt' dt \\ &= \int_{-T_I/2}^{T_I/2}\int_{-T_J/2}^{-T_I/2} e^{-2\pi i \Delta f \rho} d\tau' d\tau + \int_{-T_I/2}^{T_I/2} e^{-2\pi i \Delta f \rho} d\tau' d\tau + \int_{T_I/2}^{T_J/2} e^{-2\pi i \Delta f \rho} d\tau' d\tau dt' dt \\ &= \int_{-T_I/2}^{T_I/2} e^{-2\pi i \Delta f (t'-t)} dt' dt \int_{T_I/2}^{T_J/2} e^{2\pi i \Delta f (\tau'-\tau)} + e^{-2\pi i \Delta f (\tau'-\tau)} d\tau' d\tau + \int_{-T_I/2}^{T_I/2} e^{-2\pi i \Delta f \rho} d\tau' d\tau dt' dt \\ &= \delta_{T_I}^2(\Delta f) \int_{T_I/2}^{T_J/2} 2\cos(2\pi \Delta f (\tau' - \tau)) d\tau' d\tau + \delta_{T_I}^4(\Delta f) \\ &= \delta_{T_I}^2(\Delta f)\left(\frac{1}{\pi \Delta f}\int_{T_I/2}^{T_J/2} \sin(\pi \Delta f (T_J - 2\tau)) - \sin(\pi \Delta f (T_I - 2\tau)) d\tau + \delta_{T_I}^2(\Delta f)\right) \\ &= \delta_{T_I}^2(\Delta f)\Bigg(-\frac{1}{2(\pi\Delta f)^2}\{\cos(\pi \Delta f (T_J - T_J)) - \cos(\pi \Delta f (T_J - T_I)) \\ &\qquad - \cos(\pi \Delta f (T_I - T_J)) + \cos(\pi \Delta f (T_I - T_I))\} + \delta_{T_I}^2(\Delta f)\Bigg) \\ &= \delta_{T_I}^2(\Delta f)\left(\frac{1}{(\pi\Delta f)^2}\{\cos(\pi \Delta f \Delta T) - 1\} + \delta_{T_I}^2(\Delta f)\right) \\ &= \delta(f'-f)\delta_{T_I}(\Delta f)\left(\frac{1}{(\pi\Delta f)^2}\left\{1 - \frac{1}{2}(\pi \Delta f \Delta T)^2 + \mathcal{O}(\Delta f^4) - 1\right\} + \delta_{T_I}^2(\Delta f)\right).\end{aligned} \tag{5.117}$$

The action on a function $g \in C^\infty(\mathbb{C})$ is:

$$\begin{aligned}\int g(f')\delta_{T_I}^2\delta_{T_J}^2(f'-f)df' &= \int g(f')\delta_{T_I}(\Delta f)\left(\frac{\Delta T^2}{2} + \mathcal{O}(\Delta f^2) + \delta_{T_I}(\Delta f)^2\right)\delta(f'-f)df' \\ &= g(f)\delta_{T_I}(0)\left(\frac{\Delta T^2}{2} + \delta_{T_I}(0)^2\right) \\ &= g(f)T_I\left(\frac{\Delta T^2}{2} + T_I^2\right).\end{aligned} \tag{5.118}$$

When we plug this into the SNR we get:

$$\begin{aligned} SNR &= 2\sqrt{\frac{T_I}{T_I+\Delta T}\left(\frac{\Delta T^2}{2}+T_I^2\right)\frac{h_0^4}{P_I(|f_0|)P_J(|f_0|)}} \\ &\approx 2\left(T_I+\frac{\hat{\Omega}\cdot\Delta\boldsymbol{x}_{IJ}}{2c}\right)\frac{h_0^2}{\sqrt{P_I(f_0)P_J(f_0)}}, \end{aligned} \tag{5.119}$$

where we used the identification of the integration time with the direction of the source in Eq. (5.95).

The minimal amplitude is then given by:

$$\begin{aligned} h_{min} &= \sqrt{32}\left(\frac{(T_I+\Delta T)P_I(f)P_J(f)}{T_I\left(\frac{\Delta T^2}{2}+T_I^2\right)}\right)^{1/4} \\ &\approx \sqrt{32}\left(\frac{1}{\sqrt{T_I}}+\frac{\hat{\Omega}\cdot\Delta\boldsymbol{x}_{IJ}}{4c\sqrt{T_I}^3}\right)\sqrt[4]{P_I(f)P_J(f)}. \end{aligned} \tag{5.120}$$

Including polarizations, we have a gravitational wave $h_{ij}(t)$, which induces the signal $h_I(t)$ in detector I:

$$h_{ij}(t) = \sum_A h_A e^{2\pi i f_0(t-\frac{\hat{\Omega}\cdot\boldsymbol{x}}{c})+\varphi_A}\theta\left(t_0-\frac{\hat{\Omega}\cdot\boldsymbol{x}}{c}-t\right)e_{ij}^A \tag{5.121}$$

$$h_I(t) = \sum_A h_A F_I^A(\hat{\Omega}) e^{2\pi i f_0(t-\frac{\hat{\Omega}\cdot\boldsymbol{x}_I}{c})+\varphi_A}\theta\left(t_0-\frac{\hat{\Omega}\cdot\boldsymbol{x}_I}{c}-t\right), \tag{5.122}$$

where h_A is the amplitude of the wave in polarization A and φ_A accounts for the fact that the polarizations could be phase shifted.
For the absolute value squared of the cross correlated signals of two detectors we get:

$$\begin{aligned} |\tilde{h}_I(f)\tilde{h}_J(f)|^2 &= |\tilde{h}_I(f)|^2|\tilde{h}_J(f)|^2 \\ &= \left|\sum_A h_A F_I^A(\hat{\Omega}) e^{-\frac{2\pi i f_0}{c}\hat{\Omega}\cdot\boldsymbol{x}_I+i\varphi_A}\right|^2\left|\sum_A h_A F_J^A(\hat{\Omega}) e^{-\frac{2\pi i f_0}{c}\hat{\Omega}\cdot\boldsymbol{x}_J+i\varphi_A}\right|^2\int_{-T_I/2}^{T_I/2}\int_{-T_J/2}^{T_J/2} e^{-2\pi i(f-f_0)\rho}d^4\rho \\ &= \left|\sum_A h_A F_I^A(\hat{\Omega}) e^{i\varphi_A}\right|^2\left|\sum_A h_A F_J^A(\hat{\Omega}) e^{i\varphi_A}\right|^2\delta_{T_I}(f-f_0)\left(\frac{\Delta T^2}{2}+\delta_{T_I}(f-f_0)^2\right). \end{aligned} \tag{5.123}$$

We make the assumption, that the gravitational wave has only one of the polarizations $h = \sum_{A'} h_{A'}\delta_{A'A}$, to get the signal to noise ratio for that polarization.

$$\begin{aligned} SNR_A &:= \left.\frac{\mu}{\sigma}\right|_{h=h_A} \\ &= 2\sqrt{\frac{T_I}{T_I+\Delta T}\left(\frac{\Delta T^2}{2}+T_I^2\right)\frac{(|h_A|^2F_I^A(\hat{\Omega})F_J^A(\hat{\Omega}))^2}{P_I(|f_0|)P_J(|f_0|)}} \\ &\approx 2\left(T_I+\frac{\hat{\Omega}\cdot\Delta\boldsymbol{x}_{IJ}}{2c}\right)\frac{|h_A|^2F_I^A(\hat{\Omega})F_J^A(\hat{\Omega})}{\sqrt{P_I(f_0)P_J(f_0)}}, \end{aligned} \tag{5.124}$$

which we get by replacing $h_0^4 \mapsto (|h_A|^2F_I^A(\hat{\Omega})F_J^A(\hat{\Omega}))^2$ in Eq. (5.119).

For multiple detectors we use the maximum likelihood method and calculate the Fisher matrix. The likelihood function is given by:

$$L(\mu_{IJ},\boldsymbol{\theta}) = e^{-\sum_{(I,J)}\frac{(Y_{IJ}-\mu_{IJ})^2}{2\sigma_{IJ}^2}}, \tag{5.125}$$

where $\mu_{IJ} = \mathbb{E}[Y_{IJ}]$ is the ensemble average of the correlated signals of the detectors I and J. Its variance $\sigma_{IJ}^2 = \mathbb{V}[Y_{IJ}]$ is given by Eq. (5.111) without the filtering. Multiplying the SNR Eq. (5.119) with the noise we get:

$$\mu_{IJ} = \sqrt{T_I\left(\frac{\Delta T^2}{2}+T_I^2\right)}|\tilde{h}_I\tilde{h}_J|. \tag{5.126}$$

The matrix element $F_{AA'}$ of the Fisher matrix is then given by:

$$\begin{aligned}
F_{AA'} &= \mathbb{E}\left[\left(\partial_{|h_A|^2} \ln L\right)\left(\partial_{|h_{A'}|^2} \ln L\right)\right] \\
&= \mathbb{E}\left[\left(\sum_{(I,J)} \frac{1}{\sigma_{IJ}^2}(Y_{IJ}-\mu_{IJ})\sqrt{T_I\left(\frac{\Delta T^2}{2}+T_I^2\right)}\right)^2 \left(\partial_{|h_A|^2}|\tilde{h}_I\tilde{h}_J|\right)\left(\partial_{|h_{A'}|^2}|\tilde{h}_I\tilde{h}_J|\right)\right] \\
&= \sum_{(I,J)} \frac{1}{\sigma_{IJ}^4} \underbrace{\mathbb{E}[(Y_{IJ}-\mu_{IJ})^2]}_{\mathbb{V}[Y_{IJ}]=\sigma_{IJ}^2} T_I\left(\frac{\Delta T^2}{2}+T_I^2\right)\left(\partial_{|h_A|^2}|\tilde{h}_I\tilde{h}_J|\right)\left(\partial_{|h_{A'}|^2}|\tilde{h}_I\tilde{h}_J|\right) \\
&\quad + \sum_{(I,J)\neq(I',J')} \frac{1}{\sigma_{IJ}^2\sigma_{I'J'}^2} \underbrace{\mathbb{E}[(Y_{IJ}-\mu_{IJ})(Y_{I'J'}-\mu_{I'J'})]}_{Cov(Y_{IJ},Y_{I'J'})=0} T_I\left(\frac{\Delta T^2}{2}+T_I^2\right)\left(\partial_{|h_A|^2}|\tilde{h}_I\tilde{h}_J|\right)\left(\partial_{|h_{A'}|^2}|\tilde{h}_{I'}\tilde{h}_{J'}|\right) \\
&= \sum_{(I,J)} \frac{4T_I}{(T_I+\Delta T)P_IP_J}\left(\frac{\Delta T^2}{2}+T_I^2\right)\left(\partial_{|h_A|^2}|\tilde{h}_I\tilde{h}_J|\right)\left(\partial_{|h_{A'}|^2}|\tilde{h}_I\tilde{h}_J|\right)
\end{aligned} \tag{5.127}$$

The SNR squared of a specific polarization A is defined by dividing the square of the quantity we are looking for $|h_A|^2$ by its variance σ_A, under the condition that the incoming wave has only that polarization.

$$\begin{aligned}
SNR_A^2 &:= \left.\frac{(|h_A|^2)^2}{\sigma_A^2}\right|_{h=h_A} = \left.\frac{(|h_A|^2)^2}{(F^{-1})_{AA}}\right|_{h=h_A} \\
&= \left.\frac{(|h_A|^2)^2 \det \mathbf{F}}{\mathscr{F}_A}\right|_{h=h_A}
\end{aligned} \tag{5.128}$$

Fisher Matrix Entries

As can be seen in Appendix 5.7.3, the Fisher matrix can be written as a sum of Fisher matrices of single detector pairs, which consist of a pre-factor and two derivative terms for row and column of the entry. If $\theta_{i,j}$ are polarizations we have:

$$F_{ij} \propto \left(\partial_{\theta_i}|\tilde{h}_I\tilde{h}_J|\right)\left(\partial_{\theta_j}|\tilde{h}_I\tilde{h}_J|\right), \tag{5.129}$$

where $\boldsymbol{\theta} = (\theta, \phi, +, \times, x, y, b, l)$ are the parameters we are looking for.

Here we calculate those derivative terms.
We start by writing out the absolute value squared of the correlation signal.

$$|\tilde{h}_I\tilde{h}_J|^2 = \left|\sum_A h_A F_I^A \sum_{A'} h_{A'} F_J^{A'}\right|^2, \tag{5.130}$$

where the phase φ_A of the polarization A is integrated in the complex valued amplitude $h_A \in \mathbb{C}$.

We split the multiplied signals up into sums over terms where the polarizations coincide and where they are different:

$$
\begin{aligned}
|\tilde{h}_I\tilde{h}_J|^2 &= \left|\sum_A h_A^2 F_I^A F_J^A + \sum_{A\neq A'} h_A h_{A'} F_I^A F_J^{A'}\right|^2 \\
&= \left(\sum_A h_A^2 F_I^A F_J^A\right)\left(\sum_B h_B^2 F_I^B F_J^B\right)^* + \left(\sum_A h_A^2 F_I^A F_J^A\right)\left(\sum_{B\neq B'} h_B h_{B'} F_I^B F_J^{B'}\right)^* \\
&\quad + \left(\sum_{A\neq A'} h_A h_{A'} F_I^A F_J^{A'}\right)\left(\sum_B h_B^2 F_I^B F_J^B\right)^* + \left(\sum_{A\neq A'} h_A h_{A'} F_I^A F_J^{A'}\right)\left(\sum_{B\neq B'} h_B h_{B'} F_I^B F_J^{B'}\right)^* \\
&= \sum_A \left(|h_A|^2 F_I^A F_J^A\right)^2 + \sum_{A\neq B}(h_A h_B^*)^2 F_I^A F_J^A F_I^B F_J^B \\
&\quad + \sum_A h_A|h_A|^2 F_I^A F_J^A \sum_{B\neq A} h_B^*(F_I^A F_J^B + F_I^B F_J^A) + \sum_{A\neq B\neq B'} h_A^2 F_I^A F_J^A h_B^* h_{B'}^* F_I^B F_J^{B'} \\
&\quad + \sum_B h_B^*|h_B|^2 F_I^B F_J^B \sum_{A\neq B} h_A(F_I^B F_J^A + F_I^A F_J^B) + \sum_{A\neq A'\neq B} h_A h_{A'} F_I^A F_J^{A'}(h_B^*)^2 F_I^B F_J^B \\
&\quad + \sum_{A\neq A'} |h_A|^2|h_{A'}|^2\left[(F_I^A F_J^{A'})^2 + F_I^A F_J^{A'} F_I^{A'} F_J^A\right] \\
&\quad + \sum_A |h_A|^2 \sum_{\substack{B\neq B'\\ B,B'\neq A}} h_B h_{B'}^*\left[(F_I^A)^2 F_J^B F_J^{B'} + F_I^A F_J^A(F_I^B F_J^{B'} + F_I^{B'} F_J^B) + (F_J^A)^2 F_I^B F_I^{B'}\right] \\
&\quad + \sum_{A\neq A'\neq B\neq B'} h_A h_{A'} h_B^* h_{B'}^* F_I^A F_J^{A'} F_I^B F_J^{B'}.
\end{aligned}
\tag{5.131}
$$

When we take the derivative after $|h_A|^2$ all sums which do not contain such a term vanish.

$$
\begin{aligned}
\partial_{|h_A|^2}|\tilde{h}_I\tilde{h}_J| = \frac{1}{2\sqrt{|\tilde{h}_I\tilde{h}_J|}}\Bigg\{ & 2|h_A|^2(F_I^A F_J^A)^2 + h_A F_I^A F_J^A \sum_{B\neq A} h_B^*(F_I^A F_J^B + F_I^B F_J^A) \\
& + h_A^* F_I^A F_J^A \sum_{B\neq A} h_B(F_I^A F_J^B + F_I^B F_J^A) + \sum_{A'\neq A}|h_{A'}|^2\left[(F_I^A F_J^{A'})^2 + 2F_I^A F_J^{A'} F_I^{A'} F_J^A + (F_I^{A'} F_J^A)^2\right] \\
& + \sum_{\substack{B\neq B'\\ B,B'\neq A}} h_B h_{B'}^*\left[(F_I^A)^2 F_J^B F_J^{B'} + F_I^A F_J^A(F_I^B F_J^{B'} + F_I^{B'} F_J^B) + (F_J^A)^2 F_I^B F_I^{B'}\right]\Bigg\}.
\end{aligned}
\tag{5.132}
$$

We add the condition, that we have an incoming wave with polarization A_0 and therefore all terms proportional to two different polarizations are zero.

$$
\begin{aligned}
\partial_{|h_A|^2}|\tilde{h}_I\tilde{h}_J|\Big|_{h=h_{A_0}} &= \frac{1}{2\sqrt{\left(|h_{A_0}|^2 F_I^{A_0} F_J^{A_0}\right)^2 + 0}}\left\{2\delta_{AA_0}|h_A|^2(F_I^A F_J^A)^2\right. \\
&\quad \left. + (1-\delta_{AA_0})|h_{A_0}|^2\left[(F_I^A F_J^{A_0})^2 + 2F_I^A F_J^{A_0} F_I^{A_0} F_J^A + (F_I^{A_0} F_J^A)^2\right]\right\} \\
&= F_I^A F_J^A + (1-\delta_{AA_0})\frac{1}{2}\left[\frac{(F_I^A)^2 F_J^{A_0}}{F_I^{A_0}} + \frac{(F_J^A)^2 F_I^{A_0}}{F_J^{A_0}}\right]
\end{aligned}
\tag{5.133}
$$

If we calculate a matrix element in the θ or ϕ row or column, we cannot pull the term $\sqrt{T_I\left(\frac{\Delta T^2}{2} + T_I^2\right)}$ out in front, so the general Fisher matrix element looks like:

$$
\begin{aligned}
F_{ij} &= \mathbb{E}\Big[(\partial_{\theta_i}\ln L)(\partial_{\theta_j}\ln L)\Big] \\
&= \sum_{(I,J)}\frac{1}{\sigma_{IJ}^2}\left(\partial_{\theta_i}\sqrt{T_I\left(\frac{\Delta T^2}{2} + T_I^2\right)}|\tilde{h}_I\tilde{h}_J|\right)\cdot\left(\partial_{\theta_j}\sqrt{T_I\left(\frac{\Delta T^2}{2} + T_I^2\right)}|\tilde{h}_I\tilde{h}_J|\right)
\end{aligned}
\tag{5.134}
$$

The variance of the true signal Y_{IJ} is dependent on the true time difference and we can treat it as a parameter when we take the derivative after the estimated θ-value.

$$\mathbb{V}[Y_{IJ}] = \sigma_{IJ}^2 = \frac{T_I + \Delta T}{4} P_I P_J, \qquad \Delta T = \frac{\hat{\omega} \cdot \Delta \boldsymbol{x}_{IJ}}{c}, \tag{5.135}$$

where $\hat{\omega}$ is the true direction of the source.

The derivative term for the angle θ for a wave with polarization A_0 is given by:

$$\begin{aligned} &\partial_\theta \sqrt{T_I \left(\frac{\Delta T^2}{2} + T_I^2 \right)} |\tilde{h}_I \tilde{h}_J| \Big|_{h=h_{A_0}} \\ &= \frac{T_I \Delta T}{2\sqrt{T_I \left(\frac{\Delta T^2}{2} + T_I^2 \right)}} \frac{\hat{\Omega}_{,\theta} \cdot \Delta \boldsymbol{x}_{IJ}}{c} |h_{A_0}|^2 F_I^{A_0} F_J^{A_0} + \sqrt{T_I \left(\frac{\Delta T^2}{2} + T_I^2 \right)} |h_{A_0}|^2 \left(F_{I,\theta}^{A_0} F_J^{A_0} + F_I^{A_0} F_{J,\theta}^{A_0} \right) \end{aligned} \tag{5.136}$$

Chapter 6

Detecting Additional Polarization Modes with LISA

L. Philippoz, P. Jetzer

Based on works published in J. Phys.: Conf. Ser. **840***, 012057 (2017) and Proceedings of the 52nd Rencontres de Moriond, ASRIF (2017) pp. 69-72.*

Abstract

Within the frame of GR, GW possess two tensorial polarizations (h_+ and $h_\times$), whereas more general metric theories of gravity predict the existence of additional modes: up to 2 vector and 2 scalar modes. Moreover, if the detection of a strong enough stochastic GW background (SGWB) of cosmological origin were to happen, its analysis could tell us more about the physics of the early universe; without assuming a particular theory of gravitation, such a signal is thus expected to contain a mixture of up to 6 polarizations with no dominant mode.

We addresse the question of whether a given LISA configuration can provide a sufficient sensitivity to detect additional polarization modes and then allow the extraction of the latter in order to determine the GW spectrum for each mode. The application of an auto-correlation technique could overcome the apparent limitations of a smaller detector design (a single cluster containing only four links).

6.1 Introduction

The recent detections of gravitational waves (GW) by the LIGO Collaboration [43, 68–72] represent a milestone in GW research and open new perspectives in the study of general relativity and astrophysics. Many projects are still under way, one of them being the next ESA L3 mission, namely the Laser Interferometer Space Antenna (LISA)[44, 80]. The scope of LISA is to detect and study low-frequency gravitational radiation in the range from 0.1 mHz to 1 Hz, offering a complementary window of observation to the earth-based experiments. Phenomena such as the merger of supermassive black holes at cosmological distances, or binary systems composed of close white dwarves would produce a signal within the reach of LISA.

Alternative gravitation theories can influence the dynamics of those mergers, and LISA is thus expected to be able to measure the inprints of some alternative theories since this future space-borne detector will offer access to an unprecedented signal sensitivity. The proposed design [80] will allow the detection of possible additional polarization modes of GW, which is an invaluable tool to explore GW in alternative theories of gravity, e.g. $f(R)$ and scalar-tensor theories. Depending if additional polarizations are found or not in a detected signal, our knowledge of gravitation could have to be extended beyond GR, but we could in any case exclude some theoretical models according to which modes are actually detected, as well as put better constraints on compatible models. Moreover, the detection of a stochastic GW background (SGWB) could tell us more about the early stages of the universe . The polarization content of such a signal would also be of use to discriminate between existing gravitation theories.

6.2 Definitions

Within the frame of GR, gravitational waves possess two tensorial polarizations, the so-called h_+ and $h_\times$ modes, whereas more general metric theories of gravity predict the existence of additional modes: up to 2 vector and 2 scalar modes. The perturbed metric corresponding to a propagating gravitational wave can be expressed as:

$$h_{ij}(\omega t - \mathbf{k}\cdot\boldsymbol{x}) = \sum_A h_A(\omega t - \mathbf{k}\cdot\boldsymbol{x}) e^A_{ij} \tag{6.1}$$

with $A = +, \times, x, y, b, l$ the six possible polarization modes, h_A the GW amplitude of the mode A, and the following polarization tensors (tensor ($+$, $\times$), vector (x, y) and scalar (b, l) modes) for a GW propagating in the z-direction [89]:

$$\begin{aligned}
e^+_{ij} &= \begin{pmatrix} 1 & 0 & 0 \\ 0 & -1 & 0 \\ 0 & 0 & 0 \end{pmatrix} \quad e^x_{ij} = \begin{pmatrix} 0 & 0 & 1 \\ 0 & 0 & 0 \\ 1 & 0 & 0 \end{pmatrix} \quad e^b_{ij} = \begin{pmatrix} 1 & 0 & 0 \\ 0 & 1 & 0 \\ 0 & 0 & 0 \end{pmatrix} \\
e^\times_{ij} &= \begin{pmatrix} 0 & 1 & 0 \\ 1 & 0 & 0 \\ 0 & 0 & 0 \end{pmatrix} \quad e^y_{ij} = \begin{pmatrix} 0 & 0 & 0 \\ 0 & 0 & 1 \\ 0 & 1 & 0 \end{pmatrix} \quad e^l_{ij} = \sqrt{2}\begin{pmatrix} 0 & 0 & 0 \\ 0 & 0 & 0 \\ 0 & 0 & 1 \end{pmatrix}
\end{aligned} \tag{6.2}$$

The polarization tensors are normalized as

$$e^A_{ij} e^{ij}_{A'} = 2\delta_{AA'}. \tag{6.3}$$

If we now consider the coordinate systems represented in Fig. 6.1, where $\hat{\boldsymbol{\Omega}}$ points in the direction of a GW, and $\hat{\boldsymbol{m}}$,

$\hat{n}$ are the vectors in the plane transversal to the propagation, the polarization tensors can then be written as:

$$e+ = \hat{m} \otimes \hat{m} - \hat{n} \otimes \hat{n} \tag{6.4a}$$
$$e^{\times} = \hat{m} \otimes \hat{n} - \hat{n} \otimes \hat{m} \tag{6.4b}$$
$$e^{x} = \hat{m} \otimes \hat{\Omega} + \hat{\Omega} \otimes \hat{m} \tag{6.4c}$$
$$e^{y} = \hat{n} \otimes \hat{\Omega} + \hat{\Omega} \otimes \hat{n} \tag{6.4d}$$
$$e^{b} = \hat{m} \otimes \hat{m} - \hat{n} \otimes \hat{n} \tag{6.4e}$$
$$e^{l} = \sqrt{2}\hat{\Omega} \otimes \hat{\Omega} \tag{6.4f}$$
$$\tag{6.4g}$$

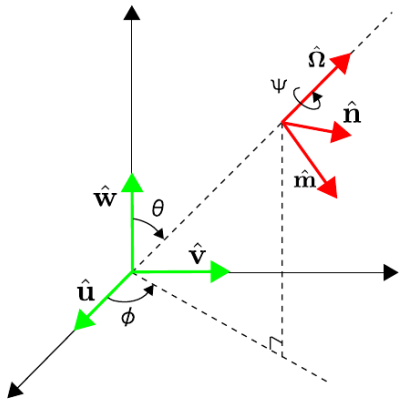

Figure 6.1: *Coordinate system for a GW travelling toward an observer. Picture from [85].*

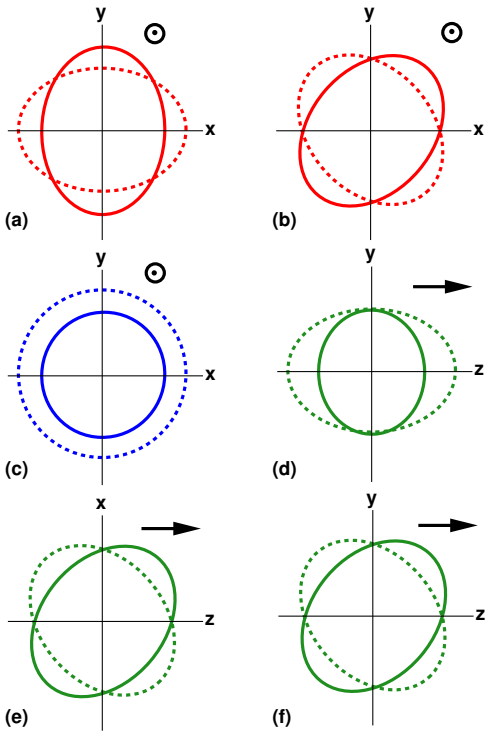

Figure 6.2: *All possible polarizations of GW. (a)-(b): + and × tensor modes. (c)-(d): breathing b and longitudinal l scalar modes. (e)-(f): x and y vector modes. Picture from [11].*

Without assuming a particular theory of gravitation, a GW signal is expected to contain a mixture of up to 6 polarizations, and it is consequently important to determine the detection threshold for a SGWB, described as [86]

$$h(t,\boldsymbol{x}) = \sum_A \int_{S^2} d\hat{\boldsymbol{\Omega}} \int_{-\infty}^{\infty} df\ \tilde{h}_A(f,\hat{\boldsymbol{\Omega}}) e^{2\pi i f(t-\hat{\boldsymbol{\Omega}}\boldsymbol{x}/c)} \boldsymbol{e}^{\boldsymbol{A}}, \tag{6.5}$$

as well as find a way of extracting its polarization content.

6.3 LISA sensitivity to polarization modes

LISA sensitivity to various TDI

The current LISA mission [80] consists in a combination of three satellites placed on an equilateral triangle with sides of length 2.5×10^6 km, placed in orbit around the Sun at a distance of about 20° behind the Earth. Each side of the cluster is covered by two lasers connecting each two satellites, which effectively corresponds to two giant interferometers sensitive in a frequency band of 0.1 mHz to about 1 HZ.

The determination of the sensitivity to additional polarization modes was discussed for an earlier version of the LISA project [90–95] but it is necessary to establish the appropriate sensitivity curves according to the future design. We start by give the noise spectra for the six possible time-delay interferometric (TDI) combinations (i.e. different combinations of the signals depending on the number of laser links between the satellites)[91]:

$$\begin{aligned}
S_X(f) &= [8\sin^2(4\pi f L) + 32\sin^2(2\pi f L)]S_y^{\rm tm} + 16\sin^2(2\pi f L)S_y^{\rm op} && (6.6)\\
S_\alpha(f) &= [8\sin^2(3\pi f L) + 16\sin^2(\pi f L)]S_y^{\rm tm} + 6S_y^{\rm op} && (6.7)\\
S_\zeta(f) &= 24\sin^2(2\pi f L)S_y^{\rm tm} + 6S_y^{\rm op} && (6.8)\\
S_E(f) = S_P(f) &= [32\sin^2(\pi f L) + 8\sin^2(2\pi f L)]S_y^{\rm tm} + [8\sin^2(\pi f L) + 8\sin^2(2\pi f L)]S_y^{\rm op} && (6.9)\\
S_U(f) &= [16\sin^2(\pi f L) + 8\sin^2(2\pi f L) + 16\sin^2(3\pi f L)]S_y^{\rm tm} && (6.10)\\
&\quad +[4\sin^2(\pi f L) + 8\sin^2(2\pi f L) + 4\sin^2(3\pi f L)]S_y^{\rm op} && (6.11)
\end{aligned}$$

where

$$\begin{aligned}
S_y^{\rm tm} &= 2.5\cdot 10^{-48}(f/(1{\rm Hz}))^{-2}\ {\rm Hz}^{-1} && (6.12)\\
S_y^{\rm op} &= 1.8\cdot 10^{-37}(f/(1{\rm Hz}))^{2}\ {\rm Hz}^{-1} && (6.13)
\end{aligned}$$

are the test mass spectrum (stray acceleration) and the optical path power spectrum (displacement noise), respectively. Their values based on the most recent designed are updated to [80, 96]:

$$\begin{aligned}
S_a^{1/2} &= 3\cdot 10^{-15}\frac{{\rm m\ s^{-2}}}{\sqrt{\rm Hz}}\sqrt{1+\left(\frac{0.4{\rm mHz}}{f}\right)^2}\sqrt{1+\left(\frac{f}{8{\rm mHz}}\right)^4} && (6.14)\\
S_{\rm ifo}^{1/2} &= 10\cdot 10^{-12}\frac{\rm m}{\sqrt{\rm Hz}}\sqrt{1+\left(\frac{2{\rm mHz}}{f}\right)^4} && (6.15)
\end{aligned}$$

An example in the case of the X TDI-combination is given in Fig. 6.3.

6.4 Network of detectors

An easy way of investigating how to extract the polarization content of a GW signal consists in first considering a network of LISA-like space detectors. A detector would measure a signal produced by a SGWB with the following form:

$$h(t,\boldsymbol{x}) = \sum_A \int_{S^2} d\hat{\boldsymbol{\Omega}} \int_{-\infty}^{\infty} df\ \tilde{h}_A(f,\hat{\boldsymbol{\Omega}}) e^{2\pi i f(t-\hat{\boldsymbol{\Omega}}\boldsymbol{x}/c)} F_A(\hat{\boldsymbol{\Omega}}), \tag{6.16}$$

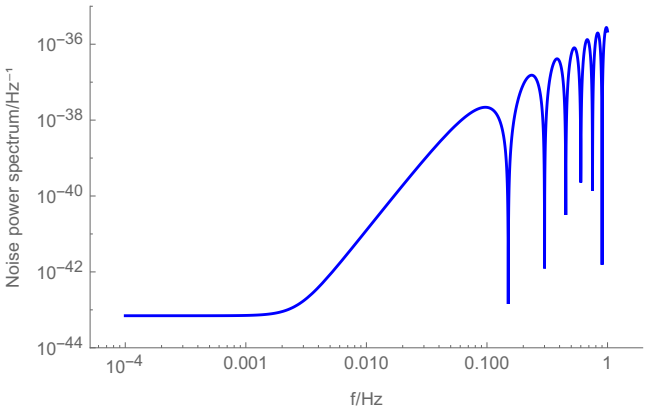

Figure 6.3: *Noise power spectrum for the X TDI-combination*

with F_A the antenna pattern function of a single detector (which describes its geometry), and h_A the GW amplitude of the mode A. In its current proposed design (3 satellites with 3 arms, i.e. 3 times 2 laser links between the satellites), LISA is actually equivalent to two single detectors; we will describe this arrangement of three satellites as a cluster. In a single detector, the vectors $\hat{u}$ and $\hat{v}$ give the direction of each arm and one can define the detector tensor D as

$$D_{ij} = \frac{1}{2}(\hat{u}_i\hat{u}_j - \hat{v}_i\hat{v}_j), \tag{6.17}$$

which gives the response of that detector to a signal.

If one now considers a network of several identical clusters [84, 85, 97], the first step consists in determining the so-called overlap reduction functions (ORFs), defined for a pair of detectors I and J separated by $\Delta\boldsymbol{x}$ as

$$\gamma_{IJ}^{M}(f) = \frac{1}{\sin^2(\chi)}\left(\rho_1^M(\alpha)D_I^{ij}D_{ij}^J + \rho_2^M(\alpha)D_{I,k}^{i}D_J^{kj}\hat{d}_i\hat{d}_j + \rho_3^M(\alpha)D_I^{ij}D_J^{kl}\hat{d}_i\hat{d}_j\hat{d}_k\hat{d}_l\right), \tag{6.18}$$

with M denoting the tensor (T), vector (V) or scalar (S) polarization modes, $\sin^2(\chi) = 1-(\hat{u}\cdot\hat{v})^2$ a geometry factor (which is $\frac{3}{4}$ for an equilateral-triangle-shaped cluster such as LISA), $\rho_i^M = f(j_0(\alpha), j_2(\alpha), j_4(\alpha))$ a linear combination of spherical Bessel functions:

$$\begin{pmatrix}\rho_1^T(\alpha)\\ \rho_2^T(\alpha)\\ \rho_3^T(\alpha)\end{pmatrix} = \frac{1}{14}\begin{pmatrix}28 & -40 & 2\\ 0 & 120 & -20\\ 0 & 0 & 25\end{pmatrix}\begin{pmatrix}j_0(\alpha)\\ j_2(\alpha)\\ j_4(\alpha)\end{pmatrix}, \tag{6.19a}$$

$$\begin{pmatrix}\rho_1^V(\alpha)\\ \rho_2^V(\alpha)\\ \rho_3^V(\alpha)\end{pmatrix} = \frac{2}{7}\begin{pmatrix}7 & 5 & -2\\ 0 & -15 & 20\\ 0 & 0 & -35\end{pmatrix}\begin{pmatrix}j_0(\alpha)\\ j_2(\alpha)\\ j_4(\alpha)\end{pmatrix}, \tag{6.19b}$$

$$\begin{pmatrix}\rho_1^S(\alpha)\\ \rho_2^S(\alpha)\\ \rho_3^S(\alpha)\end{pmatrix} = \frac{1}{7}\begin{pmatrix}14 & 20 & 6\\ 0 & -60 & -60\\ 0 & 0 & 105\end{pmatrix}\begin{pmatrix}j_0(\alpha)\\ j_2(\alpha)\\ j_4(\alpha)\end{pmatrix}, \tag{6.19c}$$

D_I^{ij} the detector tensor of the interferometer I, $\hat{d}_i = \dfrac{\Delta\boldsymbol{x}}{|\Delta\boldsymbol{x}|}$, $\alpha = \dfrac{2\pi f\,|\Delta\boldsymbol{x}|}{c}$. An ORF tells how much degree of correlation is preserved when one correlates the output of two detectors, according to their relative orientation. Examples for three different angles are given in Fig. 6.4, 6.5 and 6.6.

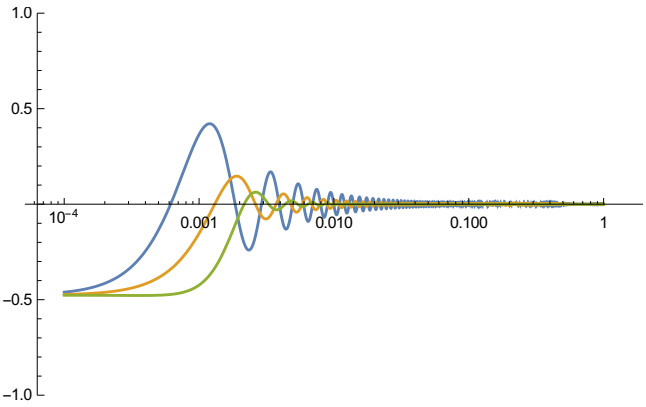

Figure 6.4: *ORF $\gamma^M(f)$ for T (blue), V (orange), S (green), and $\theta = \pi/6$*

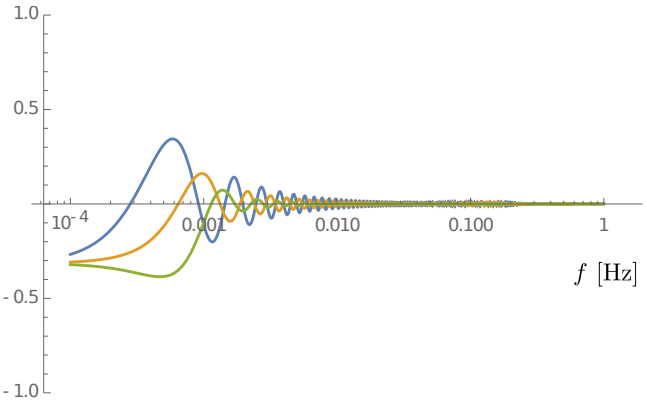

Figure 6.5: *ORF $\gamma^M(f)$ for T (blue), V (orange), S (green), and $\theta = \pi/2$*

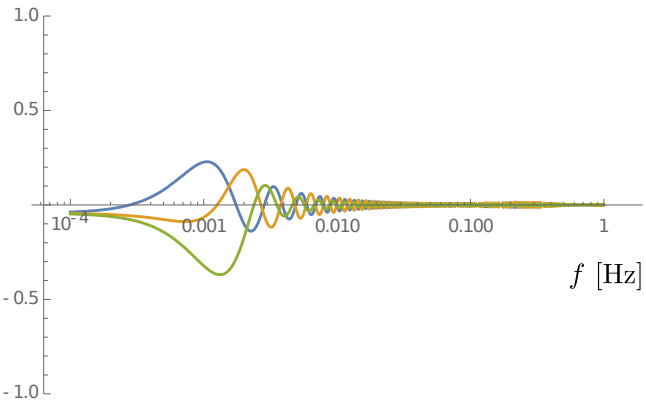

Figure 6.6: *ORF $\gamma^M(f)$ for T (blue), V (orange), S (green), and $\theta = 5\pi/6$*

Note that, schematically, the signal $h(t) + n(t)$ measured by a detector is composed of the GW signal $h(t)$ as well as the noise $n(t)$. Next, we can thus consider the one-sided power spectral density S_h^A:

$$\langle \tilde{h}_A^*(f, \hat{\mathbf{\Omega}}) \tilde{h}_{A'}(f', \hat{\mathbf{\Omega}}') \rangle = \delta(f - f') \frac{1}{4\pi} \delta^2(\hat{\mathbf{\Omega}}, \hat{\mathbf{\Omega}}') \delta_{AA'} \cdot \frac{1}{2} S_h^A(|f|), \tag{6.20}$$

as well as the noise spectrum $P_I(f)$:

$$\langle \tilde{n}_I(f) \tilde{n}_J(f') \rangle = \frac{1}{2} \delta(f - f') \delta_{IJ} \cdot P_I(|f|), \tag{6.21}$$

and the GW background energy density

$$\Omega_{\rm gw}^{M}(f) = \frac{1}{\rho_c}\frac{d\rho_{\rm gw}^{M}}{d\ln(f)} = \left(\frac{2\pi^2}{3H_0^2}\right) f^3 S_h^A(f), \tag{6.22}$$

with

$$\Omega_{\rm gw}^{T} = \Omega_{\rm gw}^{+} + \Omega_{\rm gw}^{\times}, \tag{6.23a}$$
$$\Omega_{\rm gw}^{V} = \Omega_{\rm gw}^{x} + \Omega_{\rm gw}^{y}, \tag{6.23b}$$
$$\Omega_{\rm gw}^{S} = \Omega_{\rm gw}^{b} + \Omega_{\rm gw}^{l}. \tag{6.23c}$$

It is possible to find the optimal signal-to-noise ratio (SNR) necessary to separately detect the modes:

$$SNR^{M} = \frac{9H_0^2}{40\pi^2}\left[2\int_0^{\infty} df\, \frac{(\Omega_{\rm gw}^{M}(f))^2 \det \mathbf{F}(f)}{f^6 \mathscr{F}_M(f)}\right]^{1/2}, \tag{6.24}$$

where $\mathbf{F}$ is a (3×3)-matrix whose elements are given by

$$F_{MM'} = \sum_{\substack{\text{detector}\\ \text{pairs } (I,J)}} \int_0^{T_{\rm obs}} {\rm d}t\, \frac{\gamma_{IJ}^{M}(t,f)\gamma_{IJ}^{M'}(t,f)}{P_I(f)P_J(f)},$$

($T_{\rm obs}$ is the mission duration) and $\mathscr{F}_M(f)$ is the determinant of the matrix obtained by removing all the M-elements from the matrix $\mathbf{F}$.

The separation of the modes can then be achieved as follows [84]: we first define the statistics

$$\begin{aligned} Z_{IJ} &\propto \left|f^3\right| \tilde{s}_I^*(f)\tilde{s}_J(f) \\ &= \sum_M \Omega_{\rm GW}^{M}\gamma_{IJ}^{M}(f) + \text{ noise }. \end{aligned} \tag{6.25}$$

By averaging it, one gets the matrix equation

$$\langle Z_{IJ}\rangle = \sum_M \Omega_{\rm GW}^{M}\gamma_{IJ}^{M}(f) \tag{6.26}$$

or shortly $\mathbf{Z} = \mathbf{\Pi}\,\mathbf{\Omega}$. By inverting the so-called correlation matrix $\mathbf{\Pi}$ containing the ORF:

$$\mathbf{\Pi} = \begin{pmatrix} \gamma_{12}^{T} & \gamma_{12}^{V} & \gamma_{12}^{S} \\ \gamma_{23}^{T} & \gamma_{23}^{V} & \gamma_{23}^{S} \\ \gamma_{31}^{T} & \gamma_{31}^{V} & \gamma_{31}^{S} \end{pmatrix} \tag{6.27}$$

(as long as $\det(\mathbf{\Pi}) \neq 0$), one can finally find the mode densities $\mathbf{\Omega}$.

This method thus gives the detection threshold for each mode and is valid for a network of independant detectors in space, i.e. several clusters (for instance 2 independant LISA-like clusters, or 4 clusters such as in the DECIGO project [81]), in the low frequency limit and for a full polarized GW background. Moreover, it allows to extract from a signal the energy density of each mode.

6.5 Single detector

A previous analysis of the sensitivity to additional polarization modes has been performed for an earlier version of LISA (cluster with 3 arms) and the sensitivity curves for each mode and various TDI simply need to be updated

regarding the new proposed design [94]. However, it is nevertheless worth investigating a minimal version consisting of a cluster with only 2 arms, which could be useful to consider in case of hypothetical technical difficulties reducing the number of usable arms. It could also be of use for future space detectors of reduced size. Such an alternative solution focusing only on a single 2-arm detector in space makes use of the so-called autocorrelation method [98]. If, as previously, we write the output data of the detector as $h(t)+n(t)$, with $n(t)$ the noise and $h(t)$ the GW signal, the autocorrelation of the signal reads

$$\langle \tilde{h}(f)\tilde{h}^*(f')\rangle = \frac{1}{2}\delta(f-f')S_h(|f|), \tag{6.28}$$

and similarly for the noise density P_n:

$$\langle \tilde{n}(f)\tilde{n}^*(f')\rangle = \frac{1}{2}\delta(f-f')P_n(|f|), \tag{6.29}$$

and in that case, it is possible to find the optimal SNR to detect a signal as

$$SNR = \left(\frac{T_{\text{obs}}}{2}\int_{-\infty}^{\infty} df\ \frac{S_h(|f|)^2}{[S_h(|f|)+P_n(|f|)]^2}\right)^{1/2}. \tag{6.30}$$

This method applies to a single-detector and is valid in the high-frequency limit. Since this analysis did not assume a particular polarization content, it only gives a detection threshold for a GW signal, but it will be necessary to generalize it in order to take into account all the possible modes, similarly to the network analysis.

6.6 Conclusion

As we have seen, the current analysis method for a network of space-borne detectors requires the use of multiple LISA-like clusters and presents the advantage of considering a general polarization of the signal. A second method involves only the exploitation of a single cluster. One can also focus on a single 2-arm detector, but this method does not yet address the polarization of the signal and needs to be generalized in order to fully treat the polarization content.

With the proposed LISA design as well as future possible project of space-borne inteferometers, it is therefore necessary to investigate both methods in order to set limits on the detectability of each polarization mode potentially present in a SGWB.

Chapter 7

Conclusion

"We do not know what the rules of the game are; all we are allowed to do is to watch the playing. Of course, if we watch long enough, we may eventually catch on to a few of the rules. The rules of the game are what we mean by fundamental physics."

Richard Feynman

General relativity has come a long way since its first formulation more than one hundred years ago, and so far, it has passed all the experimental tests, even the one provided by gravitational waves. Throughout this thesis, we have seen that GW can indeed be used as a powerful tool to test GR, but also act as a way to discriminate between alternative theories of gravitation, or put constraints on some of them. For this purpose, we have focused on the notion of GW polarization. Since only two tensor polarizations are expected to be detected within the framework of GR, any detection of additional vector or scalar modes could be a crucial indication of the limits of GR. And even the non-detection of additional modes can be of use, since it would allow to clarify the zoo of alternative theories.

We have first shown that in metric $f(R)$ four polarizations are expected to arise, thus showing a significant difference with GR which could be explored with future observations. Some upper bounds have already been put on additional modes for a stochastic GW background [99], and additional detectors will definitely help to refine these constraints.

We have also investigated various ways of combining future detectors, being on Earth or in space, in order to detect the polarization content of a stochastic GW background. The detection of such a signal would be crucial for two reasons: first of all, the detection itself would confirm the existence of a SGWB and give us a direct access to the very first instants of the Universe; in that sense, we could for instance directly test inflation theories. But the polarization content of the signal could once again be used to test GR and alternative theories. The achievable sensitivities of future network are in any case sufficiently low to put such a detection within the realm of the possible.

Finally, we want to note that the detection of the first BNS merger opened a new chapter for astrophysical observations, since we can now combine electromagnetic observations with GW ones, and thus start a so-called multimessenger astronomy which would allow to observe the Universe with our eyes and our ears, to put it in a poetic way. In that context, GW polarization could also play an important role when considering for instance gamma ray bursts produced in BNS, and the combination of those two signals - GW and light - could definitely tell us more about that phenomenon. In any case, GW have opened a new window on our Universe, through which we are only starting to observe, and exciting times are for sure just ahead of us.

References

[1] R. Kausar, L. Philippoz, and P. Jetzer, "Gravitational wave polarization modes in $f(R)$ theories," Phys. Rev. D **93**, 124071 (2016).

[2] R. Kausar, L. Philippoz, and P. Jetzer, "Gravitational wave polarization modes in $f(R)$ theories," in *The Fourteenth Marcel Grossmann Meeting* (World Scientific, 2017) pp. 1220–1226.

[3] L. Philippoz, A. Boîtier, and P. Jetzer, "Gravitational wave polarization from combined Earth-space detectors," Phys. Rev. D **98**, 044025 (2018).

[4] L. Philippoz and P. Jetzer, "Detecting additional polarization modes with LISA," J. Phys.: Conf. Ser. **840**, 012057 (2017).

[5] L. Philippoz and P. Jetzer, "Detecting additional polarization modes with LISA," in *Proceedings of the 52nd Rencontres de Moriond* (ASRIF, 2017) pp. 69–72.

[6] C. Misner, K. Thorne, and J. Wheeler, *Gravitation. Volume I.* (W.H. Freeman, San Francisco, USA, 1973).

[7] R. Wald, *General Relativity, With Applications to Astrophysics* (University of Chicago Press, Chicago, USA, 1984).

[8] N. Straumann, *General Relativity*, 2nd ed. (Springer, New York, USA, 2013).

[9] M. Maggiore, *Gravitational Waves. Vol. 1: Theory and Experiments*, 1st ed. (Oxford University Press, New York, USA, 2008).

[10] A. Buonanno, "Gravitational waves," (2007), arXiv:0709.4682 .

[11] C. M. Will, "The Confrontation between General Relativity and Experiment," Living Rev. Relativity **17**, 4 (2014).

[12] J. Gair, M. Vallisneri, S. Larson, and J. Baker, "Testing General Relativity with Low-Frequency, Space-Based Gravitational-Wave Detectors," Living Rev. Relativity **16**, 7 (2013).

[13] N. Yunes and X. Siemens, "Gravitational-Wave Tests of General Relativity with Ground-Based Detectors and Pulsar-Timing Arrays," Living Rev. Relativity **16**, 9 (2013).

[14] Y. Fujii and K.-I. Maeda, *The Scalar-Tensor Theory of Gravitation* (Cambridge University Press, Cambridge, England, 2003).

[15] R. Mirshekari and C. Will, "Compact binary systems in scalar-tensor gravity: Equations of motion to 2.5 post-Newtonian order," Phys. Rev. D **87**, 084070 (2013).

[16] R. Lang, "Compact binary systems in scalar-tensor gravity. II. Tensor gravitational waves to second post-Newtonian order," Phys. Rev. D **89**, 084014 (2014).

[17] B. Bertotti, L. Iess, and P. Tortora, "A test of general relativity using radio links with the Cassini spacecraft," Nature **425**, 374 (2003).

[18] C. Will and N. Yunes, "Testing alternative theories of gravity using LISA," Class. Quantum Gravity **21**, 4367 (2004).

[19] H. Zaglauer, "Neutron stars and gravitational scalars," ApJ **393**, 685 (1992).

[20] B. Famaey and S. McGaugh, "Modified Newtonian Dynamics (MOND): Observational Phenomenology and Relativistic Extensions," Living Rev. Relativity **15**, 10 (2012).

[21] N. Yunes and F. Pretorius, "Fundamental theoretical bias in gravitational wave astrophysics and the parametrized post-Einsteinian framework," Phys. Rev. D **80**, 122003 (2009).

[22] K. Yagi, L. Stein, N. Yunes, and T. Tanaka, "Post-Newtonian, quasicircular binary inspirals in quadratic modified gravity," Phys. Rev. D **85**, 064022 (2012).

[23] P. Pani and V. Cardoso, "Are black holes in alternative theories serious astrophysical candidates? The case for Einstein-dilaton-Gauss-Bonnet black holes," Phys. Rev. D **79**, 084031 (2009).

[24] S. Alexander and N. Yunes, "Chern-Simons modified general relativity," Phys. Rep. **480**, 1 (2009).

[25] A. Ashtekar and J. Lewandowski, "Background independent quantum gravity: a status report," Class. Quantum Gravity **21**, R53 (2004).

[26] W. Hartnell *et al.*, "Time and relative dimension in space," Mon. Not. Gall. Soc. **13**, 900 (1963).

[27] A. D. Felice and S. Tsujikawa, "$f(R)$ Theories," Living Rev. Relativity **13**, 3 (2010).

[28] L. Rubbo, N. Cornish, and O. Poujade, "Forward modeling of space-borne gravitational wave detectors," Phys. Rev. D **69**, 082003 (2004).

[29] N. Seto, "Effects of finite armlength of LISA on analysis of gravitational waves from massive-black-hole binaries," Phys. Rev. D **66**, 122001 (2002).

[30] N. Cornish and L. Rubbo, "LISA response function," Phys. Rev. D **67**, 022001 (2003).

[31] L. Finn, "Gravitational radiation sources and signatures," (1999), arXiv:gr-qc/9903107 .

[32] M. Vallisneri, "Use and abuse of the Fisher information matrix in the assessment of gravitational-wave parameter-estimation prospects," Phys. Rev. D **77**, 042001 (2008).

[33] C. Huwyler, *Testing General Relativity with Gravitational Waves* (PhD Thesis, Univ. Zurich, 2014).

[34] C. Rodriguez, B. Farr, W. Farr, and I. Mandel, "Inadequacies of the Fisher information matrix in gravitational-wave parameter estimation," Phys. Rev. D **88**, 084013 (2013).

[35] N. Cornish and E. Porter, "MCMC exploration of supermassive black hole binary inspirals," Class. Quantum Gravity **23**, S761 (2006).

[36] N. Cornish, L. Sampson, N. Yunes, and F. Pretorius, "Gravitational wave tests of general relativity with the parameterized post-Einsteinian framework," Phys. Rev. D **84**, 062003 (2011).

[37] L. Sampson, N. Cornish, and N. Yunes, "Gravitational wave tests of strong field general relativity with binary inspirals: Realistic injections and optimal model selection," Phys. Rev. D **87**, 102001 (2013).

[38] T. Littenberg and N. Cornish, "Separating gravitational wave signals from instrument artifacts," Phys. Rev. D **82**, 103007 (2010).

[39] T. Sotiriou and V. Faraoni, "$f(R)$ theories of gravity," Rev. Mod. Phys. **82**, 451 (2010).

[40] C. Brans and R. Dicke, "Mach's Principle and a Relativistic Theory of Gravitation," Phys. Rev. **124**, 925 (1961).

[41] J. Casas, J. Garcia-Bellido, and M. Quiros, "On the gravity theories and cosmology from strings," Nucl. Phys. B **361**, 713 (1991).

[42] M. Capone and M. Ruggiero, "Jumping from metric $f(R)$ to scalar-tensor theories and the relations between post-Newtonian parameters," Class. Quantum Gravity **27**, 125006 (2010).

[43] B. P. Abbott *et al.*, "Observation of Gravitational Waves from a Binary Black Hole Merger," Phys. Rev. Lett. **116**, 061102 (2016).

[44] P. Amaro-Seoane *et al.*, "eLISA: Astrophysics and cosmology in the millihertz regime," GW Notes **6**, 4–110 (2013).

[45] B. Abbott *et al.*, "Tests of General Relativity with GW150914," Phys. Rev. Lett. **116**, 221101 (2016).

[46] S. Capozziello, C. Corda, and M. Laurentis, "Massive gravitational waves from $f(R)$ theories of gravity: Potential detection with LISA," Phys. Lett. B **669**, 255 (2008).

[47] S. Capozziello and S. Vignolo, "Metric-affine $f(R)$-gravity with torsion: an overview," Ann. Phys. **19**, 238 (2010).

[48] S. Capozziello, R. Cianci, M. Laurentis, and S. Vignolo, "Testing metric-affine $f(R)$-gravity by relic scalar gravitational waves," Eur. Phys. J. C **70**, 341 (2010).

[49] C. Corda, "Massive gravitational waves from the R^2 theory of gravity: production and response of interferometers," Int. J. Mod. Phys. A **23**, 1521 (2008).

[50] C. Corda, "An oscillating Universe from the linearized R^2 theory of gravity," Gen. Relativ. Gravit. **40**, 2201 (2008).

[51] C. Corda, "The production of matter from curvature in a particular linearized high order theory of gravity and the longitudinal response function of interferometers," J. Cosmol. Astropart. Phys. **04**, 009 (2007).

[52] P. Prasia and V. Kuriakose, "Detection of massive Gravitational Waves using spherical antenna," Int. J. Mod. Phys. D **23**, 1450037 (2014).

[53] S. Capozziello and C. Corda, "Scalar gravitational waves from scalar-tensor gravity: production and response of interferometers," Int. J. Mod. Phys. D **15**, 1119 (2006).

[54] E. Newman and R. Penrose, "An Approach to Gravitational Radiation by a Method of Spin Coefficients," J. Math Phys. **3**, 566 (1962), see errata, ibid. **4**, 998 (1963).

[55] D. M. Eardley, D. L. Lee, and A. P. Lightman, "Gravitational-Wave Observations as a Tool for Testing Relativistic Gravity," Phys. Rev. D **8**, 3308 (1973).

[56] M. Alves, O. Miranda, and J. de Araujo, "Probing the $f(R)$ formalism through gravitational wave polarizations," Phys. Lett. B **679**, 401 (2009).

[57] M. Alves, O. Miranda, and J. de Araujo, "Extra polarization states of cosmological gravitational waves in alternative theories of gravity," Class. Quantum Gravity **27**, 145010 (2010).

[58] C. Berry and J. Gair, "Linearized $f(R)$ gravity: Gravitational radiation and Solar System tests," Phys. Rev. D **83**, 104022 (2011).

[59] S. Capozziello and M. Laurentis, "Extended Theories of Gravity," Phys. Rep. **509**, 167–321 (2011).

[60] C. Corda, "Massive relic gravitational waves from $f(R)$ theories of gravity: production and potential detection," Eur. Phys. J. C **65**, 257–267 (2010).

[61] M. Ferraris, M. Francaviglia, and I. Volovich, "The universality of vacuum Einstein equations with cosmological constant," Class. Quantum Gravity **11**, 1505–1517 (1994).

[62] J. Näf, P. Jetzer, and M. Sereno, "On gravitational waves in spacetimes with a nonvanishing cosmological constant," Phys. Rev. D **79**, 024014 (2009).

[63] C. Will, "The Confrontation between General Relativity and Experiment," Living Rev. Relativity **9**, 3 (2006).

[64] B. Sathyaprakash and B. Schutz, "Physics, Astrophysics and Cosmology with Gravitational Waves," Living Rev. Relativity **12**, 2 (2009).

[65] M. Alves, P. Moraes, J. de Araujo, and M. Malheiro, "Gravitational waves in the $f(R,T)$ theory of gravity," (2016), arXiv:1604.03874v1 .

[66] K. Bamba *et al.*, "No further gravitational wave modes in $F(T)$ gravity," Phys. Lett. B **727**, 194 (2013).

[67] A. Stabile and S. Capozziello, "Post-Minkowskian Limit and Gravitational Waves solutions of Fourth Order Gravity: a complete study," (2015), arXiv:1501.02187 .

[68] B. P. Abbott *et al.*, "GW151226: Observation of Gravitational Waves from a 22-Solar-Mass Binary Black Hole Coalescence," Phys. Rev. Lett. **116**, 241103 (2016).

[69] B. P. Abbott *et al.*, "GW170104: Observation of a 50-Solar-Mass Binary Black Hole Coalescence at Redshift 0.2," Phys. Rev. Lett. **118**, 221101 (2017).

[70] B. P. Abbott *et al.*, "GW170608: Observation of a 19 Solar-mass Binary Black Hole Coalescence," Astrophys. J. Lett. **851**, L35 (2017).

[71] B. P. Abbott *et al.*, "GW170814: A Three-Detector Observation of Gravitational Waves from a Binary Black Hole Coalescence," Phys. Rev. Lett. **119**, 141101 (2017).

[72] B. P. Abbott *et al.*, "GW170817: Observation of Gravitational Waves from a Binary Neutron Star Inspiral," Phys. Rev. Lett. **119**, 161101 (2017).

[73] B. P. Abbott *et al.*, "Multi-messenger Observations of a Binary Neutron Star Merger," Astrophys. J. Lett. **848**, 2 (2017).

[74] C. Everitt *et al.*, "Gravity Probe B data analysis status and potential for improved accuracy of scientific results," Class. Quantum Grav. **25**, 114002 (2008).

[75] P. Touboul *et al.*, "The MICROSCOPE mission: first results of a space test of the Equivalence Principle," Phys. Rev. Lett. **119**, 231101 (2017).

[76] KAGRA Collaboration, "Construction of KAGRA: an Underground Gravitational Wave Observatory," Progr. Theor. Exp. Phys. **2018**, 013F01 (2018).

[77] IndIGO Consortium, "LIGO-India: Proposal for an interferometric gravitational-wave observatory," (2011).

[78] ET Science Team, "Einstein gravitational wave Telescope conceptual design study," ET-0106C-10 **4** (2011).

[79] M. Armano *et al.*, "Beyond the Required LISA Free-Fall Performance: New LISA Pathfinder Results down to 20 μHz," Phys. Rev. Lett. **120**, 061101 (2018).

[80] LISA Consortium, "LISA: A proposal in response to the ESA call for L3 mission concepts," (2017), arXiv:1702.00786 .

[81] S. Kawamura *et al.*, "The Japanese space gravitational wave antenna - DECIGO," Class. Quantum Grav. **23**, S125 (2006).

[82] K. Yagi and N. Seto, "Detector configuration of DECIGO/BBO and identification of cosmological neutron-star binaries," Phy. Rev. D **83**, 044011 (2011).

[83] S. Isoyama, H. Nakano, and T. Nakamura, "Multiband Gravitational-Wave Astronomy: Observing binary inspirals with a decihertz detector, B-DECIGO," (2018), arXiv:1802.06977v1 .

[84] A. Nishizawa, A. Taruya, K. Hayama, S. Kawamura, and S. Masa-aki, "Probing nontensorial polarizations of stochastic GWB with ground-based laser interferometers," Phys. Rev. D **79**, 082002 (2009).

[85] A. Nishizawa, A. Taruya, and S. Kawamura, "Cosmological test of gravity with polarizations of stochastic GW around 0.1-1 Hz," Phys. Rev. D **81**, 104043 (2010).

[86] B. Allen and J. D. Romano, "Detecting a stochastic background of gravitational radiation: Signal processing strategies and sensitivities," Phys. Rev. D **59**, 102001 (1999).

[87] The LIGO Scientific Collaboration, "Advanced LIGO," Class. Quantum Grav. **32**, 074001 (2015).

[88] D. V. Martynov *et al.*, "The Sensitivity of the Advanced LIGO Detectors at the Beginning of Gravitational Wave Astronomy," Phys. Rev. D **93**, 112004 (2016).

[89] D. M. Eardley, D. L. Lee, A. P. Lightman, R. V. Wagoner, and C. M. . Will, "Gravitational-Wave Observations as a Tool for Testing Relativistic Gravity," Phys. Rev. Lett. **30**, 884 (1973).

[90] J. Armstrong, F. Estabrook, and M. Tinto, "Time-delay interferometry for space-based gravitational wave searches," ApJ **527**, 814 (1999).

[91] F. Estabrook, M. Tinto, and J. Armstrong, "Time-delay analysis of LISA GW data: Elimination of spacecraft motion effects," Phys. Rev. D **62**, 042002 (2000).

[92] M. Tinto, J. Armstrong, and F. Estabrook, "Discriminating a gravitational wave background from instrumental noise in the LISA detector," Phys. Rev. D **63**, 021101 (2000).

[93] M. Tinto, F. Estabrook, and J. Armstrong, "Time-delay interferometry for LISA," Phys. Rev. D **65**, 082003 (2002).

[94] M. Tinto and M. E. Alves, "LISA sensitivities to GW from relativistic metric theories of gravity," Phys. Rev. D **82**, 122003 (2010).

[95] M. Tinto and S. V. Dhurandhar, "Time-Delay Interferometry," Living Rev Relativity **17**, 6 (2014).

[96] C. J. Moore, R. H. Cole, and C. P. L. Berry, "Gravitational-wave sensitivity curves," Class. Quantum Gravity **32**, 015014 (2015).

[97] A. Nishizawa and K. Hayama, "Probing for massive stochastic gravitational-wave background with a detector network," Phys. Rev. D **88**, 064005 (2013).

[98] M. Tinto and J. W. Armstrong, "Single-detector searches for a stochastic backgroung of gravitational radiation," (2012), arXiv:gr-qc/1205.4620v1 .

[99] B. Abbott *et al.*, "Search for Tensor, Vector, and Scalar Polarizations in the Stochastic Gravitational-Wave Background," Phys. Rev. Lett. **120**, 201102 (2018).

PHILIPPOZ Lionel — Curriculum Vitae

Personal information

Date of birth 31 March 1988

Nationality Swiss

Place of origin Leytron VS

Education

2013–2018 **Doctorate** (Dr. sc. nat.)
Physik-Institut, Universität Zürich
Supervisor: Prof. Dr. P. Jetzer
Thesis title: "On the Polarization of Gravitational Waves"

2010–2012 **MSc** in Theoretical Physics
ETH Zürich
Supervisors: Prof. Dr. V. Desjacques, Prof. Dr. G.M. Graf
Title: "Testing Inflationary Models with Galaxy Clustering"

2007–2010 **BSc** in Physics
EPFL

2002–2007 **Matura** with focus on mathematics and physics
Lycée-Collège des Creusets, Sion (VS)

Publications

2016 "Gravitational wave polarization modes in $f(R)$ theories"
R.H. Kausar, L. Philippoz, P. Jetzer - *Physical Review D,* **93** *124071, 2016*.

2017 "Gravitational wave polarization modes in $f(R)$ theories"
R.H. Kausar, L. Philippoz, P. Jetzer - *Proceedings of the 14th Marcel Grossmann Meeting, held 12-18 July 2015 at the University of Rome "La Sapienza", Italy. World Scientific, December 2017, 1220-1226*.

2017 "Detecting additional polarization modes with LISA"
L. Philippoz, P. Jetzer - *Proceedings of the 11th LISA Symposium, held 5-9 September 2016 at Irchel Campus, University of Zürich, Switzerland. J.Phys.: Conf. Ser., Vol.* **840** *012057, 2017*.

2017 "Detecting additional polarization modes with LISA"
L. Philippoz, P. Jetzer - *Proceedings of the 52nd Rencontres de Moriond, held 25 March - 1 April 2017 at La Thuile, Aosta Valley, Italy. ARISF, 2017*.

2018 "Gravitational wave polarizations from combined Earth-space detectors"
L. Philippoz, A. Boîtier, P. Jetzer - *Physical Review D,* **98** *044025, 2018*.

Conferences, Schools and Talks

6-7 Feb 2014 Swiss Cosmo Days
ETH, Zürich, Switzerland

12-13 Mar 2014 eLISA Consortium Progress Meeting #3
University of Zürich, Zürich, Switzerland

18-23 May 2014 10th LISA Symposium
University of Florida, Gainesville, USA
Poster "Detecting additional polarization modes with eLISA"

15-20 Sep 2014 DPG School on Physics - GR@99
Bad Honnef, Germany

6-7 Feb 2015 Swiss Cosmo Days
University of Geneva, Geneva, Switzerland

25-28 Mar 2015 International School of Gravitational Wave Physics
University of Kyoto, Kyoto, Japan
Talk and poster "Detecting additional polarization modes with eLISA"

13-18 Dec 2015 28th Texas Symposium on Relativistic Astrophysics
International Conference Center, Geneva, Switzerland

11-12 Feb 2016 Swiss Cosmo Days
EPFL, Lausanne, Switzerland

5-9 Sep 2016 11th LISA Symposium
University of Zürich, Zürich, Switzerland
Poster "Detecting additional polarization modes with LISA"

25-1 Apr 2016 52nd Rencontres de Moriond - Gravitation
La Thuile, Aosta Valley, Italy
Talk "Detecting additional polarization modes with LISA"

28-3 Feb 2017 48th Saas-Fee course: Black hole formation and growth
Saas-Fee, Switzerland

Experience

Aug 2013 – Jul 2017 **Assistant for Mathematics**
Departement of Business Administration - University of Zürich
Teaching mathematics to bachelor students in economics. Series corrections, exam preparation and correction.

Aug 2015 – Jul 2016 **Coordinator of the Mathematics Lecture**
Departement of Business Administration - University of Zürich
Coordination of a team of up to 10 assistants and tutors. Exercices and exam planification.

Jan 2015 – Jul 2016 **Head of Marking and Moderation, Academic Committee**
International Physics Olympiad 2016 - University of Zürich
Academic committee of the IPhO 2016 held in Zürich. Problem preparation. Training and coordination of the markers (around 100 members of the Physics Departement) during the correction and discussion of the problems.

Jul 2017 – Feb 2018 **Assistant for Physics**
Departement of Physics - ETH Zürich
Teaching general relativity to master students in physics. Series corrections, oral exam co-examiner.